Characterization of CAMTA1 and Nkx2.2 in the context of glioblastoma cancer stem cell biology

Dissertation zur Erlangung des Doktorgrades der Naturwissenschaften (Dr. rer. nat.) der Fakultät für Biologie und Vorklinische Medizin der Universität Regensburg

vorgelegt von

Ludwig Wankerl

aus

Regensburg

im Jahr

2015

Das Promotionsgesuch wurde eingereicht am:

03. Juli 2015

Die Arbeit wurde angeleitet von:

Prof. Dr. rer. nat. Gunter Meister

Unterschrift:

Our greatest weakness lies in giving up.

The most certain way to succeed is always to try just one more time.

Thomas A. Edison

Abstract

Glioblastoma multiforme (glioblastoma) is the most malignant type of tumor in the human brain. For glioblastomas and several other cancer types, the existence of so called "cancer stem cells" was described. Cancer stem cells are characterized by stem cell-like traits such as the capacity of self-renewal and differentiation. Moreover, there is evidence that these cells contribute to cancer recurrence after therapy.

Several molecular-pathological factors are crucial for the emergence of glioblastomas in general and for glioblastoma cancer stem cells in particular. For example, certain microRNAs (miRNAs) such as the miRNA pair miR-9/9* are specifically enriched in glioblastoma cancer stem cells. This miRNA pair acts as oncogene for glioblastomas by repressing the tumor suppressor Calmodulin-binding transcription activator 1 (CAMTA1).

In this thesis, the upstream and downstream pathways of the CAMTA1 transcription factor were investigated in terms of their relevance in cancer biology. Therefore, siRNAs and antibodies against CAMTA1 were generated and established. Beyond that, a potential interaction partner of CAMTA1, Nkx2.2, was identified. Nkx2.2 is an important transcription factor for neural development and is also a potential tumor suppressor for glioblastomas. The tumor-suppressive effect of Nkx2.2 reported previously was further confirmed by this thesis. In this regard, it was shown that an overexpression of Nkx2.2 affected glioblastoma cancer stem cells negatively and impaired the proliferation of glioma cells. Additionally, a positive correlation between Nkx2.2 expression and survival of glioma patients was revealed.

Furthermore, it was hypothesized that Nkx2.2 and CAMTA1 act in concert to stimulate the transcription of *NPPA,* which encodes for the precursor of the natriuretic

peptide (ANP). This activation was thought to be the main mechanism for these two transcription factors to cause their tumor-suppressive effects. Consistently, it was shown that an overexpression of Nkx2.2 elevated the NPPA mRNA levels and that Nkx2.2 can strongly induce the *NPPA* promoter.

Nkx2.2 was further characterized in terms of additional interaction partners and a potential regulation by miRNAs.

The findings of this thesis allow to postulate a model which describes a possible regulatory network important for understanding glioblastomas, in particular the formation and traits of glioblastoma cancer stem cells. This will advance therapy strategies that "tackle" these persistent cells.

Zusammenfassung

Glioblastoma multiforme (Glioblastom) ist eine Tumorform, die im Gehirn auftritt und unter den Gehirntumoren den höchsten Grad an Malignität aufweist. Für Glioblastome und diverse andere Krebsarten wurde die Existenz von sog. "Krebs-Stammzellen" nachgewiesen. Krebs-Stammzellen zeichnen sich durch ähnliche Charakteristika aus wie Stammzellen von normalem, gesundem Gewebe, d.h. sie sind fähig, sich zu differenzieren und selbst zu erneuern.

Verschiedene molekular-pathologische Faktoren tragen zur Entstehung von Glioblastomen bzw. deren Krebs-Stammzellen bei. So sind beispielsweise bestimmte mikroRNAs (miRNAs) wie das bifunktionelle miRNA-Paar miR-9/9* vermehrt in diesen Krebs-Stammzellen exprimiert. Dieses spezielle miRNA-Paar reprimiert den Tumorsuppressor *Calmodulin-binding transcription activator 1* (CAMTA1) und wirkt dadurch onkogen für Glioblastome.

In dieser Arbeit sollte das zelluläre Netzwerk von CAMTA1, durch welches die tumor-suppressive Wirkung hervorgerufen wird, näher untersucht werden. Dazu wurden siRNAs und Antikörper gegen CAMTA1 generiert und auf ihre Funktionalität überprüft. Darüber hinaus konnte der Transkriptionsfaktor Nkx2.2 als ein potentieller Interaktionspartner von CAMTA1 identifiziert werden. Nkx2.2 spielt bei der Entwicklung des zentralen Nervensystems eine wichtige Rolle und gilt ebenfalls als potentieller Tumorsuppressor für Glioblastome. Diese tumor-suppressive Wirkung von Nkx2.2 wurde in einer früheren Studie gezeigt und konnte durch diese Arbeit bestätigt werden: Eine Überexpression von Nkx2.2 beeinflusste Glioblastom-Krebs-Stammzellen negativ und verminderte deutlich die Proliferation von Glioma-Zellen. Zudem konnte

ein Zusammenhang zwischen einer erhöhter Nkx2.2-Expression und einer höheren Überlebensrate von Patienten mit Gliomen festgestellt werden.

In dieser Arbeit wurde die Hypothese aufgestellt, dass CAMTA1 und Nkx2.2 miteinander interagieren, um die Transkription des Gens *NPPA* zu steigern. *NPPA* kodiert für den Vorläufer des atrialen natriuretischen Peptids (ANP). Die Aktivierung des *NPPA*-Gens stellt vermutlich einen zentralen Mechanismus dar, über den die beiden Transkriptionsfaktoren CAMTA1 und Nkx2.2 ihre tumor-suppressive Wirkung vermitteln. Es konnte gezeigt werden, dass eine Überexpression von Nkx2.2 tatsächlich zu einer Erhöhung der *NPPA*-Expression führte und dass Nkx2.2 in der Lage ist, den Promotor dieses Gens zu aktivieren.

Ferner wurde untersucht, ob für Nkx2.2 weitere potentielle Interaktionspartner identifiziert werden können und ob Nkx2.2 durch miRNAs reguliert wird.

Mit den in dieser Arbeit erbrachten Ergebnissen lässt sich ein Modell entwerfen, wie die Entstehung von *Glioblastoma multiforme* und dessen Krebsstam-Zellen durch einen Regulationsmechanismus potentiell unterdrückt wird. Dieses Modell kann dazu beitragen, die molekularen Mechanismen für die Entstehung von Glioblastomen, insbesondere von deren Krebs-Stammzellen, besser zu verstehen. Dadurch lassen sich möglicherweise neue Therapieansätze entwickeln.

Contents

List of Figures

List of Tables

List of Abbreviations

A	
A	(deoxy-)adenosine or ampere (context-dependent)
aa	amino acid
AEBSF	4-(2-Aminoethyl) benzenesulfonyl fluoride hydrochloride
APS	ammonium persulfate
Arabidopsis or at	*Arabidopsis thaliana*
AS	antisense
ATP	adenosine 5'-triphosphate
B	
bp	base pair(s)
BSA	bovine serum albumin
C	
C	(deoxy-)cytidine
C. elegans or ce	*Caenorhabditis elegans*
cDNA	complementary DNA
cGMP	cyclic guanosine monophosphate
CSC(s)	cancer stem cell(s)
CSC(s)	cancer stem cell(s)
C-terminus	carboxyl-terminus
D	
d	deoxy- or day(s) (context-dependent)
DAPI	4',6-diamidino-2-phenylindole
DMEM	Dulbecco's Modified Eagle's Medium
DMSO	dimethyl sulfoxide
DNA	deoxyribonucleic acid
DNase	deoxyribonuclease
Drosophila or dm	*Drosophila melanogaster*

DTT	dithiothreitol
E	
E. coli	*Escherichia coli*
EDTA	ethylenediaminetetraacetic acid
ERK	extracellular-signal-regulated kinases
F	
F	FLAG-tag
FBS	fetal bovine serum
G	
G	(deoxy-)guanosine
g	gram or standard gravity (≈ 9.81 m/s^2) (context-dependent)
GAPDH	glyceraldehyde 3-phosphate dehydrogenase
GFP	green fluorescent protein
GMP	guanosine monophosphate
GST	glutathione S-transferase
GTP	guanosine 5'-triphosphate
H	
H	HA-tag
HA	hemagglutinin
HBS	HEPES buffered saline
HEPES	4-(2-hydroxyethyl)-1-piperazineethanesulfonic acid
HMGA2	high-mobility group AT-hook 2
hs or hsa	*Homo sapiens*
I	
IgG	immunoglobulin G
IF	immunofluorescence
IP	immunoprecipitation
IPTG	isopropyl β-D-1-thiogalactopyranoside
K	
kb	kilo bases (1,000 bp)
L	
LB	lysogeny broth
M	
MEK	mitogen-activated protein kinase kinase

mm	*Mus musculus*
mRNA	messenger RNA
N	
N-terminus	amino-terminus
O	
OD	optical density
P	
PA	polyacrylamide
PABP	poly(A)-binding protein
PACT	protein activator of the interferon-induced protein kinase
PBS	phosphate buffered saline
PCR	polymerase chain reaction
Q	
qRT-PCR	quantitative real-time PCR
R	
r	ribo-
Ras	rat sarcoma
RNA	ribonucleic acid
RNase	ribonuclease
S	
S	sense
SDS	sodium dodecyl sulfate
siRNA	small interfering RNA
T	
T	(deoxy-)tymidine
TBS	TRIS-buffered saline
TEMED	tetramethylethylenediamine
TEV	tobacco etch virus
TRBP	transactivation-responsive RNA-binding protein
TRIS	tris(hydroxymethyl)-aminomethan
tRNA	transfer RNA
U	
U	uridine or units (context-dependent)
UTR(s)	untranslated region(s)

UV	ultraviolet
V	
v/v	volume per volume
W	
w/v	weight per volume
WB	western blot
X	
X-gal	5-bromo-4-chloro-3-indolyl-β-D-galactopyranoside

Units were abbreviated according to the international system of units (SI-units). For amino acids 3-letter or 1-letter abbreviations were used according to the recommendations of the International Union of Pure and Applied Chemistry (IUPAC).

1. Introduction

1.1. Cancer stem cells

Cancer describes a very diverse disease, which can emerge in almost every tissue of the human body. The progression of the several types of cancer is rather complex and involves disruptions of various cellular networks on different levels including alterations of the genome, transcriptome, proteome, and/or interactome.

In cancer research, it was thought for a long time that tumors are bulks of cells characterized by de-regulated proliferation. However, during the last twenty years, this simplified view of cancer has drastically changed: Many tumors form sophisticated and heterogeneous, almost organ-like, tissues which are sometimes also called "tumor microenvironment". This microenvironment is essential for the survival of the tumor and also for its distribution throughout the body by metastasis or migration. For example, it recruits blood vessels to supply tumor cells with nutrients and oxygen or it protects the tumor against the immune system (*1*).

But how can one single transformed cell or a small population of abnormal cells generate such a diversity? A likely explanation for this would be given by the existence of so-called cancer stem cells (CSCs) or tumor initiating cells (TICs). It was postulated that these CSCs behave like their normal counterparts in the body, i.e. these cells are capable of self-renewal and differentiation as normal stem cells are (Figure 1.1). By means of these stem cell-like abilities such cancer cells can constantly renew the tumor and generate the heterogeneous, differentiated tumor mass (*1, 2*).

The cancer stem cell hypothesis emerged at the end of the last century when for human acute myeloid leukemia a distinct, relatively small population of cells was identified (*3, 4*). The isolated cells differed from other cells of this cancer type regarding their

phenotype and functionality: These cells expressed the same pattern of cell surface proteins as normal hematopoietic stem cells. Furthermore, they were capable of self-renewal and promoted the formation of human leukemia when these cells were injected into (immuno-deficient) mice (*3, 4*). In 2003, CSCs were also found for breast cancer (*5*) and for brain tumors (*6*). The latter CSCs were isolated from human brain tumors (gliomas and medulloblastomas) and characterized by the expression of the cell surface protein CD133 (*6, 7*), which is normally a specific marker for neural stem cells (*8*). Remarkably, the injection of only 100 CD133-positve ($CD133^+$) cells into brains of immuno-deficient mice was sufficient to initiate the formation of new tumors, whereas even the injection of 100,000 CD133-negative ($CD133^-$) could not (*7*). Characteristics of CSCs in human brain tumors, particularly in *glioblastoma multiforme*, are described in more detail below (see paragraph 1.2.).

This hierarchical concept of a small subpopulation of CSCs and the residual differentiated tumor cells forming the bulk of the tumor was also reported for further types of cancer such as pancreatic (*9*), colon (*10*), or lung cancer (*11*). Hence, today, the cancer stem cell hypothesis is widely accepted.

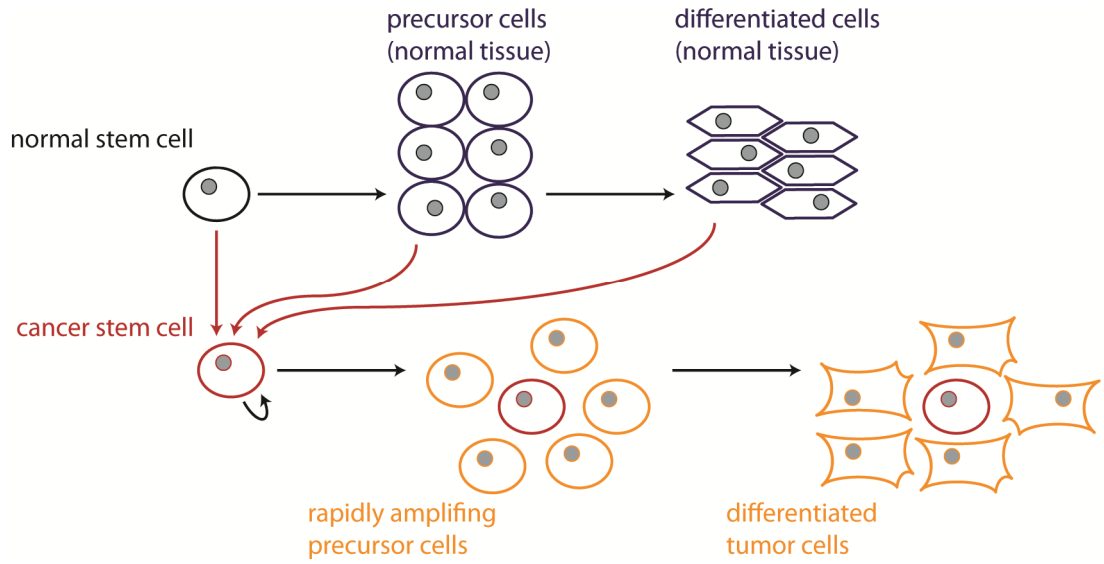

Figure 1.1: The concept of cancer stem cells (CSCs). CSCs possess the abilities of self-renewal and to differentiate comparable to normal stem cells. In the tumor, CSCs represent a relatively small sub-population whereas the tumor mass is constituted of more differentiated cancer cells. [Figure adapted and modified from (*12*)].

Interestingly, signaling pathways such as Sonic Hedgehog (SHH) or Notch, which are important for differentiation from pluripotent stem cells and strictly regulated during normal development, are often found to be de-regulated in CSCs (*2, 13*). This also illustrates that CSCs seem indeed to be abnormal counterparts of normal stem cells. But what kind of cell is transformed into a CSCs? Up to now, this remains largely unknown and depends probably on the cellular origin from which the tumor emerges. It is generally assumed that cells in every phase of their individual differentiation process can possibly transform into a CSCs (Figure 1.1) (*1, 2*).

1.2. *Glioblastoma multiforme*

Origin, molecular characteristics, and therapy

Glioblastoma multiforme[1] is not only the most frequent brain tumor in humans but also the most malignant. The World Health Organization (WHO) classifies human brain tumors into four grades due to their malignancy (*14*). In this regard, glioblastoma belongs to the highest WHO grade IV (lower-grade gliomas are for example astrocytomas) (*14*). Indeed, the median survival after diagnosis with best proceeding therapy is only 15 months, which drastically illustrates its malignancy. One reason for the fatal prognosis for glioblastomas is the fact that their cancer cells show a high degree of diffuse invasiveness into surrounding healthy brain tissue. Although the occurrence of glioblastomas is rare compared to other forms of cancer, glioblastomas are the most common type of all malignant gliomas (60 - 70 %) and they represent about 30 % of all human brain tumors (*15-17*).

As the name "glioblastoma" already implicates, it is thought that the origin of this brain tumor are most likely glia cells or their progenitor cells (*16*). Figure 1.2 illustrates the potential lineage origin of human brain tumors including glioblastomas. It also shows that glioblastomas are histological heterogeneous due to their cellular lineage origins. This heterogeneity can also be observed on the molecular-pathological level. In this

[1] Hereinafter shortened called glioblastoma

regard, Verhaak *et al.* classified glioblastomas, on the basis of genomic aberrations and corresponding alterations in expression levels of a large number of genes, into four distinct subtypes: classical, mesenchymal, proneural, and neural (*18*). The classical subtype is characterized by a massive *EGFR* amplification (encodes for the epidermal growth factor receptor). A hemizygous deletion of the *NF1* containing locus (encodes for neurofibromin 1, a known tumor suppressor) is the main feature of the mesenchymal subtype (*18*). For the proneural subtype, a significant higher (compared to the other subtypes) amplification for *Pdgfra* (encodes for Pdgf receptor α, a receptor tyrosine kinase) as well as point mutations in *IDH1* (encodes for isocitrate dehydrogenase 1) were observed (*18*). The neural subtype is characterized by the expression of certain neuron markers, e.g. neurofilament light polypeptide (NEFL) (*18*). Furthermore, Verhaak *et al.* linked all these characterized subtypes to cellular lineages of normal brain cell types: The proneural class reflected a oligodendrocytic signature but not the astrocytic signature which was in contrast associated with the classical type (*18*). The neural subtype showed both signatures as well as a neuron expression pattern and the mesenchymal type was associated with astroglial lineage (*18*).

Moreover, glioblastomas can be classified into primary and secondary glioblastomas: Primary glioblastomas arise *de novo* (i.e. due to a transformation of a normal cell of the brain), whereas secondary glioblastomas originate from lower-grade gliomas such as astrocytomas. Most glioblastomas are primary (*15, 16, 19*). Although there is no difference between primary and secondary glioblastomas concerning their morphological and malignant features, distinctions were identified at the molecular level: For example, primary glioblastomas show a frequent amplification of *EGFR*, in contrast to secondary glioblastomas which are characterized by *TP53* mutations (encodes for the tumor suppressor p53) (*15, 16, 19*).

Besides removal by surgery (which is often only possible to a limited extent without causing damage in healthy brain regions), combined radio- and chemotherapy applying the alkylating reagent temozolomide is the usual treatment (*20*). However, even with optimal therapy the survival of patients can only be extended for a few months.

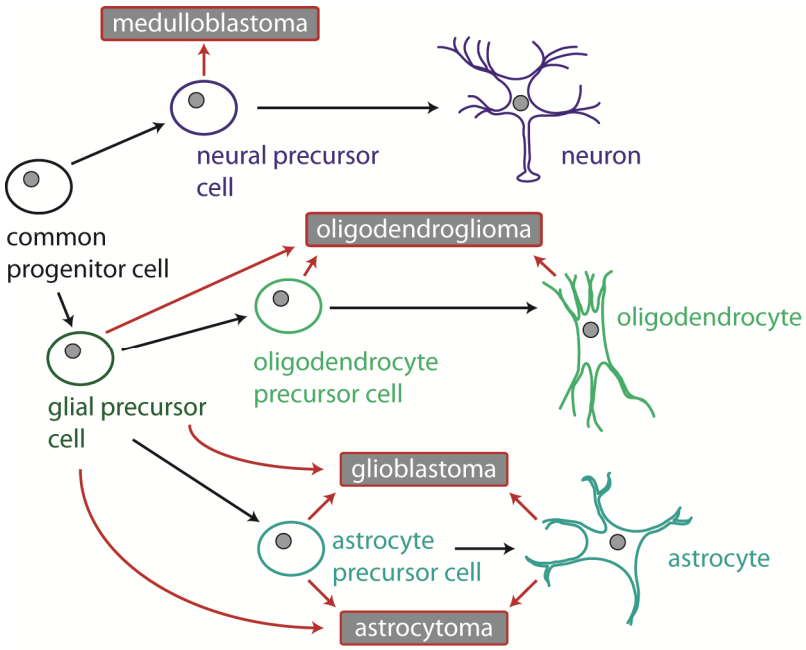

Figure 1.2: Suggested cellular origins of human brain tumors (medulloblastomas and gliomas). Red arrows indicate the possible transformation of a normal cell. Lineage origin based on histological and/or molecular features. It was suggested that glioblastoma emerge in the subventricular zone in the brain where (in adults) neural stem and progenitor cells can be found (*21*). [Figure adapted from (*16*)].

Glioblastoma cancer stem cells

As already mentioned in paragraph 1.1., CSCs expressing CD133 were identified about ten years ago in glioblastomas. In this work, Singh *et al.* showed that CD133-positive cells effectively induce the emergence of new tumors when they are injected into mouse brains. Notably, the newly formed tumors contained both $CD133^+$ and $C133^-$ cells although only $CD133^+$ cells were injected. This demonstrated that the CD133-positive cells can differentiate (*7*). Furthermore, Singh *et al.* showed a constant renewal and proliferation of the $CD133^+$ pool (*7*). Besides their capability of self-renewal and differentiation, these cells are also more resistant to irradiation and chemotherapeutics such as temozolomide (*22-24*). These traits of glioblastoma CSCs gives a possible explanation for the poor therapy success for glioblastomas.

Furthermore, it was demonstrated by Bao *et al.* that these cells secret the vascular endothelial growth factor (VEGF) which causes angiogenesis, the formation of blood

vessels by the surrounding tissue (*25*). This is essential for supplying the tumor with oxygen and nutrients.

The population of the CD133-positive CSCs within the tumor is small compared to the other differentiated cells of the tumor. Though, primary and secondary glioblastomas are divergent regarding their respective portion of CD133-positive cells: Primary glioblastomas contain significantly more CD133-positive cells than secondary glioblastomas (*26*). However, also glioblastoma CSCs were identified which do not express the CD133 marker but show tumorigenicity to a similar extent as CD133-positive cells (*26*). Thus, also other (more general) markers were suggested to define glioblastoma CSCs, e.g. the stage specific embryonic antigen 1 (SSEA1 or CD15) (*27*) or Nestin (*28*).

When primary glioblastoma cells, in particular CD-133 positive cells, are cultured *in vitro* under normal stem-cell like growth conditions, they form non-adherent spheres, called "neurosphere-like clones/colonies" (Figure 1.3). In this way cultured glioblastoma CSCs maintain their stem cell-like features and their capability to induce tumor formation *in vivo (26, 29, 30)*.

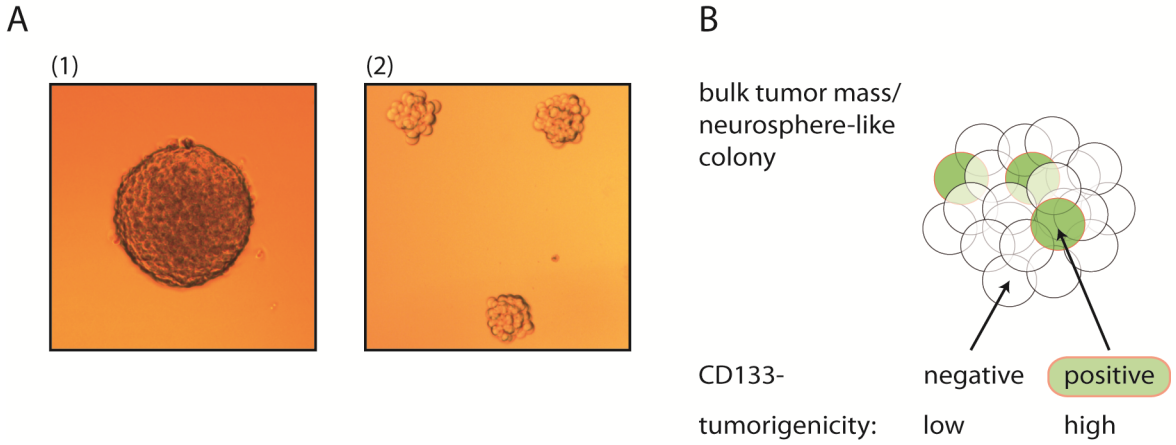

Figure 1.3: Cultured primary glioblastoma cells form neurosphere-like clones when cultured under stem cell-like growth conditions. A: Primary glioblastoma cells used in this thesis: (1) R11, (2) ZH161. **B:** Schematic illustration of a neurosphere-like colony.

1.3. The role of microRNAs in glioblastoma biology

MicroRNAs (miRNAs, miRs) are small non-coding RNAs that regulate fundamental cellular processes and are hence crucial factors for development, differentiation, and cell metabolism (*31-33*). Since miRNAs are important regulators, a de-regulation of miRNA expression is often associated with several types of diseases including cancer. Such miRNAs are also often referred to as "oncomiRs" (*34, 35*). On the one hand, oncomiRs can either act as tumor suppressors targeting oncogenes, on the other hand as oncogenes themselves inhibiting certain tumor suppressors (*34, 35*). Latter oncomiRs are often overexpressed and thus promote cancer progression. This paragraph focuses on several miRNAs (miR-26a, miR-17, miR-9/9*) which act as oncomiRs during glioblastoma progression. But first, the biogenesis of miRNAs and their mechanism of transcript regulation in mammals will be described.

1.3.1. miRNA biogenesis and miRNA-directed transcript regulation

MiRNA genes are normally transcribed by RNA-polymerase II, which leads to primary miRNA transcripts (pri-miRNAs) (*36*). These transcripts were first processed by a protein complex called microprocessor, which contains the RNase III Drosha and its co-factor DiGeorge syndrome critical region 8 (DGCR8). This processing step results in the miRNA precursor (pre-miRNA), which is characterized by a hairpin structure and a two nucleotide-overhang at the 3'-end (*37-39*). The precursor is afterwards exported by Exportin 5 from the nucleus into the cytoplasm (*40-42*), where the hairpin is cleaved off by another RNase III enzyme, Dicer. This yields a double-stranded miRNA (miRNA-duplex) with a length of about 22 nucleotides (*43, 44*). One strand of the duplex, the mature miRNA, is loaded into a protein of the Argonaute family whereas the other is usually degraded (referred to as miRNA*). Argonaute (Ago) proteins are the core components of the miRNA-induced silencing complex (miRISC) (*45*). The miRNA within the miRISC guides the silencing complex to the 3'-UTR of its target mRNA, whereas Ago recruits a member of the GW protein family (termed TNRC6A, B, and C in humans). TNRC6 proteins act by inhibiting translation or

inducing mRNA degradation and are therefore important mediators of miRNA-guided target repression (*46*, *47*). For the target recognition by the miRNA itself, the nucleotides 2 to 8 of the miRNA are important. This so called "seed sequence" is complementary to the target site within the particular mRNA (*32*). The biogenesis of miRNAs and its mRNA-mediated gene silencing are illustrated in Figure 1.4.

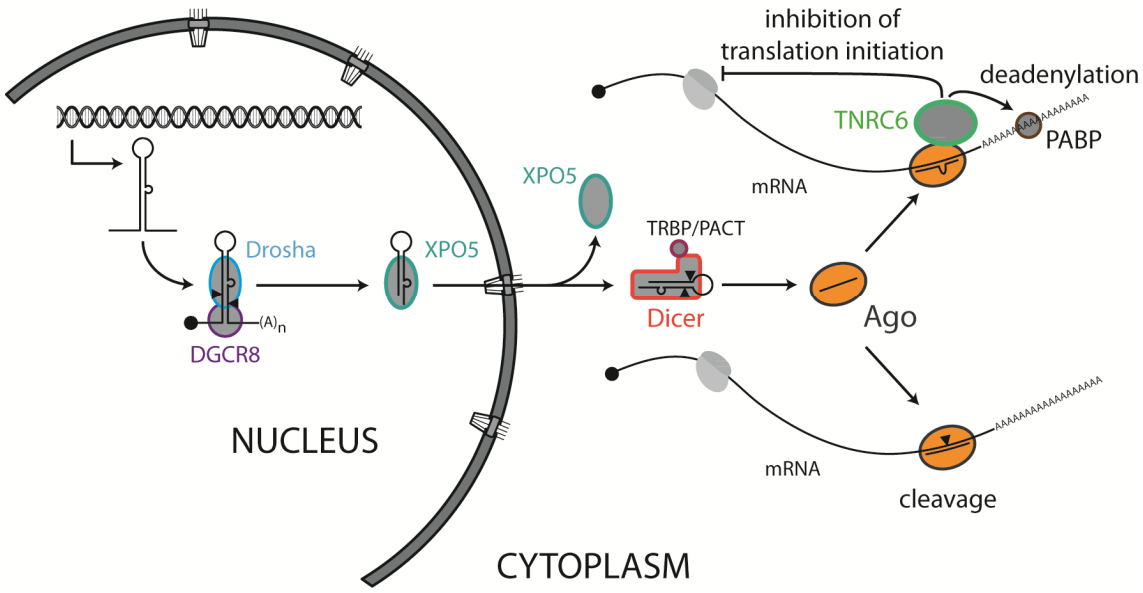

Figure 1.4: miRNA biogenesis and miRNA-induced transcript silencing. The first steps of the miRNA biogenesis take place in the nucleus and the maturation process is completed in the cytoplasm by transferring one strand of the miRNA duplex into an Ago protein. A rare event in mammals is a direct cleavage of mRNAs by cleavage-competent Ago2 loaded with a miRNA that is fully complementary to its target (*45*). This mechanism is comparable to an siRNA-directed knockdown.

1.3.2. Several miRNAs are important for glioblastoma progression and glioblastoma cancer stem cell maintenance

Various studies previously reported altered expression for many different miRNAs in gliomas, respectively in glioblastomas. This paragraph highlights four miRNAs important in glioblastoma biology.

miR-26a

In high-grade gliomas, miR-26a is frequently overexpressed (*48*). This results from a gene amplification of one of two *miR-26a* genomic loci (*miR-26a-2*) (*48*). Interestingly, this amplification is associated with a monoallelic deletion of *PTEN* (but was not observed for a homozygous *PTEN* deletion) (*48*). *PTEN* encodes for Phosphatase and Tensin homolog, which acts as a tumor suppressor and is a direct target of miR-26a in glioblastomas (*48*). It has been suggested that during glioblastoma progression, the monoallelic deletion of *PTEN* occurs before the gene amplification of *miR-26a-2 (48)*. The remaining PTEN is then post-transcriptionally repressed by the overexpressed miR-26a. This mechanism is basically equal to a homozygous loss of *PTEN*.

miR-17

Mammalian primary miRNA transcripts are often polycistronic, i.e. one primary transcript is transcribed from a cluster of various miRNA genes (*49*). This single primary transcript gives rise to several distinct mature miRNAs. MiR-17 is part of the miR-17~92 cluster. This particular miRNA is a well characterized oncogenic miRNA for several types of cancer (*35, 50*) and was found to be significantly higher expressed in glioblastomas (*51, 52*). Moreover, inhibition of all miR-17~92 cluster members in primary glioblastoma cells led to a decrease of proliferation on the one hand and had a stimulating effect on apoptosis on the other hand (*52*). In addition, miR-17-5p belongs to group of miRNAs, which are specifically enriched in CD133-positive glioblastoma cancer stem cells (*53*). An inhibition of this particular miRNA significantly reduces formation of neurosphere-like colonies of cultured CD133-postive glioblastoma cells (*53*). Other miRNAs showing also specific expression in CD133-positive cells are miR-106b, which is part of a miR-17~92 paralogous cluster (miR-106b~25) and has the same seed sequence as miR-17-5p (*50*), and the miRNA pair miR-9/9* (*53*).

*miR-9/9**

The miR-9/9* duplex belongs to a type of miRNA duplexes characterized by a functional guide and passenger strand (*54*). Different from the usual miRNA biogenesis, where the miRNA* strand is normally degraded, both strands are loaded to Ago, yielding two distinct miRISCs each with particular targets.

MiR-9/9* is mainly expressed in the nervous system where it is an important factor for neurogenesis (*54, 55*). In this context, the transcription factor REST (repressor element-1 silencing transcription factor) was identified to be a target for miR-9 and its co-factor CoREST is regulated by miR-9* (*54*). REST and CoREST are highly expressed in neural stem cells, but not in differentiated neural cells. By repression of both factors via miR-9/9*, neural stem cells differentiate (*54*). Furthermore, the specific inhibition of miR-9 strongly decreased the proliferation rate of differentiating neural precursor cells and increased cell migration (*55*). Both effects are caused by stathmin, which is important for microtubule dynamics and a target of miR-9 (*55*).

Besides its role in neural development, a de-regulation of miR-9/9*, indicated by high expression levels, was observed in brain tumors like glioblastomas (*56*) and also in other cancers such as breast cancer (*57*). For glioblastomas, Schraivogel *et al.* showed that miR-9/9* is highly abundant in CD133-positive glioblastoma stem cells (*53*). Importantly, a specific inhibition of miR-9 and miR-9* led in both cases to a drastic decrease of neurosphere-like clones and to a significant reduction of the CD133-positive cell population (*53*). Moreover, the inhibition also promoted differentiation of these cancer stem cells (*53*).

Taken together, these observations by Schraivogel *et al.,* indicate that miR-9/9* are important for maintaining the stem cell character of glioblastoma cancer stem cells. This raised the question for transcripts regulated by miR-9/9*. In this context, Schraivogel *et al.* identified the mRNA of the Calmodulin-binding transcription activator 1 (CAMTA1) as a potential target for miR-9/9* (*53*).

1.4. The Calmodulin-binding transcription activator 1 is a tumor suppressor for glioblastomas

1.4.1. The CAMTA family of transcription factors: Protein organization

Human CAMTA1 belongs to a family of transcription factors, which can be found in plants as well as in animals. Members of this protein family were first described in plants about 15 years ago (*58-60*). The genome of *Arabidopsis thaliana* encodes six CAMTA proteins (atCAMTA1-6) whereas both in *Caenorhabditis elegans* and *Drosophila melanogaster* respectively one CAMTA protein could be identified (ceCAMTA and dmCAMTA) (*60*). Mice and humans have two representatives of this family (mmCAMTA1/hsCAMTA1[2] and mmCAMTA2/hsCAMTA2[2]) (*60, 61*).
The large CAMTA proteins (e.g. human CAMTA1 has a molecular weight of 180 kDa) contain several domains with distinct functions. The organization of these domains within the protein and their amino acid sequence is highly conserved from plants to human (Figure 1.5) (*60, 62*). By bioinformatical analysis, the following domains were identified (from the N- to the C-terminus): A DNA-binding domain, called CG-1 domain, a TIG-domain, several ankyrin repeats, and IQ-domains (*60, 62*).

CG-1 domain

The CG-1 domain was first described for a DNA binding protein in parsley (*63*) and is characteristic for the CAMTA protein family (*60, 62*) . In *Arabidopsis thaliana* a target DNA sequence with a length of 6 bp was identified for atCAMTA1 and atCAMTA3 (*59, 64-66*). This target with a consensus sequence 5'-(A/C/G)CG(C/T)G(G/T/C)-3' was termed "CGCG-box" (*59*). Moreover, it was shown that in *Arabidopsis* abscisic acid-specific *cis* elements contain this CGCG-box (ABRE and its related coupling element ABRE-CE). These ABREs significantly occur upstream of calcium-induced genes suggesting that ABREs function as calcium-responsive *cis* elements (*64, 67*). Also in *Drosophila melanogaster* this CGCG-box was indentified within the promoter region

[2] unless stated otherwise CAMTA1 or CAMTA2 refers always to the human proteins in this thesis

of the dmCAMTA target gene *dFbxl4 (68)*. Interestingly, the CG-1 domain of dmCAMTA mediates dimerization, which is important for nuclear localization of dmCAMTA (*69*). In mammals it was not known for a long time if the CG-1 domain of the mammalian CAMTA representatives binds to a similar target sequence. But recently, Long *et al.* identified a consensus sequence for murine CAMTA2 by *in vitro* binding assays (*70*). This sequence (5'-(T/C)GCA(G/A/T/C)TGCG-3') is also GC-rich as the consensus-sequence found in *Arabidopsis* but it differs from the plant sequence. Using reporter assays, Long *et al.* showed that mmCAMTA1 recognizes this motif and activates the reporter even stronger than CAMTA2 (*70*). The critical residue for DNA-binding seems to be a single lysine (K141 for mmCAMTA1 and K108 for mmCAMTA2) (*70*). Furthermore, this study suggests that mammalian CAMTA proteins bind probably as dimers to their target DNA sequence (*70*), which is in line with the previously reported dimerization of dmCAMTA (*69*). Bioinformatic analysis revealed a nuclear localization signal (NLS) within the CG-1 domain of almost all members of the CAMTA protein family (Figure 1.5) (*60, 62*). In contrast, for mmCAMTA2 the NLS was identified next to the C-terminus and a nuclear export signal (NES) in the CG-1 domain (*61*).

TIG domain

The organization of the TIG (transcription factor immunoglobulin) domain (as well as the ankyrin repeats) of the CAMTA proteins is similar to precursors p100 and p105 of the transcription factor NF-κB. The TIG domain mediates non-specific DNA contacts of NF-κB family members and is also responsible for dimerization of these proteins (*71-74*).

Ankyrin repeats

Ankyrin (ANK) repeats can be found in NF-κB family members (*74*), but also in many other eukaryotic proteins. Indeed, ANK repeats belong to the most abundant eukaryotic protein motifs and were identified in many proteins involved in a wide range of cellular functions (*75, 76*). One single ANK repeat has a length of about 30 amino acids and is

composed of two α-helices (*77*). The repeats are connected via a β-hairpin consisting of two β-sheets (*78*). These repeats are known as interfaces for protein-protein interactions (*75, 76, 78*). Due to their very frequent occurrence in many proteins with crucial cellular function, mutations disrupting protein-protein interactions via ANK repeats are often associated with human diseases such as cancer (*75, 76*).

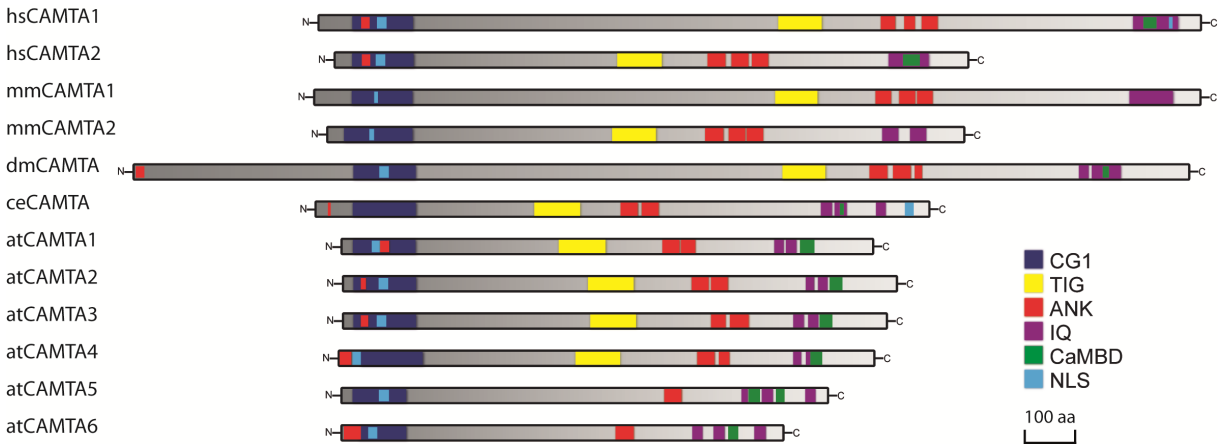

Figure 1.5: The CAMTA family of transcription factors. The particular proteins are drawn to scale: For human (hs), *Drosophila melanogaster* (dm), *Caenorhabditis elegans* (ce), and *Arabidopsis thaliana* (at) CAMTAs according to (*62*), protein information for murine (mm) CAMTAs was retrieved from http://www.uniprot.org/ [(A2A891 (mmCAMTA1) and Q80Y50 (mmCAMTA2)]. The particular, highly conserved, domains are illustrated in different colors: CG-1 DNA-binding domain, TIG transcription factor immunoglobulin domain (TIG), ankyrin repeats (ANK), IQ domain (IQ), calmodulin-binding domain (CaMBD), and nuclear localization signal (NLS).

IQ domain

The IQ domains, which are located next to the C-terminus of all CAMTA proteins, are known to bind Calmodulin (CaM) or CaM-related proteins, whereby binding can also occur in the absence of calcium (*79, 80*). These domains are characterized by the repetitive motif IQXXXRGXXXR, hence they are termed "IQ motifs" (*79, 80*). The number of IQ domains for the respective CAMTA proteins differs within the protein family: For ceCAMTA no IQ domain was identified, whereas atCAMTA6 contains five IQ domains (see also Figure 1.5) (*60*). But not only the number of IQ-domains is different, also the ability of CaM binding varies. AtCAMTA1 showed basically no

binding of its IQ domains to Ca^{2+}-CaM (*60*). In contrast, a Ca^{2+}-independent CaM-binding motif within the IQ domain was characterized for dmCAMTA (*68*).

Up to now, it remains unknown if the IQ-motifs of the mammalian CAMTA representatives can also bind CaM (neither in presence nor absence of Ca^{2+}). However, it was shown recently that an elevated intracellular calcium concentration obviously results in an increased CAMTA1 mRNA level in human mesenchymal stem cells (*81*). This gives a first hint for a possible Ca^{2+}-dependent transcription regulation of CAMTA1.

Other domains

Besides the highly conserved domains described before, some CAMTA proteins have less conserved domains. In this context, for atCAMTA1 (*60*), dmCAMTA (*68*), and mmCAMTA2 (*61*) a functional transcription activation domain (TAD) was identified. In the case of atCAMTA1 and mammalian CAMTA2, this domain is located between their particular CG-1 and TIG domains (*62*). However, no consensus sequence for this domain was found via bioinformatic analysis (*60*).

1.4.2. Function of CAMTA proteins from plants to mammals

The function of CAMTA proteins in plants was extensively investigated during the last ten years. Obviously, plant CAMTA proteins act as key mediators of cellular response to signals caused by abiotic (e.g. wounding, drought, temperature extremes, salt concentration) and biotic (e.g. pathogens) stress (*59, 65, 66, 82-85*). These proteins function as relays between intracellular signal transducers such as calcium (stress signaling commonly results in an increased cytosolic Ca^{2+} concentration) and a comprehensive transcriptome response of the cell to stress (*65, 66, 82-84*). In this context, the CAMTA target sequence described above was found in many stress-responsive genes (*65-67, 82, 83*).

In contrast, the role of CAMTA proteins and the cellular processes controlled by these proteins in animals remain vague.

DmCAMTA1 is mainly expressed in photoreceptor cells where it functions as a important regulator of the visual process (*68*). As mentioned before, dmCAMTA stimulates the transcription of the F-box gene *dFbxl4* which leads to a deactivation of light-induced rhodopsin, a G-protein coupled photoreceptor (*68*). For this transcription regulation dimerization-induced nuclear localization of dmCAMTA (*69*) and Ca^{2+}-independent CaM-binding to dmCAMTA (*68*) are essential.

For mammalian CAMTA2 it was reported previously that it has an essential function during cardiac hypertrophy which describes the hypertrophic growth of heart muscle cells. Heart hypertrophy is caused for example by mechanical stress such as elevated blood pressure and calcium is an important intracellular transducer for this cellular stress (*86, 87*). Since murine and human CAMTA2 show a specific expression in cardiac myocytes of the adult heart (*61*), it appears to be likely that there is a calcium-dependent stress response mediated by CAMTA2 (maybe in similar way as observed in plants). Song *et al.* further demonstrated that CAMTA2 acts as a co-activator of the *NPPA* gene in cardiac myocytes (see also paragraph 1.5.1.) (*61*). This co-activation is blocked by HDAC5 (*61*), a member of class II histone deacetylases, which are known as negative regulators of cardiac hypertrophy (*87*). Thereby, HDAC5 directly interacts with the ankyrin repeats of CAMTA2 (*61*).

Mammalian CAMTA1 was found to be expressed mainly in the fetal heart and in the central nervous system, in particular in the brain (*61, 88-91*). During development of the murine brain, CAMTA1 is expressed ubiquitously, whereas later in development the expression is constricted to the cerebellum, hippocampi, and the olfactory bulbs (*91*). The cerebellum is important for motor coordination. Interestingly, it was reported before that heterozygous intragenic aberrations of the human *CAMTA1* gene were associated with ataxia and in some cases with intellectual disability (*91, 92*). These aberrations concern exclusively the 5'-end of the CAMTA1 locus and are characterized by deletions of certain exons of which most are involved in coding for the CG-1 DNA-binding domain (*91, 92*). The described deletions lead either to frame shift mutations, and therefore to an early translation termination, or to non-functional protein (*91, 92*). These findings are in line with a study recently published by Long *et al.*, which describes

an ataxic phenotype observed for a neural-specific CAMTA1 knockout in mice (*70*). This phenotype was caused by a significant degeneration of Purkinje Cells in the cerebellum of CAMTA1-knockout mice. Since the organization of the cerebellum was normal in these mice, Long *et al.* concluded that CAMTA1 is less important for a proper development of the cerebellum but rather for the maintenance of cerebellar neurons (*70*). Moreover, Long *et al.* used microarray analysis to investigate which genes are de-regulated as a result of the CAMTA1 knockout. Among the down-regulated genes in CAMTA1-knockout mice are *Snhg11*, *fbxl3a*, and *Gtl2*. These genes contain the mammalian DNA-binding site for CAMTA proteins (*70*). The F-box gene *fbxl3a* is involved in protein degradation. The function of *Snhg11* is still unknown but it shows a high expression level in Purkinje cells (*70*). *Gtl2* encodes for a long non-coding RNA reported previously to act as a tumor suppressor (*93*). This might be of particular importance since CAMTA1 has also a function as a tumor suppressor (see paragraph 1.4.2.).

A further function suggested for mammalian CAMTA1 is a role in episodic memory performance. CAMTA1 expression is increased in memory-related human brain regions and a poorer memory performance seems to be associated with single nucleotide polymorphisms within the *CAMTA1* allele (*90*).

Summing up, CAMTA1 seems be an important factor for normal function of the mammalian brain, in particular for a proper motor coordination. Furthermore, it was also reported before that it acts as tumor suppressor for neural tumors such as neuroblastoma and glioblastoma. This function will be described more closely in the next paragraph.

1.4.3. CAMTA1 acts as tumor suppressor in neural tumors

It was found that deletion located in the short arm of chromosome 1 is frequently associated with tumors originating from neural tissues such as neuroblastomas and glioblastomas (*89, 94-103*). This deletion is localized at position 1p36.3, which represents the genomic locus of CAMTA1 (*89, 95-97, 99-102*). Therefore, CAMTA1

was regarded as a potential tumor suppressor protein for neuroblastomas and glioblastomas for more than a decade. In 2006, it was shown for neuroblastoma patients carrying this specific deletion that a lower level of CAMTA1 expression correlates indeed with a poor prognosis for this tumor (*99*). Neuroblastomas originate from cells of the sympathetic nervous system and occur mainly during childhood (*101*). The above described 1p-deletion can be observed in about 30 % of all neuroblastomas and thereof mainly in high-malignant forms (*94, 97*). This corresponds to a significantly lower CAMTA1-expression in higher-stage neuroblastomas (*99*). A 2011 published study by Henrich *et al.* showed further that a constitutive overexpression of CAMTA1 in inducible neuroblastoma cell lines influenced the cell cycle significantly: The overexpression changed the cell population by decreasing the proportion of cells in the S-phase and increasing the proportion of cells in the G_1/G_0-phase (*104*). Moreover, this study demonstrated *in vitro* and *in vivo* an antiproliferative effect for overexpressed CAMTA1 (*104*). Increased CAMTA1 levels also cause induction of neural differentiation markers and, *vice versa*, an up-regulation of CAMTA1 was observed by Henrich *et al.* during neuroblastoma differentiation (*104*). Furthermore, microarray analyses conducted by this group revealed several genes which were de-regulated by CAMTA1 overexpression: In general, genes involved in differentiation and cell cycle inhibition showed up-regulation whereas genes promoting for example mitosis were down-regulated by CAMTA1 (*104*).

In gliomas the deletion of the 1p36-locus is often observed in oligodendrogliomas and is also associated with lower CAMTA1 expression (in an analogous manner as described for neuroblastomas): Oligodendrogliomas characterized by this deletion show a decrease of CAMTA1 expression of about 50 % compared to oligodendrogliomas without this deletion (*89*). However, the 1p36-deletion also occurs frequently in higher-grade gliomas such as glioblastomas (*103*). These glioblastomas often have hemizygous deletions at the CAMTA1-locus (*103*), which correlates with a lower CAMTA1-expression in glioblastomas compared to lower-grade gliomas such as astrocytomas (*102*). In 2011, Schraivogel *et al.* further supported the hypothesis that CAMTA1 is a tumor suppressor candidate for glioblastomas. As already mentioned in paragraph

1.3.2., CAMTA1 was identified as a potential target for miR-9/9*. Indeed, miR-9/9* predicted target sites in the 3'-UTR of the CAMTA1 mRNA were validated by Schraivogel *et al.* (*53*). Moreover, a CAMTA1 overexpression showed a tumor-suppressive effect *in vitro* and *in vivo*: The formation of neurosphere-like clones was significantly reduced by CAMTA1 overexpression in primary glioblastoma cells and the $CD133^+$ cell population was also decreased drastically (*53*). An overexpression in these primary cells also led to a clear reduction of tumor growth when those cells were implanted in mouse brains (*53*). Interestingly, for the effect on primary glioblastoma cells the CG-1 DNA-binding domain of CAMTA1 is necessary since an overexpression of a CG-1 deletion mutant had no effect on these cells (*53*). As previously observed for CAMTA1 in neuroblastomas, an elevated CAMTA1 level correlates also here with patient survival: Patients with higher CAMTA1 levels survived significantly longer than patients with a normal or lower CAMTA1 expression. Remarkably, a CAMTA1 overexpression in stable glioblastoma cell lines also distinctly resulted in elevated NPPA mRNA levels (*53*). Therefore, it seems likely that CAMTA1 acts as (co-)activator of the *NPPA* gene as previously reported for CAMTA2 in heart. Schraivogel *et al.* furthermore demonstrated a connection between up-regulated NPPA expression and patient survival whereupon patients with increased NPPA expression survived much longer (*53*).

1.5. Nkx2.2: A glioblastoma tumor suppressor candidate

1.5.1. The Nkx protein family: Transcription factors essential for development

Nkx2.2 belongs to a family of vertebrate transcription factors characterized by a highly conserved homeobox-binding domain (HD). These transcription factors are known for more than twenty years to be important factors for proper development of different tissues. Together with other Nkx proteins such as Nkx2.1 or Nkx2.5, Nkx2.2 constitutes in vertebrates the Nk-2 class of transcription factors, whose homologs were first identified in *Drosophila melanogaster (105, 106)*. In total, eleven Nk-2 class members are known and all of them show organ-specific expression patterns (*106*).

The HD of Nkx2.1, 2.2, and 2.5 binds to a DNA sequence (NK-response element, shortened NKE) which contains the core consensus sequence 5'-AAGTG-3' (Figure 1.6 C) and is highly conserved in mammals (*107-110*). For Nkx2.2, however, also an alternative core sequence (5'-GAGT-3') was postulated in 2011 (*111*). Besides the HD, Nk-2 class proteins feature other conserved domains: A transcriptional repression TN-domain which is located at the N-terminus, an Nk-2 specific domain (NK-2 SD), and a transcription activation domain (TAD) next to the C-terminus (see Figure 1.6 A) (*105, 110*). Thereby, the Nk-2 specific domain is thought to be an intrinsic repression domain for the TAD of the C-terminus due to its hydrophobic character (*110*). Moreover, it was suggested to function as interface for specific protein-protein interactions (*110*).

Regarding their function as key factors for the development of different organs, Nkx2.1, 2.2, and 2.5 belong to the best studied members of the Nk-2 class proteins. Nkx2.1 is known for its important role during lung development (*112-114*). Consistently, *Nkx2.1* knocked out mice die soon after birth from respiratory failure caused by malformed lungs (*112, 113*). Nkx2.1 was also linked to lung cancer biology: In several studies Nkx2.1 was reported both as suppressor of malignant progression and as oncogene promoting lung adenocarcinomas. The two-sided function of Nkx proteins is discussed more closely in paragraph 3.2.3.

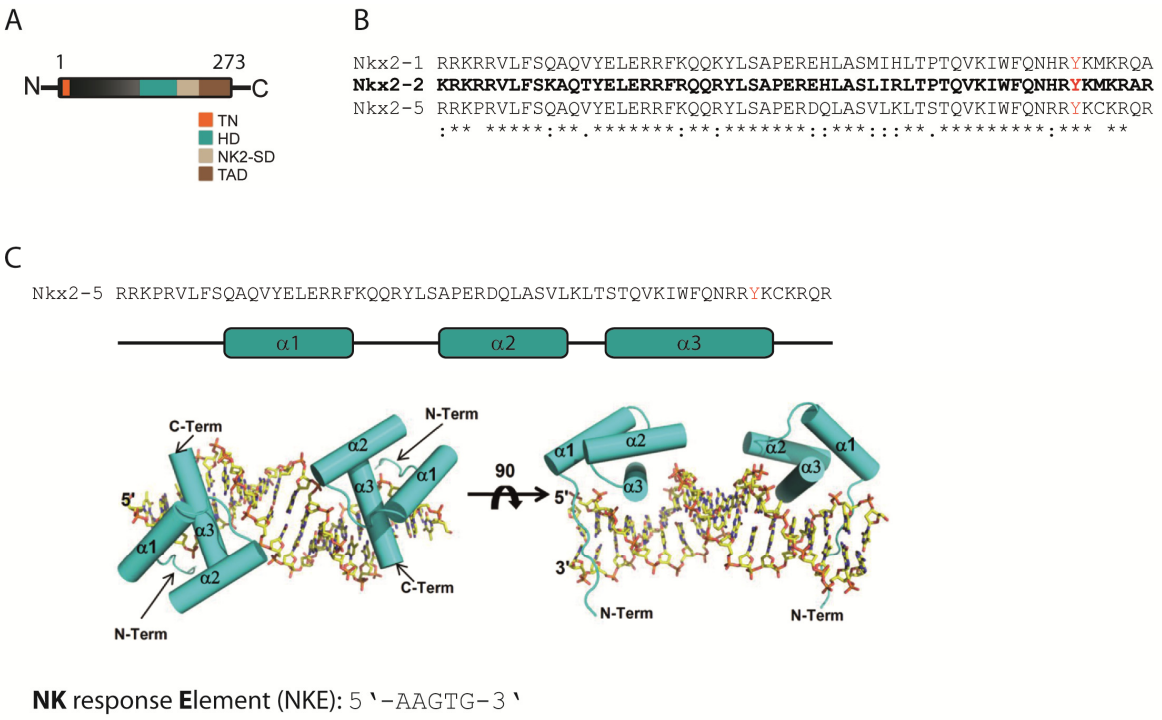

Figure 1.6: Nk-2 class of homeobox-binding domain containing transcription factors. A: Nkx2.2 with its Nk-2 class-typical domains (highlighted in different colors): Transcriptional repression domain (TN), homeobox-binding domain (HD), Nk2-specific domain (NK2-SD), and transcription activation domain (TAD). [(Illustration based on structural information available at http://www.uniprot.org/ for human Nkx2.2 (O95096)]. **B:** The HD of the Nk-2 class members Nkx2.1, Nk2.2, and Nkx2.5 is highly conserved. Sequence alignment was performed using ClustalW2 (http://www.ebi.ac.uk/). **C:** Structure of the Nkx2.5 HD. The domain consists of three α-helices of which α3 mediates specific interactions with the NK response element (NKE). Within α3 a specific tyrosine (Y191 for Nkx2.5; highlighted in red in **B** and **C**) is essential for NKE recognition. Adopted from (*115*).

Nkx2.2 is essential for neural development, in particular for glia cell maturation, which is highlighted in the next paragraph (see 1.5.2.).

The crucial role of Nkx2.5 in heart development and maintenance of a normal heart function was extensively investigated in several studies before (*109, 116-123*). In this context, it was shown previously that a homozygous knockout of *Nkx2.5* in mouse is embryonic lethal, because heart development is severely impaired (*117, 118*). As a transcriptional target for Nkx2.5, *NPPA* was identified already twenty years ago (*108, 109*). Nkx2.5 stimulates its expression via binding to the NKE sites in the *NPPA* promoter (*108, 109, 115*). NPPA in turn is the precursor of ANP, a secreted peptide

and a marker for cardiomyocyte differentiation (*124*). For the stimulation of the NPPA promoter, a member of the GATA family of transcription factors, GATA-4, was identified as an Nkx2.5 interaction partner during the maturation of cardiomyocytes (*109, 123*). Another co-inducer of *NPPA,* which can also interact with Nkx2.5, is the T-box transcription factor Tbx5 *(119, 120)*.

As already mentioned in paragraph 1.4.2., CAMTA2 is also a co-activator of *NPPA* during cardiac hypertrophy. In this context, it was shown by Song *et al.* that CAMTA2 directly interacts with Nkx2.5 to stimulate the *NPPA* promoter (*61*). This interaction is mainly mediated by the CG-1 domain of CAMTA2 and the HD of Nkx2.5 (*61*). It is believed that these two transcription factors interact to promote cardiac hypertrophy as response to cellular stress.

Recently, the binding of the Nkx2.5 HD to the NKE site of its target *NPPA* was structurally resolved: Nkx2.5 binds as a homodimer to palindromically arranged NKE sites in the *NPPA* promoter (*115*). The HD itself consists of three α-helices connected by a loop (Figure 1.6 C). Thereby, helix α3 facilitates the majority of the HD-DNA interactions (*115*). The other helices seem to be important for the stability of the entire domain (*115*). Within helix α3, several residues are important for DNA-binding, but only a single tyrosine (Y191) is essential for the sequence-specific interaction (*115*). Consistently, a mutation of this residue (Y191C) is frequently associated with human heart diseases (*125*). Furthermore, this tyrosine is highly conserved among other Nk-2 members, as illustrated in Figure 1.6 B.

1.5.2. Nkx2.2 is important for neural development and a potential tumor suppressor protein

The proper development of the central nervous system with its different classes of neurons and glia cells is very complex and requires a widespread, very accurately regulated network of signaling that turns certain transcription factors on or off at a precise time point and region during maturation of the different cell types.

In this context, Nkx2.2 has an essential function for the differentiation of oligodendrocyte progenitor cells, which is best studied for the development of the mouse and chicken spinal cord (*126-133*). During dorsal-ventral pattering of the neural tube, Nkx2.2 expression emerges in a defined ventral region of the ventricular zone as a response to Sonic Hedgehog (SHH) signaling (*126, 127*). Together with its adjacent region which is characterized by the expression of the oligodendrocyte precursor-specific factor Olig2, this most ventral region is the major region for oligodendrocyte linage determination in the developing spinal cord (*132*). Nkx2.2 and Olig2 collaborate to activate the final maturation program during late oligodendrocyte development (*131, 132, 134*). In this regard, Nkx2.2 expression is inducible by Olig2 and Nkx2.2 also becomes a co-inducer of Olig2 during later maturation (*131, 134*), each probably in an indirect manner since both proteins are thought to act as transcriptional repressors during oligodendrocyte maturation (*131*).

Nkx2.2 also prevents the premature expression of the myelin basic protein (MBP) gene by binding directly to the *MBP* promoter and by association with a repressor complex that includes histone deacetylase 1 (HDAC1) (*135*). On the other hand, Nkx2.2 is also able to induce the gene of the proteolipid protein (PLP) (*129, 132*). Both, MBP and PLP, are essential proteins for the formation of myelin sheaths by the mature oligodendrocytes. By a similar mechanism as shown for MBP, via recruiting HDAC1, Nkx2.2 negatively affects expression of Sirt2, a protein which belongs to the Sirtuin class III deacetylases (*136*). Sirt2 is another important factor during oligodendrocyte maturation since it associates with myelin (*137, 138*). Recently, it was also shown that Nkx2.2 represses *Pdgfra* via direct binding to its promoter (*133*). *Pdgfra* (Pdgf receptor α) and Pdgf signaling via its receptor is important for early oligodendrocytes lineage determination and an interruption of *Pdgfra* leads to a premature differentiation of the oligodendrocyte precursors (*139, 140*). After terminal differentiation, Nkx2.2 is down-regulated in oligodendrocytes (*128, 135*).

Besides its function in oligodendrocytes development in the spinal cord and in the brain (*128, 129*), Nkx2.2 is also essential for the generation of v3 interneurons in the spinal cord and serotonergic neurons in the developing hindbrain (*126, 127, 141*).

In 2010, it was furthermore reported that Nkx2.2 acts as a tumor suppressor for glioblastomas. For this study, Muraguchi *et al.* generated a transgenic mouse, which develops glioblastomas characterized by a human phenotype (*142*). These tumors showed only a weak Nkx2.2 expression (*142*). Moreover, an overexpression of Nkx2.2 in cancer stem cells of these tumors and in primary human glioblastoma cells negatively affected their ability for self-renewal as it led to a significant reduction of neurosphere-like colonies (*142*). The overexpression in isolated glioblastoma cells from the introduced mouse model also resulted in a drastic decrease of Nestin and, consistently, in an elevation of mature oligodendrocytes markers such as NG2 (*142*). In addition, Muraguchi *et al.* also demonstrated a tumor suppressive effect of Nkx2.2 *in vivo (142)*.
Taken together, the findings by Muraguchi *et al.* turn the important developmental transcription factor Nkx2.2 to a interesting tumor suppressor candidate in glioblastoma biology. A de-regulation of this factor could be important for progression of this type of brain cancer.

1.6. Aims and working model for this thesis

The putative transcription factor CAMTA1 acts as a tumor suppressor for glioblastomas as well as for neuroblastomas. However, the exact mechanisms of how this protein carries out this function remains largely unknown.

Hence, it was the aim of this thesis to characterize CAMTA1 in detail and to gain insight into which cellular network CAMTA1 is involved in to promote its tumor suppressive function. To achieve this, it was intended to establish tools for a functional characterization of CAMTA1, including antibodies or siRNAs. With these tools it should be further possible to examine which genes are regulated by CAMTA1 and which other proteins it interacts with.

Based on previous findings about CAMTA proteins, a working model was developed for this thesis. As mentioned before, mammalian CAMTA2 interacts with Nkx2.5 in the heart to stimulate the expression of NPPA. Hence, it was assumed that a similar interaction might take place in neural cells between CAMTA1 and Nkx2.2. Moreover, both CAMTA1 and Nkx2.2 repress self-renewal and differentiation of glioblastoma CSCs. Therefore, one could speculate that these two proteins act in concert to suppress tumor formation and that a de-regulation of one or both proteins promotes glioblastoma progression. As mentioned before, CAMTA1 overexpression causes a significant elevation of *NPPA* mRNA levels. Remarkably, for the peptide hormone ANP (which arises from the precursor NPPA) an antiproliferative effect on glioblastoma cells was reported before (*143*) and, furthermore, NPPA expression correlates with survival of glioblastoma patients (*53*). Thus, it is likely that CAMTA1 and Nkx2.2 might interact to stimulate NPPA expression, which finally causes a tumor suppressive effect. This working model is illustrated in Figure 1.7.

Besides the investigation of a potential interaction between CAMTA1 and Nkx2.2, it was further intended to examine upstream and downstream pathways involving Nkx2.2 in the context of glioblastoma biology.

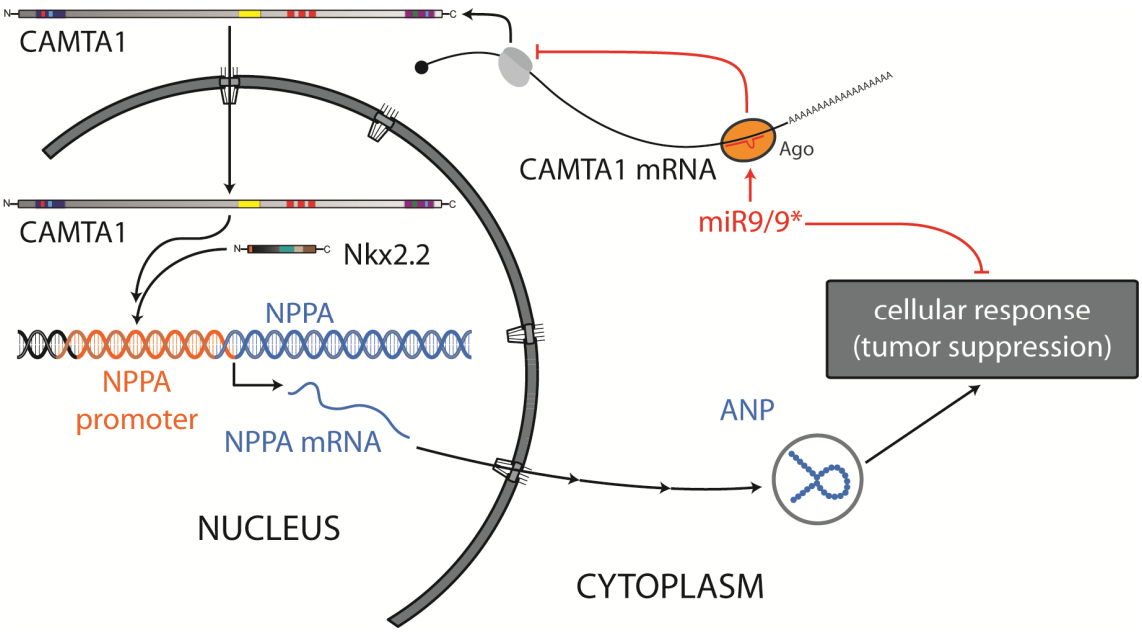

Figure 1.7: Working model for this thesis. It is hypothesized that in the mammalian brain CAMTA1 acts in concert with Nkx2.2 to stimulate the promoter of *NPPA* (in a similar manner as CAMTA2 and Nkx2.5 interacts in cardiac myocytes). The expression of NPPA, which is the precursor of ANP, would in turn cause tumor suppression. Furthermore, de-regulated miR-9/9* would probably counteract this mechanism in glioblastoma CSCs by targeting the CAMTA1 mRNA. It is assumed, that this maintains the stem cells character of these CSCs and promotes glioblastoma progression.

2. Results

2.1. Characterization of CAMTA1

CAMTA1 is a putative transcription factor, however less is known about its potential target genes and/or interaction partners. Therefore, in order to characterize the cellular function of CAMTA1, the generation and establishment of tools such as siRNAs and antibodies are essential. This is described in the following first two paragraphs of this chapter.

2.1.1. Establishing of efficient CAMTA1 knockdown strategies

SiRNA-mediated gene silencing provides a very effective tool to characterize proteins of interest in terms of their cellular functions. For the knockdown of CAMTA1, five siRNA oligonucleotides were designed. Each of these siRNAs targets a different exon and the target sites are distributed over the whole major CAMTA1 transcript, which encodes for the full-length CAMTA1 protein (Figure 2.1 A). Besides this major transcript, alternative transcripts with unknown function are predicted (illustrated in blue in Figure 2.1 A). In theory, all generated CAMTA1 siRNAs should also target these alternative transcripts except of siRNA4 with its target site in exon nine that is included only in the largest transcript.

The efficiency of the generated siRNAs for CAMTA1 knockdowns was tested via qRT-PCR (Figure 2.1 B). Three different primer pairs were used to quantify the CAMTA1 mRNA levels. All primer pairs were designed to span exon-intron junctions. Primer pair 1 (CAMTA1 p1) spans exon three to five, CAMTA p2 exon three to four, and CAMTA1 p3 exon 20 to 21. Therefore, CAMTA1 p1 and p2 should only generate

their specific amplicon only from the major CAMTA1 transcript since exon four and five are exclusively found in the main transcript. As shown in Figure 2.1 B for a CAMTA1 knockdown in primary R11 glioblastoma cells, basically all siRNAs led to a decreased mRNA level of CAMTA1 (compared to the control siRNA). Notably, the highest knockdown efficiencies were observed for siRNA1 and siRNA2.

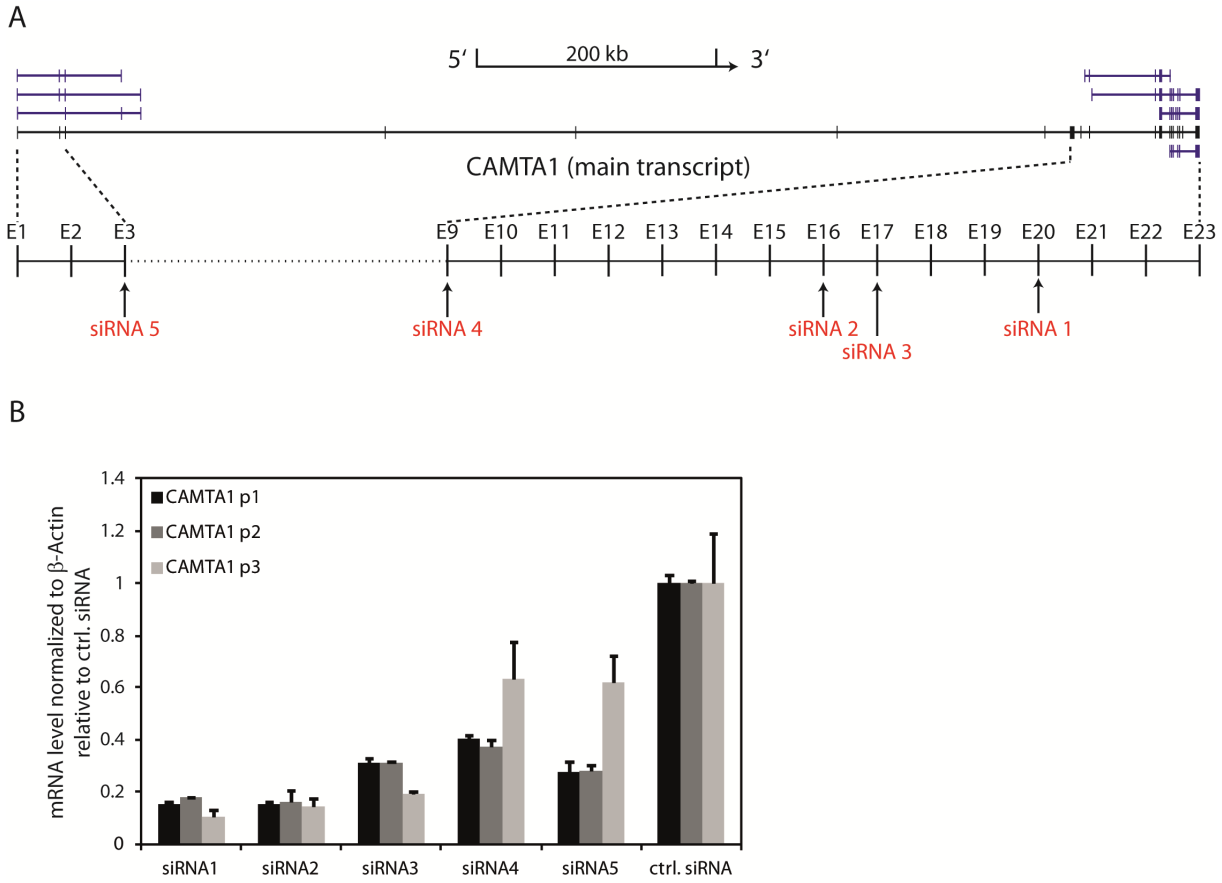

Figure 2.1: Genomic locus of CAMTA1 and siRNAs against CAMTA1. A: Schematic illustration of the CAMTA1 locus (1p36.31 - 1p36.23). Vertical lines represent exons (E). The main transcript (coding for the complete CAMTA1 protein) is depicted in black, alternative transcripts are highlighted in blue. The particular exons targeted by the generated siRNAs are shown below. The illustration was drawn according to the genomic information available at the UCSC genome browser (http://genome.ucsc.edu/). **B:** Testing the functionality of the CAMTA1 siRNAs. Primary R11 glioblastoma cells were transfected with the respective siRNAs [siRNA1 to 5 and control siRNA (ctrl. siRNA)]. Total RNA extraction and cDNA synthesis were performed four days after transfection. The efficiency of the particular knockdowns was validated via qRT-PCR using three different CAMTA1 primer pairs (p1, p2, and p3). SiRNA1 and siRNA2 showed the strongest knockdown of CAMTA1.

2.1.2. Polyclonal antibodies against CAMTA1

Besides siRNAs, specific antibodies are also highly valuable tools to characterize the function of CAMTA1. Two polyclonal rabbit antibody sera against human CAMTA1 were already available at the beginning of this thesis, named as "anti-CAMTA1 1886" and "anti-CAMTA1 1901" serum (shortened referred to as "1886" and "1901" in the following paragraphs). In order to test their functionality for detection of endogenous CAMTA1 in western blots, total protein lysates of the knockdown depicted in Figure 2.1 B (see previous paragraph) were used. Both antibodies recognize bands with a molecular weight around 180 kDa (the theoretical weight for CAMTA1). Thereby, the band with the strongest signal intensity detected by the 1886 antibody ran slightly lower and the major band revealed by the 1901 antibody was slightly bigger than 180 kDa (Figure 2.2). However, for both antibodies, the signal intensities of these bands were unchanged in all lysate samples, including CAMTA1 knockdown samples. Therefore, it is questionable if these antibodies can indeed detect endogenous CAMTA1 in western blot. Alternatively, CAMTA1 might be highly stable and CAMTA1 mRNA changes might not impact immediately its cellular protein level (discussed in paragraph 3.1.2.).

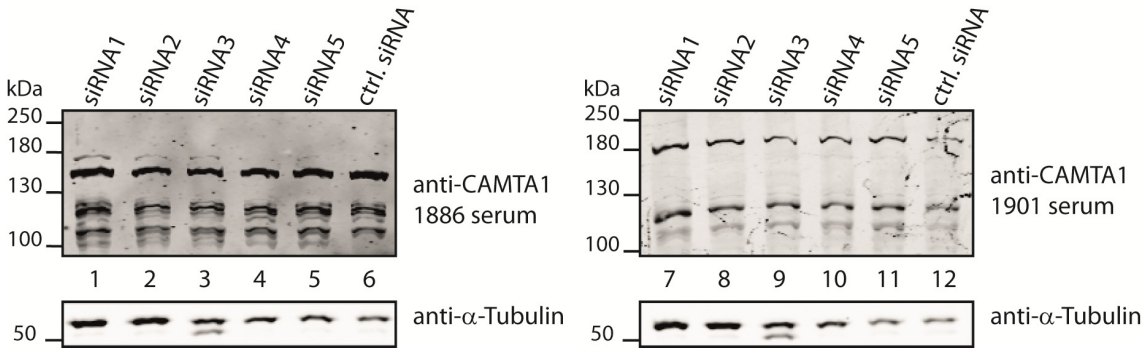

Figure 2.2: Testing the CAMTA1 antibodies 1886 and 1901 for their functionality to detect endogenous CAMTA1 in western blots. Protein samples of the CAMTA1 knockdowns shown in Figure 2.1 were used for western blot analysis. Of each particular knockdown (siRNA1 to 5) and knockdown control (ctrl.), 100 µg total protein lysate was loaded for each western blot [equal loading was controlled by western blot against α-Tubulin (lower panels)]. The respective detection pattern of both antibodies was basically unchanged for each of the individual knockdown samples.

Since it was not sure, whether the detected bands represent indeed endogenous CAMTA1, the antibodies 1886 and 1901 were tested for detection of overexpressed CAMTA1 with an N-terminally myc-tag CAMTA1 (mycCAMTA1). For this purpose, mycCAMTA1 was overexpressed in HEK293-T cells and subsequently knocked down by using siRNAs 1, 2, and 3 after 48 hours of overexpression. After further cultivation of again 48 hours, cells were harvested and split for total RNA extraction in order to validate the knockdown on the mRNA level (Figure 2.3 D) and for total protein lysates subsequently used for western blot analysis. The detection patterns of the CAMTA1 antibodies were observed and compared to an anti-myc antibody. This antibody detected mainly two bands: One band bigger than 250 kDa and a second band running slightly lower than 180 kDa. Since the signal intensity of both bands was clearly reduced by the used CAMTA1 siRNAs, it can be assumed that both bands were indeed mycCAMTA1 (Figure 2.3 C). The same bands were also detected by the 1886 and 1901 antibody (Figure 2.3 A and B), but with different signal intensities. Nonetheless, this leads to the conclusion that both antibodies can in principle detect myc-tagged CAMTA1. However, both antibodies also visualized prominent protein bands which ran different than mycCAMTA1 and were also present in the empty vector control: The 1886 antibody detected a band between 130 and 180 kDa, whereas 1901 showed a band with a strong signal running slightly bigger than 180 kDa. These bands were also detected in the western blots with CAMTA1 knockdown samples (Figure 2.2). Consistent with these western blots, the intensities of the bands detected around 180 kDa were here also not affected by the CAMTA1 siRNAs (Figure 2.3 A and B). Hence, the identities of these bands are indistinct.

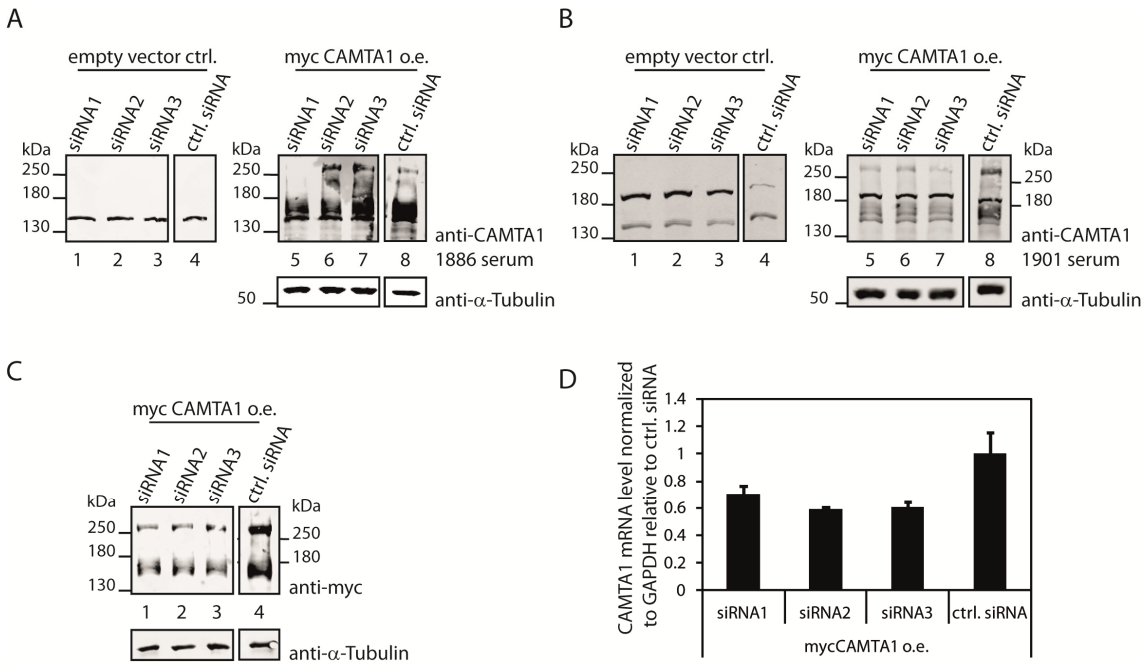

Figure 2.3: The CAMTA1 antibodies 1886 and 1901 can both detect overexpressed mycCAMTA1. Overexpressed (o.e.) mycCAMTA1 (in HEK293-T cells) was knocked down with the indicated CAMTA1 siRNAs or control siRNA (ctrl. siRNA) after 48 hours overexpression. Total RNA extraction for qRT-PCR validation and lysis for western blot analyses were performed 48 hours after siRNA transfection. For the western blot analysis 80 µg of each protein lysate was loaded (equal loading for the mycCAMTA1 knockdown samples was controlled by western blots for α-Tubulin). Both antibodies (**A:** 1886, **B:** 1901) were able to detect overexpressed mycCAMTA1 as the comparison with the western blot against the myc-tag (**C**) showed. **D:** Knockdown validation of mycCAMTA1 by qRT-PCR.

It was further tested if both sera can be used for anti-CAMTA1 immunoprecipitations (IPs). However, no clear enrichment of endogenous CAMTA1 was seen for IPs using these antibodies (data not shown).

Taken together, the utility of the two CAMTA antibodies 1886 and 1901 to characterize endogenous CAMTA1 via western blot analysis and/or IPs remains doubtful: Although both antibodies are at least able to detect overexpressed mycCAMTA1 in western blots, the identities of the most prominent protein bands detected around 180 kDa by these antibodies could not be clarified. Moreover, these antibodies showed also negative results for IPs of endogenous CAMTA1. For these reasons, a new set of antibodies against CAMTA1 was generated to further study the function of the endogenous protein.

The two CAMTA1 fragments (fragment 1 and 2) used as antigens for immunization of rabbits to produce the antibody sera 1886 and 1901 are schematically shown in Figure 2.4 A. For the generation of new polyclonal antibodies, a CAMTA1 fragment located in the linker region between the ankyrin repeats and the C-terminal IQ domain was used (fragment 3 in Figure 2.4 A). This fragment was N-terminally fused to GST for purification and stabilization ("GST-CAMTA1-F3"). Additionally, a TEV protease recognition site was introduced between GST and fragment 3. The GST-fragment 3 construct was recombinantly expressed in a Rosetta *Escherichia coli* strain. After determination of the optimal expression conditions (at 25°C for five hours), the fusion protein was purified in large scale (4 l culture volume) via fast protein liquid chromatography (Figure 2.4 B).

To get GST-CAMTA1-F3 as pure as possible for immunization, a subsequent anion exchange chromatography was necessary. Figure 2.4 B (right panel, lane 1) shows GST-CAMTA1-F3 after the final purification step. The purified GST-tagged peptide was used to immunize two rabbits for antibody production (Eurogentec, Liège, Belgium). This resulted in the generation of two additional anti-CAMTA1 antibody sera, termed as "anti-CAMTA1 SY6160" and "anti-CAMTA1 SY6161" (shortened referred to as "SY6160" and SY6161" in the following paragraphs).

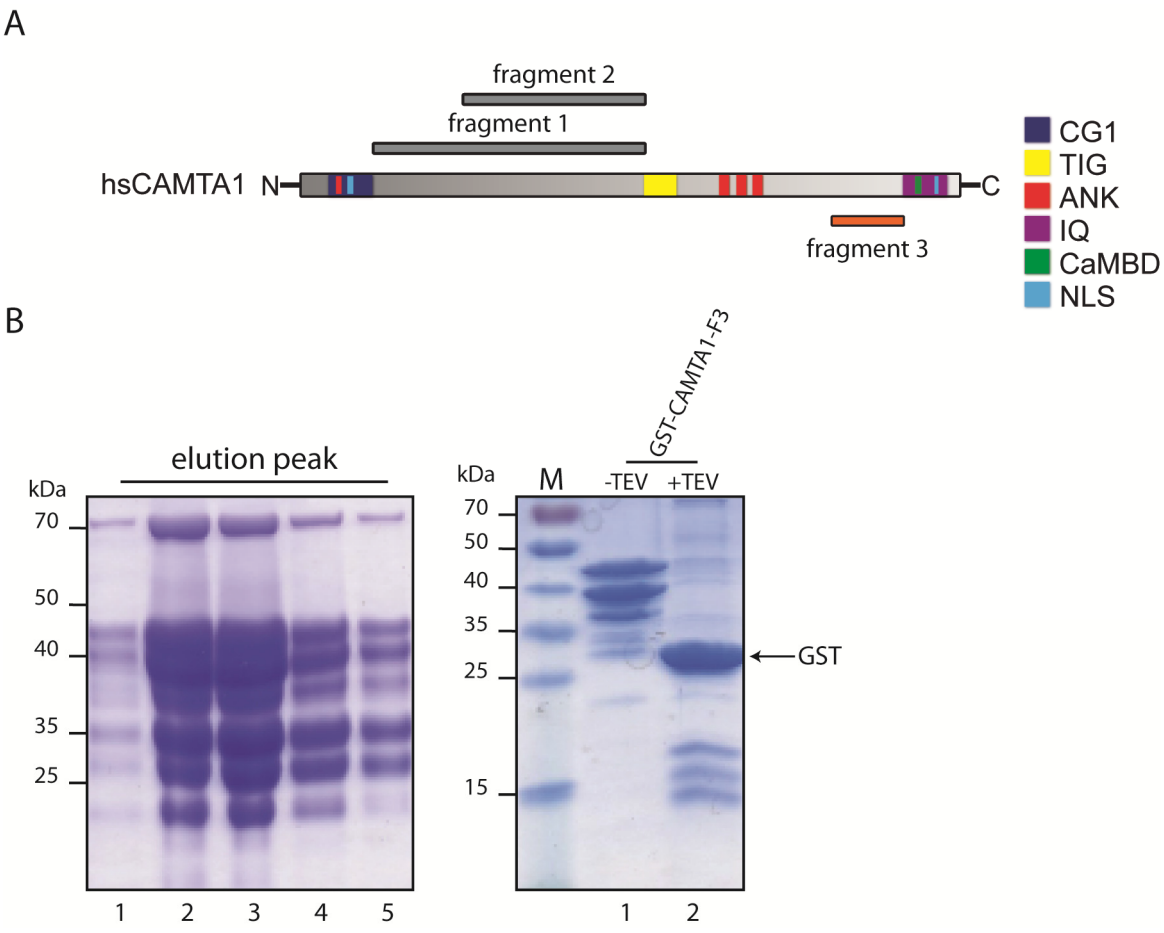

Figure 2.4: Generation of new CAMTA1 antibodies. A: Position of the particular fragments used for the production of antibodies within the CAMTA1 protein. Fragment 1 and 2 were used to generate the antibody sera 1886 and 1901. Fragment 3 was purified (as GST fusion protein) in this thesis to produce additional antibody sera. **B**: Purification of GST-CAMTA1-F3. Left panel: Elution peak of the glutathione Sepharose™ purification step (about 0.1 % of each fraction was loaded on a 15 % PA gel). Right panel: GST-CAMTA1-F3 after final purification via anion exchange chromatography (15 % PA gel). Purity was controlled by cleaving off the GST-tag by TEV protease (about 10 µg of the purified protein was used for TEV cleavage).

These new sera were first tested for their functionality in western blots using different mycCAMTA1 constructs overexpressed in HEK293-T cells (Figure 2.5 A). These constructs represent truncated versions of the CAMTA1 wildtype protein. In the case of the CAMTA1 ΔN construct, the N-terminus (including the CG1 domain) is completely deleted. The other constructs are depicted schematically in Figure 2.15 A (see page 47). As clearly shown in Figure 2.5 A, both new antibody sera detected the mycCAMTA1 constructs except of mycCAMTA1 ΔC, which lacks the entire C-

terminus (including the ankyrin repeats). This detection pattern is not surprising because the antigen used for the generation of the new sera is located in a region next to the C-terminus, which is not present in mycCAMTA1 ΔC.

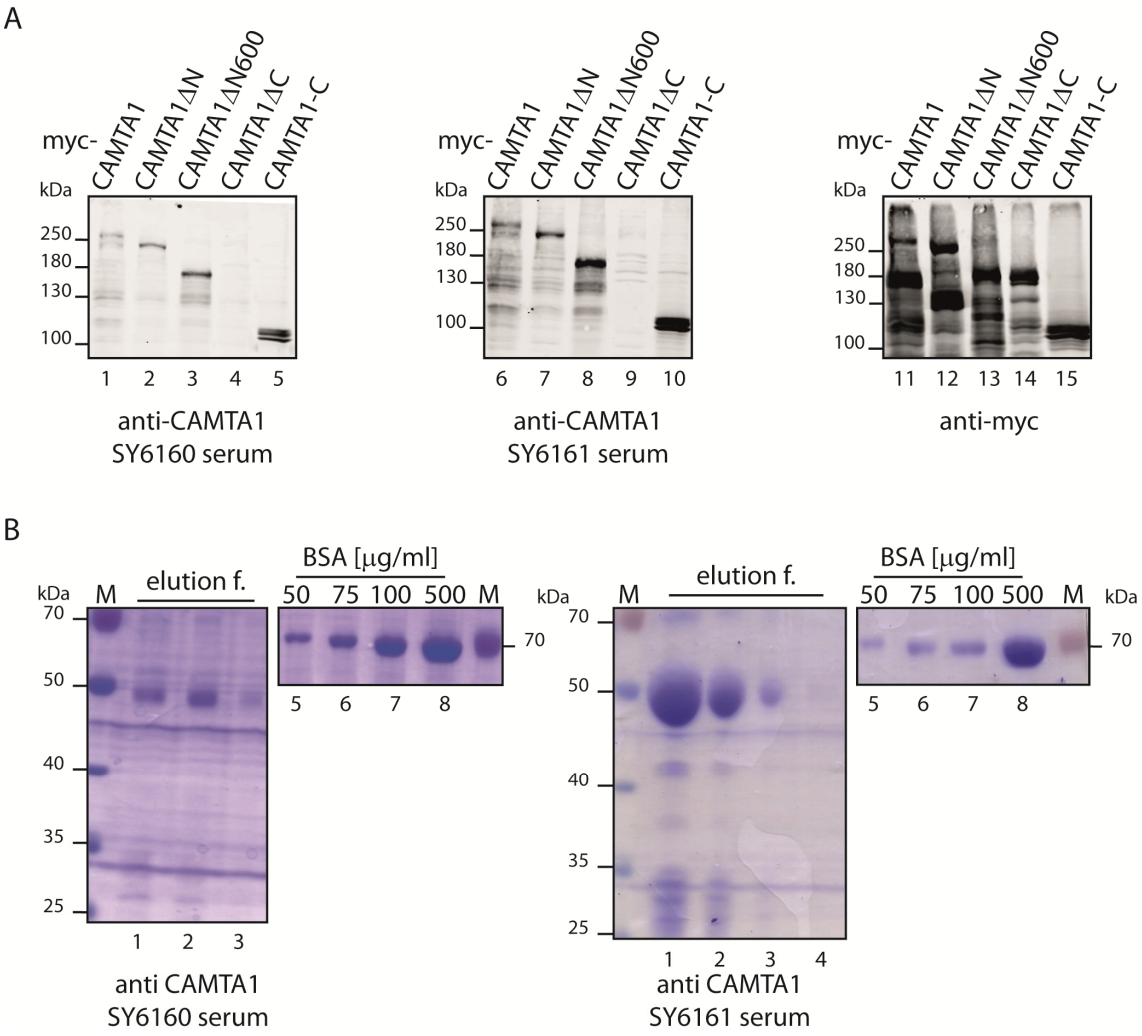

Figure 2.5: Testing and purifying the generated CAMTA1 antibody sera. A: Both antibody sera (SY6160 and SY6161) detected several mycCAMTA1 constructs (overexpressed in HEK293-T), but not mycCAMTA1ΔC, which lacks the antigen (about 2 % of each lysate was loaded for the western blots). **B:** Purification of the sera via affinity chromatography. About 1 % of each elution peak fraction (f.) was loaded. To estimate the particular concentrations of the purified antibodies, serial diluted BSA was also loaded (lanes 5 - 8). [Purification of SY6160 was carried out by Martina Tremmel (B.Sc.) under supervision of Ludwig Wankerl].

Since the two new sera indeed detect mycCAMTA1, these sera were further purified by affinity chromatography using the antigen GST-CAMTA1-F3 (Figure 2.5 B). The purified antibodies were then tested if they are capable to detect endogenous CAMTA1.

For this purpose, CAMTA1 was knocked down in stable T98G glioma cells using the efficient CAMTA1 siRNA 1 (transected twice with 48 hours of incubation in between) (Figure 2.6). Although the knockdown was efficient on mRNA level (Figure 2.6 B), the signal intensities of the bands detected by the two purified antibodies were in both cases not decreased in the knockdown sample (compared to the siRNA control sample). Notably, the purified SY6161 antibody detected in both the knockdown and the control sample a band running slightly higher than 180 kDa. This protein band probably matches with the most prominent band detected by the 1901 CAMTA1 antibody (see e.g. Figure 2.2). The possibility whether this band represents endogenous CAMTA1 is discussed in paragraph 3.1.2.

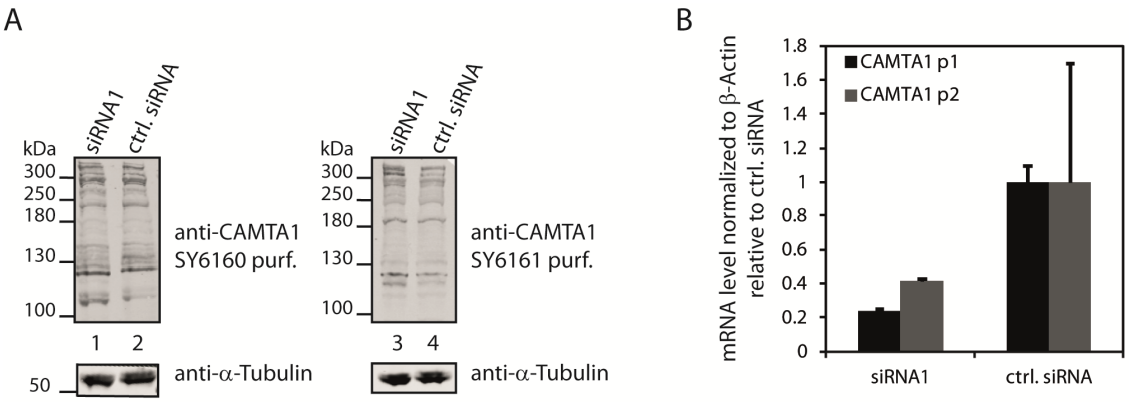

Figure 2.6: Testing the purified new CAMTA1 antibodies for their functionality to detect endogenous CAMTA1. Endogenous CAMTA1 was knocked down in T98G cells using CAMTA1 siRNA1 (transfected twice). **A:** Western blot analyses using the two purified (purf.) antibodies (100 µg of each protein lysate was loaded; equal loading controlled by western blots for α-Tubulin). The individual detection patterns of both antibodies were not affected by the knockdown. **B:** Knockdown validation via qRT-PCR.

Analogous to the antibody tests of the "old" sera (1886 and 1901), it was also examined if the new antibodies can be used to immunoprecipitate endogenous CAMTA1. For the IPs[3] total protein lysates of HEK293-T and stable T98G glioma cells were used. The western blot analysis of the IP eluates revealed that the purified CAMTA1 antibody SY6161 clearly precipitated a protein with the expected molecular weight of CAMTA1 from the HEK293-T as well as from the T98G lysate (Figure 2.7). Since this protein has the expected molecular weight and was not detected in the IP control with rabbit IgG, it can be assumed that the precipitated protein is indeed endogenous CAMTA1.

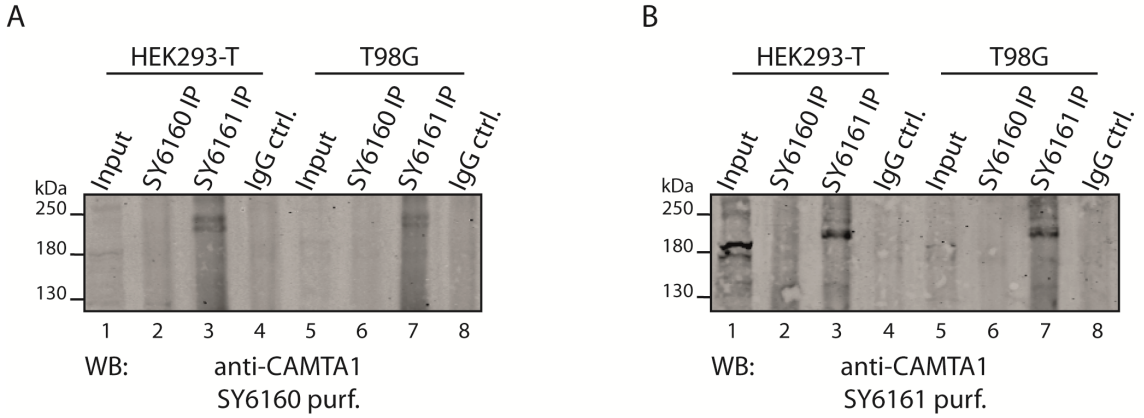

Figure 2.7: Immunoprecipitation of endogenous CAMTA1 from HEK293-T and T98G cells via the generated antibodies. The purified (purf.) antibody SY6161 precipitated CAMTA1 from HEK293-T and T98G total protein lysates. **A:** Western blot analysis of the IPs using the purified SY6160 antibody for CAMTA1 detection. For each IP, material form three 15-cm culture dishes were lysed (about 1 % IP-input and 50 % IP-eluate were loaded). **B:** Western blot result using the SY6161 CAMTA1 antibody (of each sample the same amount as in A was loaded).

[3] carried out by Martina Tremmel (B.Sc.) under supervision of Ludwig Wankerl

2.1.3. Localization of CAMTA1

The nuclear localization for atCAMTA1 (*59, 60*), dmCAMTA (*68*) as well as for mammalian CAMTA2 (*61*) was already shown previously. Hence, it was assumed that human CAMTA1 should also mainly be localized in the nucleus.

To investigate the subcellular localization of human CAMTA1, all polyclonal antibodies motioned in paragraph 2.1.2. were used for immunofluorescence (IF) staining of CAMTA1. A first screening using different cell lines (HEK293-T as well as the stable glioma cell lines LNT229 and T98G) revealed that for all antibodies the strongest signal intensity was observed in T98G cells (data not shown). Therefore, these cells were used to further examine the localization of CAMTA1 and to confirm that the observed signals indeed originate from endogenous CAMTA1. For this purpose, CAMTA1 was knocked down in these cells using CAMTA1 siRNA1 and siRNA2. The knockdown was also validated on mRNA level via qRT-PCR resulting in an approximately 50 % decrease of the CAMTA1 mRNA level for siRNA 1 (compared to the control siRNA). However, no knockdown was measured on mRNA level in the case of siRNA 2 (data not shown). In the IFs, the antibodies showed clearly different detection patterns. For the 1886 antibody a nuclear signal was detected, which was also decreased in the cells transfected with siRNA 1 (Figure 2.8). In contrast, the 1901 antibody caused a signal that was distributed over the whole cell (Figure 2.9, page 39). The intensity of this signal was not reduced in the siRNA1-knockdown cells. The antibodies SY6160 and SY6161 which were generated in this thesis show similar detection patterns: Here, the strongest signal was observed in a region adjacent to the nucleus. However, this signal was not changed by the knockdown [see Figure 2.10 (page 40) for SY6160 and Figure 2.11 (page 41) for SY6161]. Besides this signal, for both antibodies a faint nuclear signal was also observed, but it was difficult to determine if this signal is indeed reduced within the cells when CAMTA1 was knocked down.

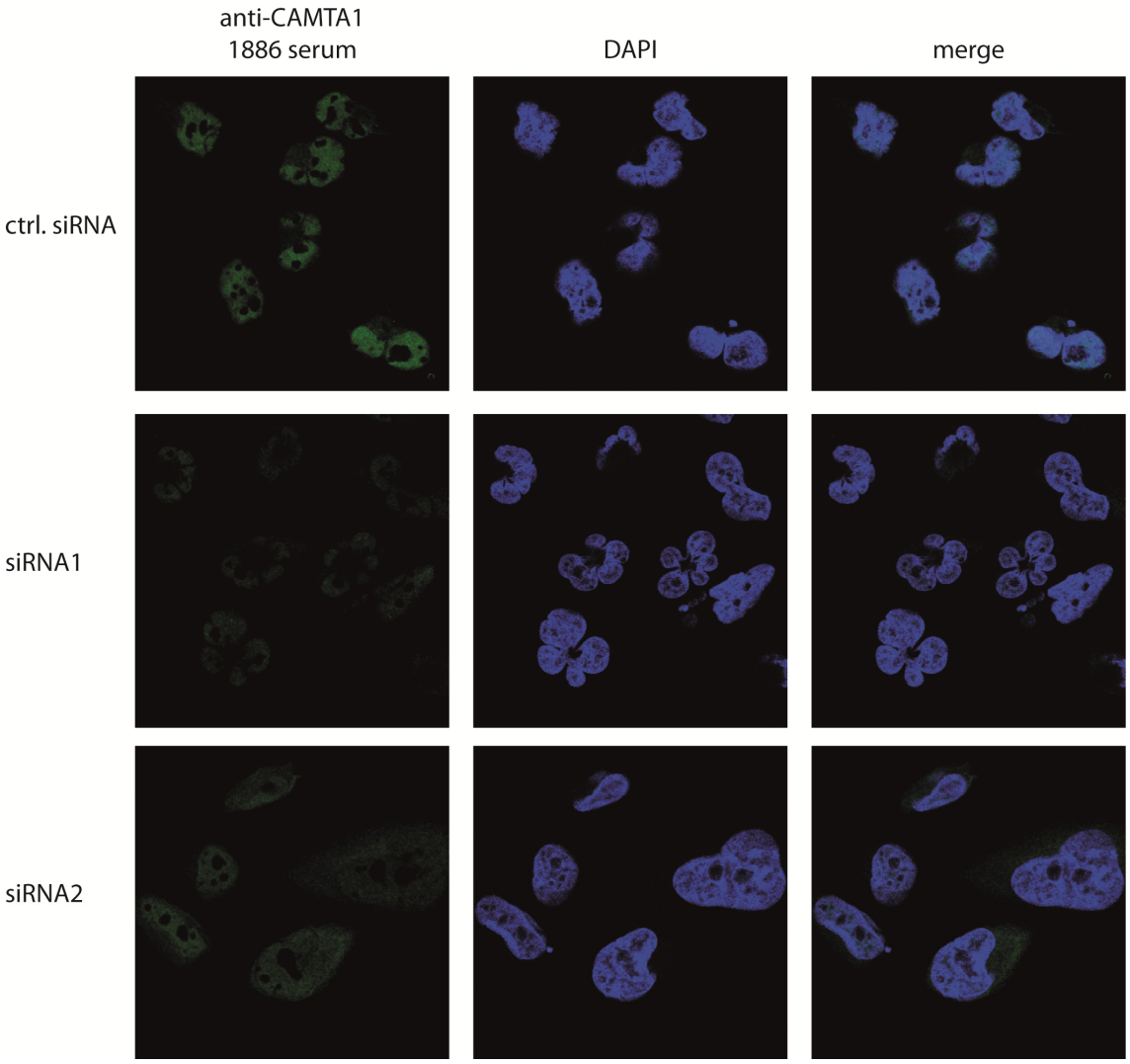

Figure 2.8: Immunofluorescence of endogenous and knocked down CAMTA1 using the 1886 antibody. Knockdown for subsequent IF was performed in T98G cells transfected twice with the indicated siRNAs. The 1886 antibody showed a clear nuclear signal which was decreased for CAMTA1 siRNA1 [for this knockdown also a reduction of CAMTA1 mRNA of approximately 50 % compared to control siRNA (ctrl. siRNA) was measured via qRT-PCR; data not shown].

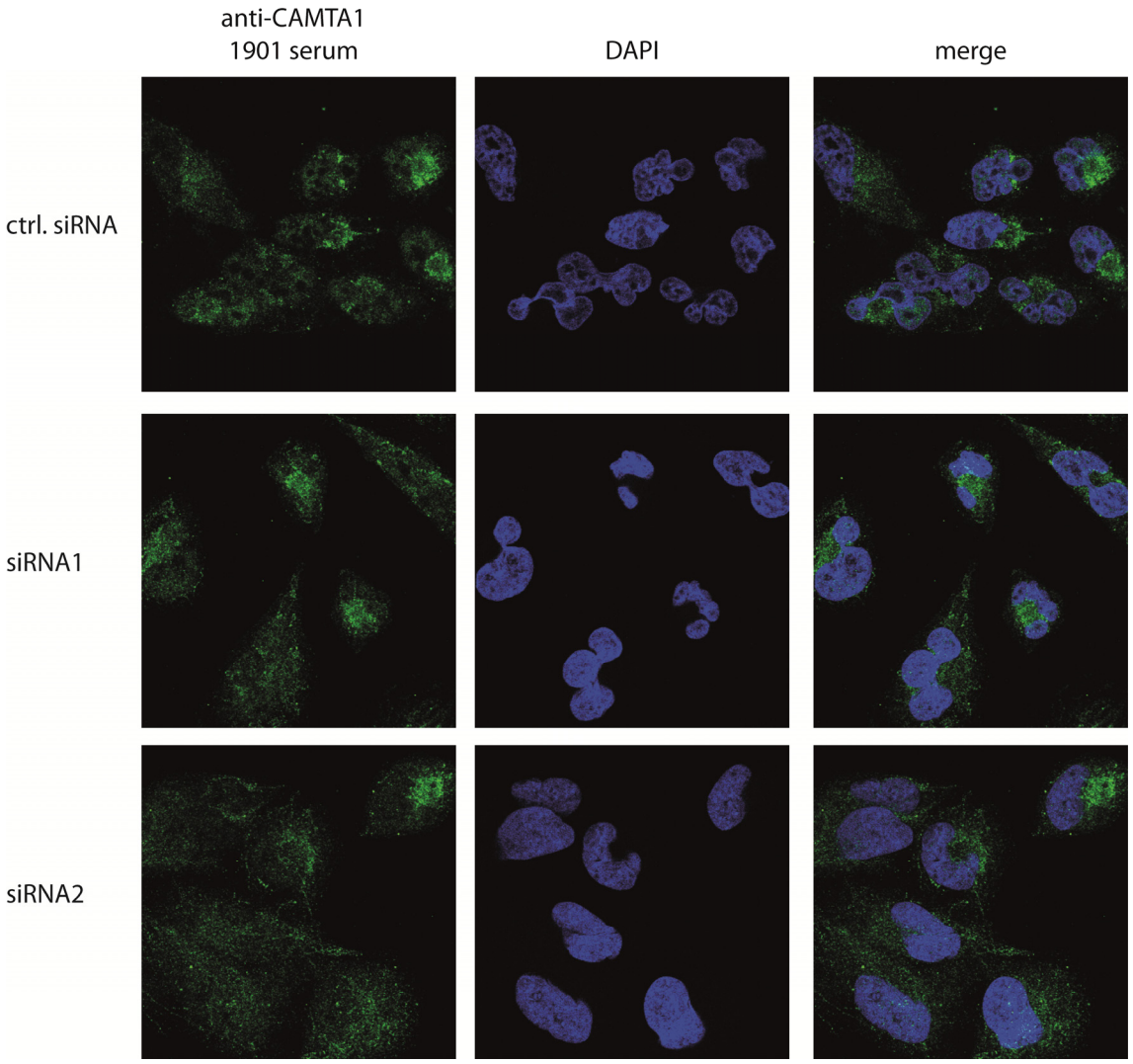

Figure 2.9: Immunofluorescence of endogenous and knocked down CAMTA1 using the 1901 antibody. This IF reflects the same CAMTA1 knockdown as depicted in Figure 2.8. In contrast to the 1886 antibody, the 1901 antibody showed no specific nuclear signal and also no signal decrease for CAMTA1 siRNA1-transfected cells.

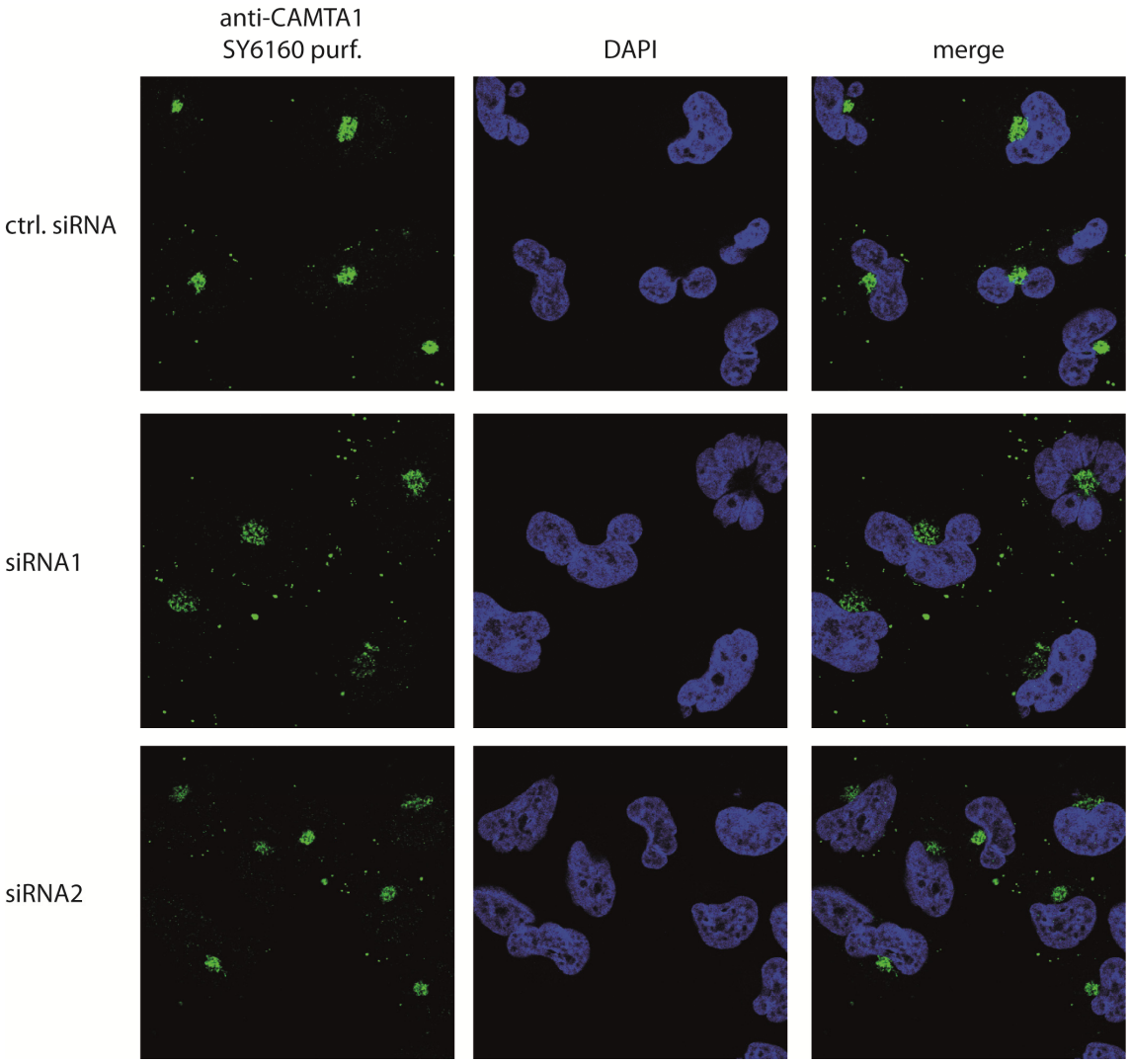

Figure 2.10: Immunofluorescence of endogenous and knocked down CAMTA1 using the purified SY6160 antibody. This IF reflects the same CAMTA1 knockdown as depicted in Figure 2.8. For this antibody, the strongest signal was observed close to nucleus, whereas the nuclear signal was only faint. However, basically no change of the signal intensities was observed for the CAMTA1-knockdown cells.

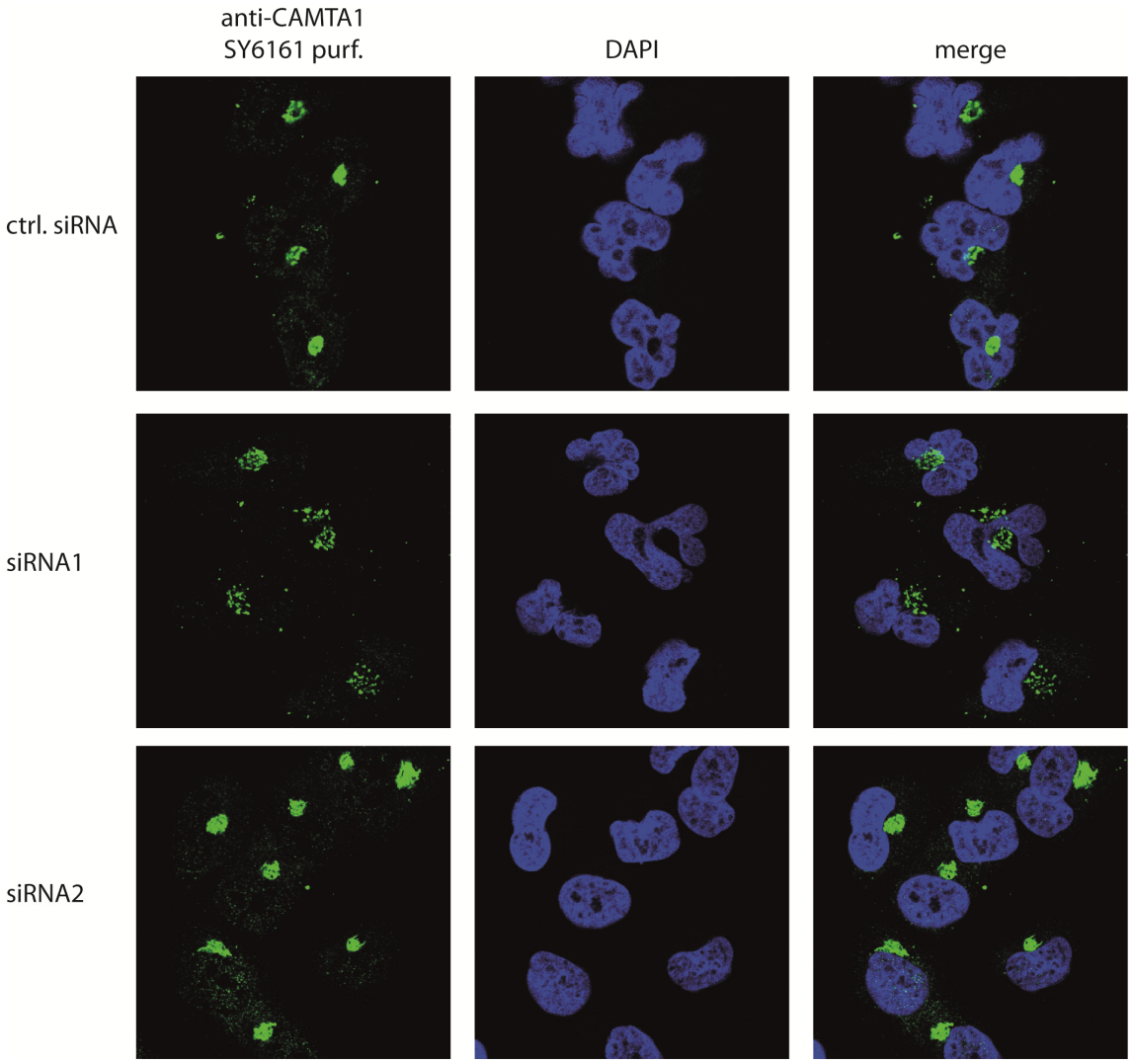

Figure 2.11: Immunofluorescence of endogenous and knocked down CAMTA1 using the purified SY6161 antibody. This IF reflects the same CAMTA1 knockdown as depicted in Figure 2.8. The SY6161 antibody had a similar detection pattern as the SY6160 antibody. However, the overall signal intensity observed was stronger compared to SY6160. Also for this antibody a (weak) nuclear signal was detected. This signal seemed to be reduced in siRNA1-knockdown cells.

It was also investigated if CAMTA1 shows nuclear localization in western blots using subcellular fractions. Therefore, nuclear extracts were prepared from HEK293-T and HeLa cells.

As before, the previously described CAMTA1 antibodies showed different detection patterns in western blots of cytoplasmic and nuclear fractions from HEK293-T cells (Figure 2.12). The 1886 antibody detected a band running at 180 kDa, which had the same intensity in cytoplasmic and nuclear fractions. In the nuclear fraction the most intense signal, however, was a double band slightly lower than 180 kDa. This double band was less intense in the cytoplasmic fraction (Figure 2.12 A, left panel, lane 1). In contrast, the band with the strongest signal visualized by the 1901 antibody (slightly bigger than 180 kDa) was equally intense in cytoplasmic and nuclear fractions (Figure 2.12 A, right panel). In the case of the SY6160 antibody, several bands appeared in the nuclear fraction. Among these, a band slightly bigger than 180 kDa was most intense and was detected with lower intensity in the cytoplasmic fraction (Figure 2.12 B, left panel, lane 1). The SY6161 antibody visualized a band around 180 kDa, which was equally strong in both fractions, similar to the detection pattern of the 1901 antibody (Figure 2.12 B, right panel). Additionally, this antibody detected also a band running a little bit lower than 180 kDa, that appeared exclusively in the nuclear fraction (Figure 2.12 B, right panel, lane 2).

The newly generated antibodies (SY6160 and SY6161) were also used in western blots with subcellular fractions of HeLa-S3 suspension culture cells. For the preparation of these fractions, the raw nuclear fraction was further purified resulting in a soluble and insoluble nuclear fraction. In case of the SY6160 antibody, several bands appeared (Figure 2.13 A, page 44). One band around 180 kDa was detected in the whole cell lysate (lane 1) as well as in the cytoplasmic (lanes 2 and 3) and nuclear fraction (lanes 4 and 5). Also a smaller band (between 130 and 180 kDa) was observed in the nuclear fraction (lanes 4 to 6), but not in the cytoplasmic fraction. The SY6161 antibody showed a similar result, however the detection pattern for this western seems to be more specific compared to the SY6160 antibody (Figure 2.13 B). Interestingly, the detected band running slightly lower than 180 kDa was observed within the nuclear fraction

mainly in the raw nuclear extract and in the sample containing the insoluble parts of the nucleus, but was not present in the cytoplasmic fraction (Figure 2.13 B).

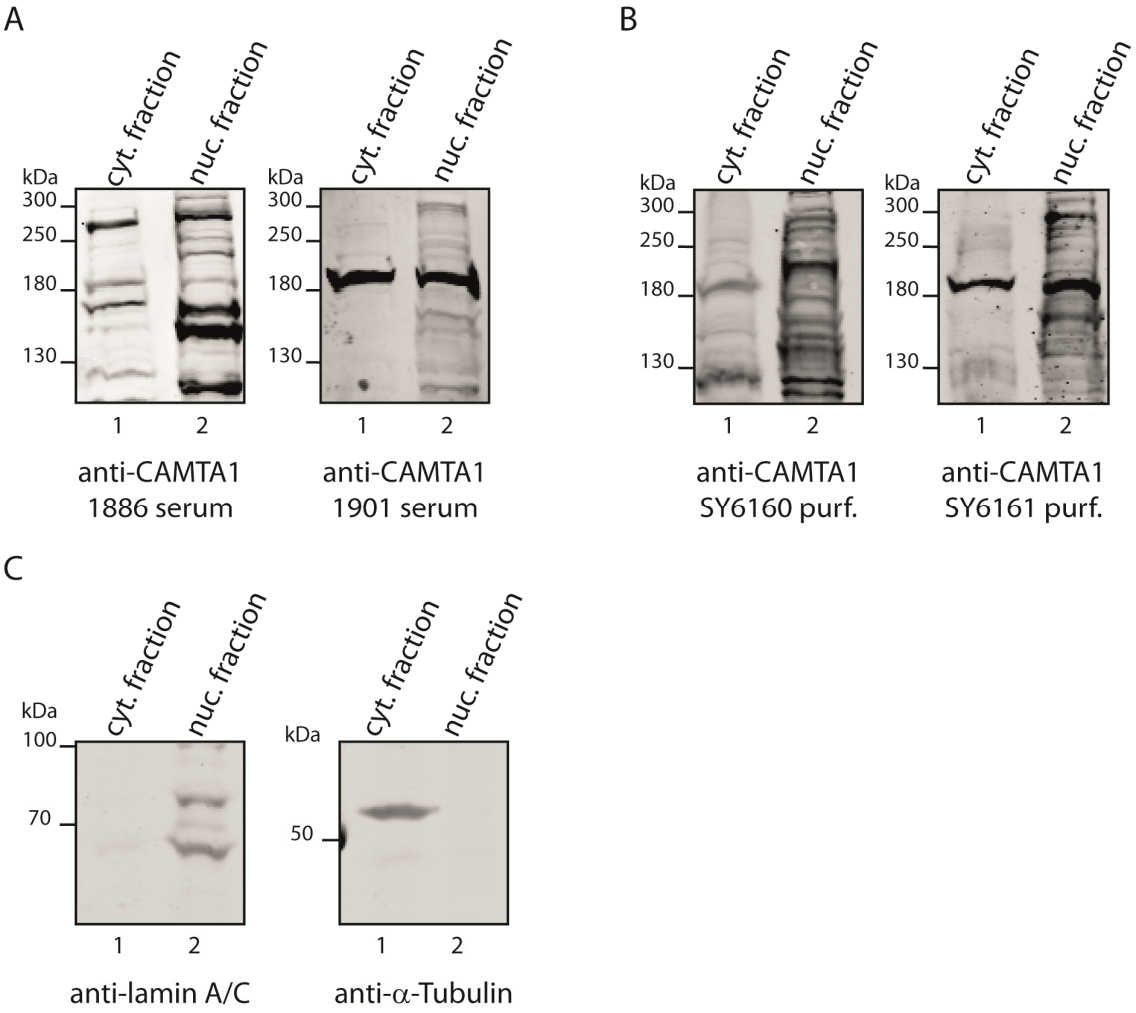

Figure 2.12: Subcellular fractionation of HEK293-T cells for CAMTA1 localization. For the fractionation, material form eight 15-cm cell culture dishes were lysed. Comparable amounts of cytoplasmic (cyt.) and nuclear fraction (nuc.) were loaded for the particular western blots. **A:** Western blot results using the CAMTA1 antibodies 1886 (left panel) and 1901 (right panel). The (double) band with strongest signal detected by the 1886 antibody ran slightly lower than 180 kDa and was more intense in the nuclear fraction. Using the 1901 antibody, a band running higher than 180 kDa was detected with high intensity (equal in both fractions). **B:** Western blot analyses with the new generated, purified (purf.) CAMTA1 antibodies. Multiple bands in cyt. and nuc. fractions were detected by the SY6160 antibody. In contrast, the SY6161 antibody showed a similar detection pattern as the 1901 antibody. **C:** Purity of the cyt. and nuc. fraction was controlled by western blots for lamin A/C (left panel) and α-Tubulin (right panel).

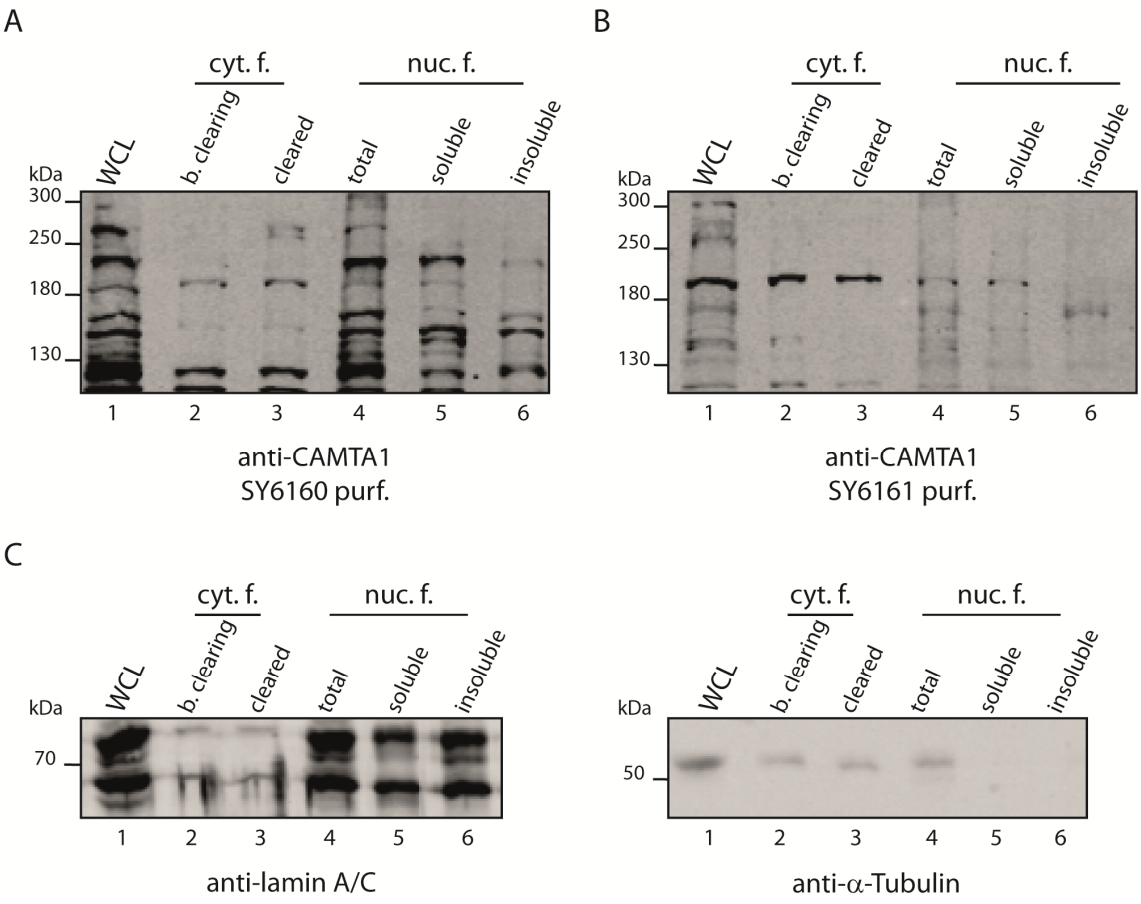

Figure 2.13: Subcellular fractionation of HeLa-S3 suspension culture cells to detect endogenous CAMTA1 by the generated antibodies. Comparable amounts of each fraction was loaded for the particular western blots. **A:** Western blot analysis using the purified (purf.) SY6160 antibody: SY6160 detected a band around 180 kDa, which was observed in the whole cell lysate (WCL; lane 1), the cytoplasmic (cyt.) fractions (lane 2 and 3), as well as in the total (lane 4) and soluble (lane 5) nuclear (nuc.) fractions. The same band was also detected by the SY6161 antibody **(B)**. However, this antibody visualized also a band slightly lower than 180 kDa, which was exclusively found (besides the WCL) in the total and insoluble nuc. fractions (lanes 4 and 6). **C:** Purity of the cyt. and nuc. fractions was controlled by western blots for lamin A/C (left panel) and α-Tubulin (right panel).

2.1.4. A potential CAMTA1 interaction partner: Nkx2.2

As pointed out in the working model for this thesis (see paragraph 1.6), we hypothesized that Nkx2.2 could be an interaction candidate for CAMTA1. It was thought, that this potential interaction is similar to the interaction between Nkx2.5 and CAMTA2 in the heart, which was reported previously (*61*).

To provide first evidences for an interaction between both proteins, mycCAMTA1 and N-terminally FLAG/HA-tagged Nkx2.2 (FH-Nkx2.2) were simultaneously overexpressed in HEK293-T cells. After 48 hours of overexpression, mycCAMTA1 was immunoprecipitated using anti-myc Sepharose® beads. In subsequent western blot analysis of the eluate, the co-precipitation of FH-Nkx2.2 was examined. As controls, N-terminally myc-tagged constructs of wildtype human Dicer, Exportin 5 (XPO5), Argonaute 2 (Ago2), and Target of EGR1 protein 1 (TOE1) were used. Additionally, instead of FH-Nkx2.2, FH-GFP was overexpressed together with each of the above mentioned myc-tagged proteins. As shown in Figure 2.14, FH-Nkx2.2 was detected in the eluate of the mycCAMTA1 precipitation (lane 6 of the anti-HA western blot) but not for the immunoprecipitations of the other myc-tagged proteins (lanes 7 to 10 of the anti-HA western blot).

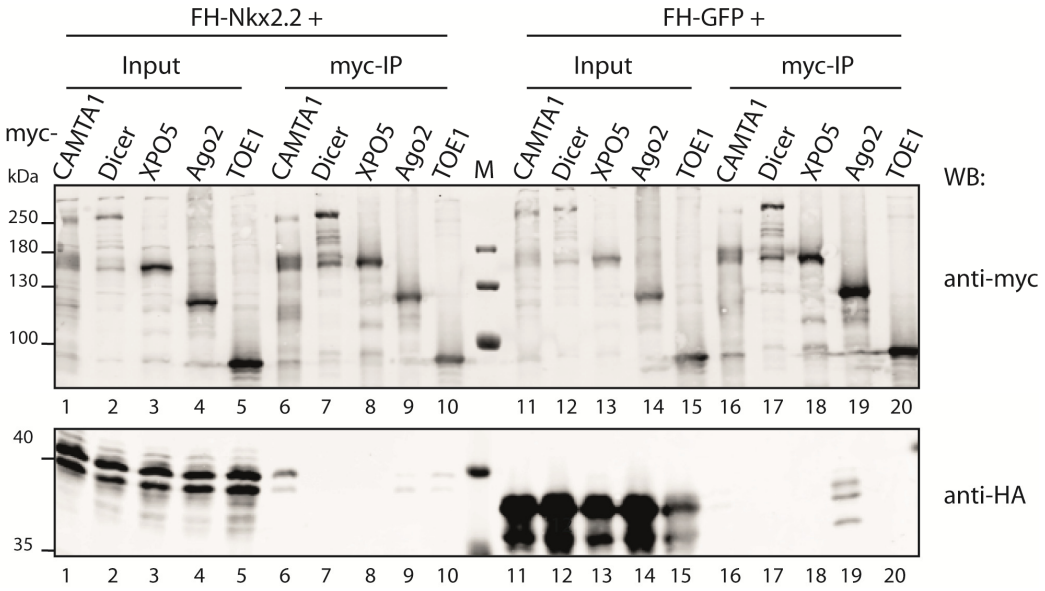

Figure 2.14: Interaction between mycCAMTA1 and FLAG/HA-Nkx2.2. The indicated myc-tagged proteins were overexpressed either together with FH-Nkx2.2 or with FH-GFP. Lane 6 of the anti-HA western blot (lower panel) showed a distinct signal for FH-Nkx2.2, which was co-immunoprecipitated by mycCAMTA1 (anti-myc western blot, upper panel). For western blot analysis about 1 % IP-input and 20 % IP-eluate was loaded.

This interaction was studied more in detail by mapping CAMTA1 for a potential Nkx2.2 interaction region. Therefore, several deletion mutants or truncated versions of CAMTA1 (all N-terminally myc-tagged) were generated as illustrated schematically in Figure 2.15 A. For CAMTA2 it was reported before that the CG-1 domain, which is located in close proximity to the N-terminus, is responsible for interaction with Nkx2.5 and that the TAD probably stabilizes this interaction (*61*). Accordingly, the corresponding region of CAMTA1 was completely deleted resulting in a truncated CAMTA1 version lacking the amino acids from 1 to 600. This construct was termed as "CAMTA1 ΔN600". In another construct ("CAMTA1 ΔC") the complete C-terminus was deleted including the ankyrin repeats. Further constructs were "CAMTA1 N+C", which is characterized by the fusion of the N- and C-terminus and lacks the region between amino acid 600 and 1054, "CAMTA1 M" consisting exclusively of the middle region of CAMTA1 bearing the TIG domain, and "CAMTA1 C", which is basically the CAMTA1 C-terminus including the ankyrin repeats.

Each of the mycCAMTA1 constructs was overexpressed in HEK293-T cells either together with FH-Nkx2.2 or with FH-GFP, followed up by anti-myc IPs. The eluate of each IP was analyzed via western blot for detection of FH-Nkx2.2 [Figure 2.15 B(2)]. Remarkably, FH-Nkx2.2 was co-precipitated for every CAMTA1 construct. However, minor differences in the signal intensity were observed: The co-IP by mycCAMTA1 M construct showed the strongest signal for FH-Nkx2.2 in western blots [Figure 2.15 B(2), lane 10], whereas the FH-Nkx2.2 signal was weakest for mycCAMTA1 C. FH-Nkx2.2 was detected with similar signal intensity in each eluate of the co-IPs with the other mycCAMTA1 constructs (wildtype CAMTA1, CAMTA1 ΔN600, CAMTA1 N+C, and CAMTA1 ΔC).

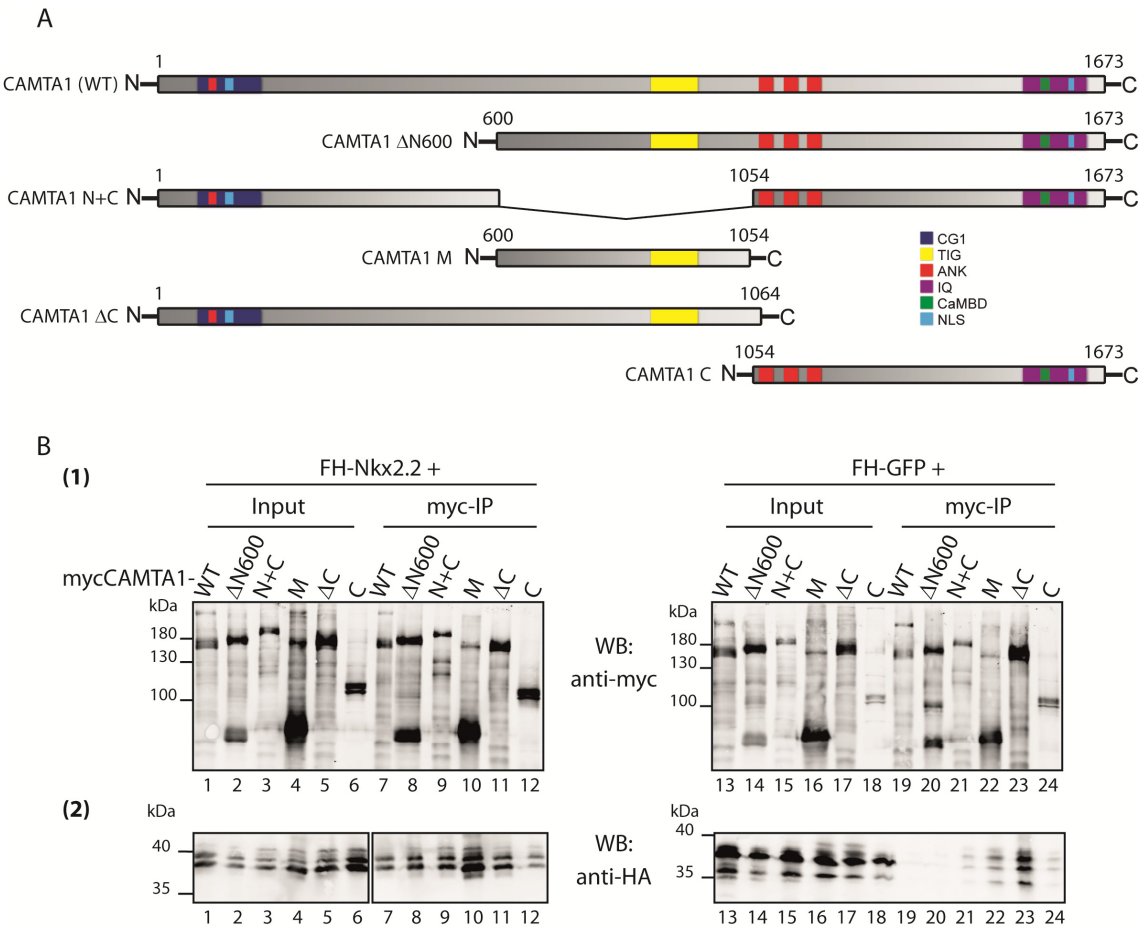

Figure 2.15: Mapping the interaction between CAMTA1 and Nkx2.2. A: Schematic illustration of the different mycCAMTA1 constructs to reveal a potential interaction site. **B:** The indicated constructs were overexpressed in HEK293-T cells together either with FH-Nkx2.2 or FH-GFP. (1) Western blot against myc-tag (about 1 % IP-input and 20 % IP-eluate was loaded). (2) Western blot against HA-tag (1 % IP-input and 30 % IP-eluate was loaded). FH-Nkx2.2 was detected for basically all mycCAMTA1 constructs. However, the signal for FH-Nkx2.2 was strongest in the mycCAMTA1 M co-IP (lane 10) and only weak in the mycCAMTA1 C co-IP (lane 12).

For the above-mentioned studies, interactions between overexpressed (tagged) proteins were examined. To further prove a potential CAMTA1/Nkx2.2 interaction, it was investigated if also the endogenous proteins form a complex that can be immunoprecipitated. Since stable LNT229 glioma cells show a strong nuclear signal for endogenous Nkx2.2 in immunofluorescence (see paragraph 2.2.1.), these cells were used for the endogenous co-immunoprecipitations.

Figure 2.16 shows the western blot result for a co-IP of endogenous CAMTA1. Since the purified CAMTA1 antibody SY6161 was efficient to immunoprecipitate endogenous CAMTA1 from total cell lysates of HEK293-T and T98G (Figure 2.7.), this antibody was used for the CAMTA1 co-IP. Moreover, the subsequent western blot analysis for CAMTA1 was also performed with this antibody. For the co-IP, LNT229 cells were lysed using IP-lysis buffer 1 (containing sodium deoxycholate, see also paragraph 4.2.3.2.), which was supplemented with a nuclease (Benzonase®).

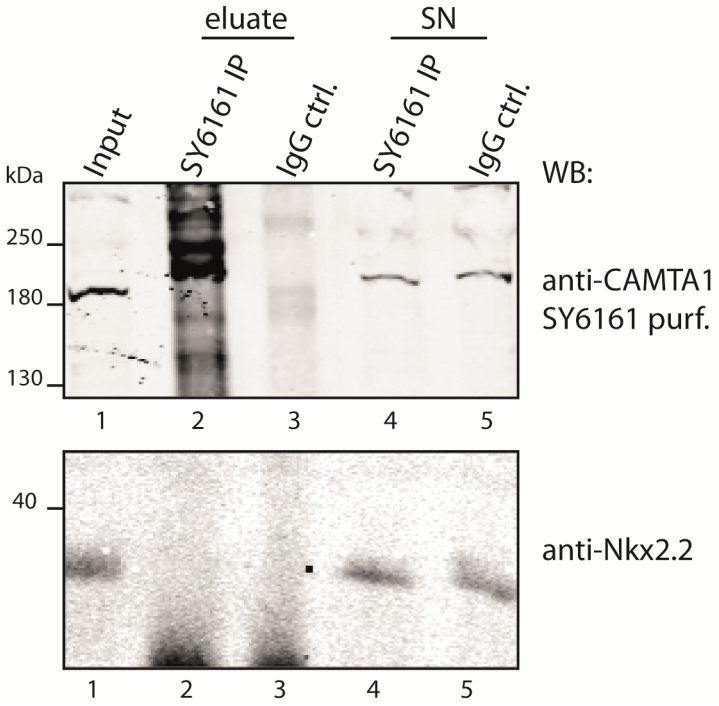

Figure 2.16: Immunoprecipitation of endogenous CAMTA1 to investigate a potential interaction with Nkx2.2 in LNT229 cells. The IP of endogenous CAMTA1 was performed using the purified (purf.) SY6161 CAMTA1 antibody. Western blot analysis of the IPs was performed with the SY6161 antibody (upper panel) and a Nkx2.2 specific antibody (lower panel). CAMTA1 was immunoprecipitated (lane 2, upper panel) but endogenous Nkx2.2 was not co-precipitated (lane 2, lower panel). For the IP and the IP-control (IgG ctrl.) material from ten 15-cm cell culture plates were used each; about 0.2 % IP-input/IP-supernatant (SN) and 50 % IP-eluate were loaded.

By using a monoclonal antibody against Nkx2.2 in the western blot analysis, the endogenous protein was only detected in the input and IP-supernatant samples, but not in the IP-eluate (Figure 2.16, lower panel).

When endogenous Nkx2.2 was immunoprecipitated, an interaction between the two endogenous proteins was also not observed (Figure 2.17). Thereby, the co-IP eluates were analyzed for CAMTA1 co-immunoprecipitation via western blots using both newly generated CAMTA1 antibodies (SY6160 and SY6161). Since it was believed that sodium deoxycholate has possibly a negative effect on the interaction, the lysis conditions were changed for this co-IP. Here, cells were lysed by hypotonic treatment (with IP-lysis buffer 2) and the nuclear proteins were extracted by adding NaCl afterwards (see also paragraph 4.2.3.2.). Moreover, the lysis for this co-IP was carried out without using any nuclease since it was thought that DNA is maybe required for a stable interaction of CAMTA1 and Nkx2.2.

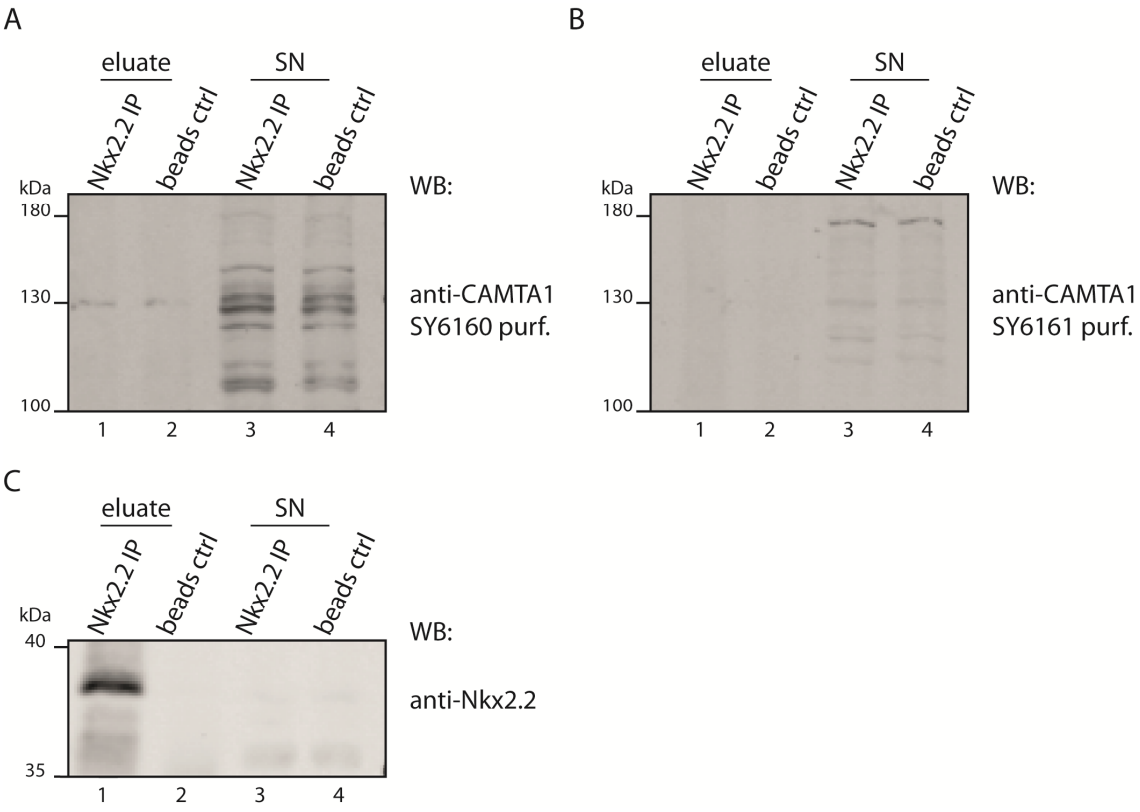

Figure 2.17: Immunoprecipitation of endogenous Nkx2.2 to investigate a potential interaction with CAMTA1 in LNT229 cells. The IP of endogenous Nkx2.2 was performed using a Nkx2.2 specific antibody. **A:** Western blot analysis of the IPs using the purified (purf.) CAMTA1 antibody SY6160. **B:** Western blot analysis with the purified SY6161 antibody. In both western blots, CAMTA1 was not detected in Nkx2.2-IP samples. **C:** The IP was validated by western blot analysis for Nkx2.2. For the IP and the beads only-control (beads ctrl.) material from ten 15-cm cell culture plates was used each; about 0.2 % IP-input/IP-supernatant (SN) and 50 % IP-eluate were loaded.

2.2. Characterization of Nkx2.2

The transcription factor Nkx2.2 was identified as a potential CAMTA1 interaction factor (as described in the previous chapter) and is known as a tumor suppressor candidate for glioblastomas. This chapter points out the further biochemical and functional characterization of Nkx2.2.

2.2.1. Nuclear localization of Nkx2.2

Hessabi *et al.* reported before that (overexpressed) Nkx2.2 showed nuclear localization and its HD contains two functional nuclear localization signals (NLS) (*144*). Both NLS are necessary for an efficient nuclear import (*144*).

Since it was thought that Nkx2.2 act as a transcription factor in glioma pathogenesis, the nuclear localization of the endogenous protein was analyzed in several different glioma-derived cell lines. This was assayed via IFs using a monoclonal antibody against endogenous Nkx2.2. Thereby, Nkx2.2 localization was investigated for the stable glioma cell lines T98G and LNT229 in comparison to the non-glioma-related cell line HEK293-T. Whereas in T98G cells, Nkx2.2 was barely detectable, HEK293-T showed a faint and LNT229 a strong nuclear fluorescence signal for Nkx2.2 (data not shown). Using an siRNA-mediated knockdown of endogenous Nkx2.2 in LNT229 cells it was proven that the detected signal originates from endogenous Nkx2.2 (Figure 2.18).

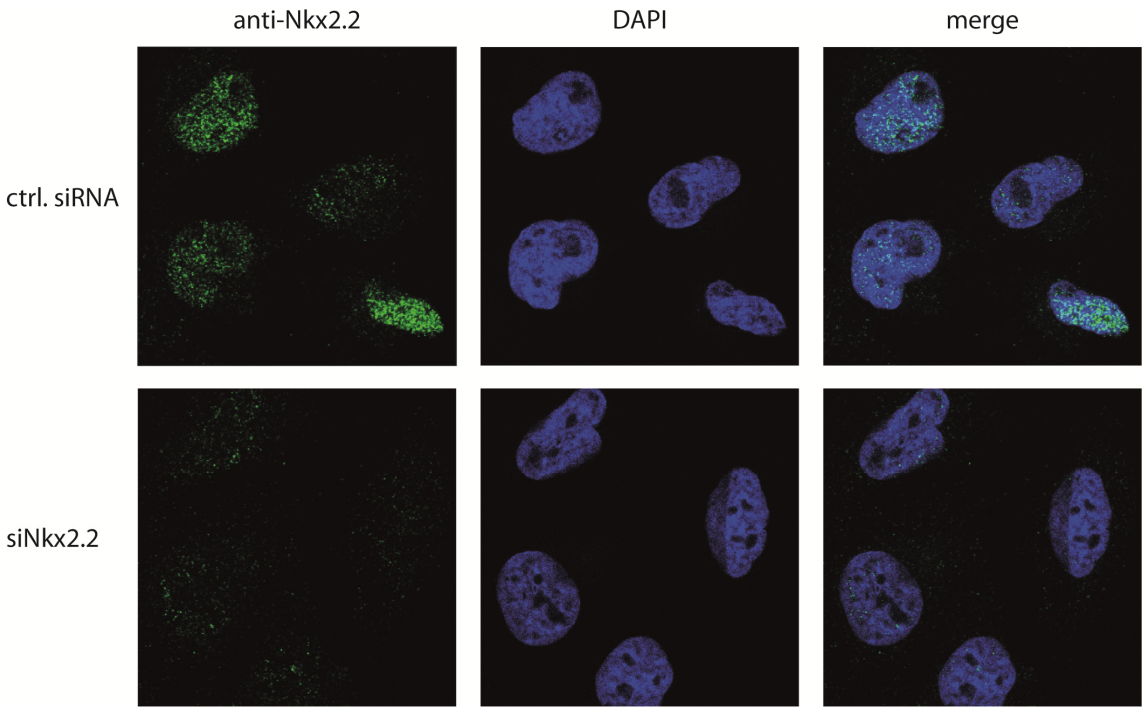

Figure 2.18: Nuclear localization of endogenous Nkx2.2 in LNT229 cells. For the IF, Nkx2.2 was knocked down using an siRNA targeting Nkx2.2. The IF was performed 48 h after siRNA transfection with a Nkx2.2-specific antibody. The IF showed a clear decrease of the nuclear Nkx2.2 signal.

2.2.2. Nkx2.2 interaction partners

In paragraph 2.1.4. it was comprehensively illustrated that CAMTA1 was considered to be a potential interaction partner for Nkx2.2. To validate this and to identify other putative interaction partners, overexpressed FH-Nkx2.2 was immunoprecipitated and co-immunoprecipitated proteins were analyzed using mass spectrometry. As negative controls, the empty expression vector and a FH-GFP encoding plasmid were used. Immunoprecipitation was performed with pre-coupled anti-FLAG agarose. The IP efficiency was controlled by western blot with 20 % of each eluate (Figure 2.19 A, page 53). Afterwards, 50 % of each eluate was used for a second SDS-polyacrylamide gel electrophoresis. This gel was then stained with silver nitrate until specific bands were clearly visible (Figure 2.19 B). Finally, several bands that appeared exclusively in the eluate of the FH-Nkx2.2 IP (named a to n in Figure 2.19 B) were cut out and analyzed by mass spectrometry. To identify proteins, mass spectrometric raw data were

interpreted using the Mascot software tool (see paragraph 4.2.3.8.). Table 2.1 (page 54) shows for each band the identified protein that appears at the first position with the highest Mascot protein score. In general, the higher the score value is, the more peptides were identified from a particular protein, which correlates with the significance of a match for a distinct protein. A complete list for mass spectrometric analysis of the FH-Nkx2.2 IP can be found in the appendix (see page 151).

In band k to n, Nkx2.2 was identified at top position, indicating a clear enrichment of FH-Nkx2.2 by the IP. This is also reflected by the western blot analysis of the IP (Figure 2.19 A). Interestingly, band m and n contain also Nkx2.3 (another Nk-2 class protein) with a relative high score (around 200). However, neither CAMTA1 nor previously reported Nkx2.2 interaction partners such as histone deacetylase I (*135*) or Olig2 (*145*) were detected for this co-IP. Among the other proteins identified are some nuclear proteins (e.g. Structural maintenance of chromosomes protein 1A), but it is difficult to determine if indeed specific Nkx2.2 interaction partners were co-immunoprecipitated. Yet, based on the identities and functions (if known) of these proteins as well as on the knowledge about previously studied cellular processes involving Nkx2.2, none of these was considered to be a reasonable candidate for Nkx2.2 interaction.

Although the IP of FH-Nkx2.2 was successful, the other proteins identified by mass spectrometry were most likely non-specifically co-precipitated, with the exception of Nkx2.3. This co-IP of Nkx2.3 was presumably a result of a heterodimerization between FH-Nkx2.2 and Nkx2.3 (discussed in paragraph 3.2.1.).

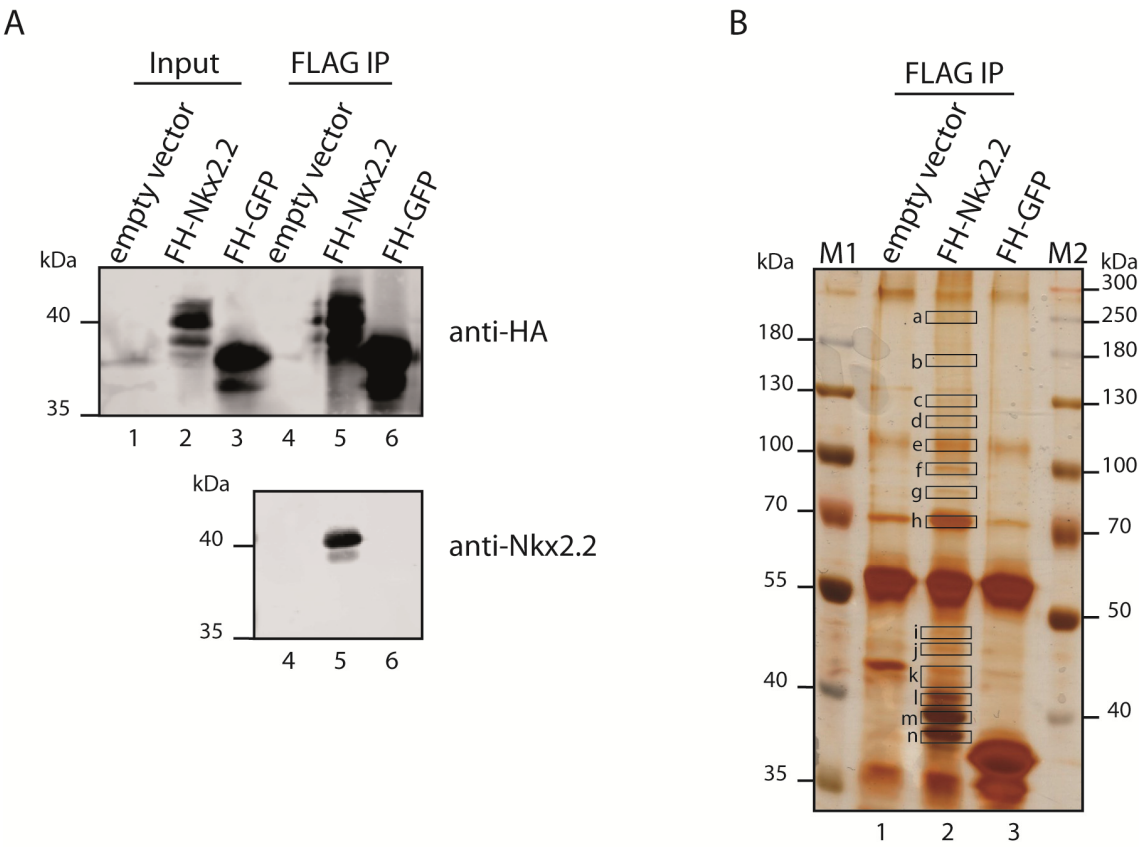

Figure 2.19: Screening for potential Nkx2.2 interaction partners. FLAG/HA-tagged Nkx2.2 (FH-Nkx2.2) was overexpressed in HEK293-T cells and subsequently precipitated (anti-FLAG IP). For each IP transfected cells from three 15-cm cell culture plates were used. **A:** Western blot control of the IPs using an antibody against the HA-tag (upper panel) and a Nkx2.2 specific antibody (lower panel). [About 1 % of the IP-inputs (lanes 1 to 3) and 20 % of each IP-eluate (lanes 4 to 6) were loaded]. **B:** PAGE and subsequent silver straining to identify unique protein bands (a to n) in the eluate of the FH-Nkx2.2 IP (lane 2). The particular bands were cut out and analyzed via mass spectrometry (for the PAGE, 50 % of each IP-eluate was loaded)

Table 2.1: Results of the mass spectrometric analysis of the FH-Nkx2.2 IP (shown in Figure 2.19). Only proteins with the highest Mascot score identified in the particular bands (a to n) were listed here. For a full list, see appendix (page 151).

band	protein identified at top position	molecular weight [kDa]	score
a	Myosin-9	226.4	842.1
b	Structural maintenance of chromosomes protein 1A	143.1	257.4
c	Heterogeneous nuclear ribonucleoprotein U	90.5	678.2
d	Kinesin-like protein KIF11	119.1	981.8
e	Importin subunit beta-1	97.1	475.9
f	X-ray repair cross-complementing protein 5	82.7	1495.8
g	78 kDa glucose-regulated protein	72.3	2489.4
h	Heat shock 70 kDa protein 1A/1B	70.0	2695.2
i	Tubulin beta chain	49.6	1245.6
j	Elongation factor Tu, mitochondrial	49.5	1293.7
k	Homeobox protein Nkx-2.2	30.1	1046.9
l	Homeobox protein Nkx-2.2	30.1	2075.1
m	Homeobox protein Nkx-2.2	30.1	3899.2
n	Homeobox protein Nkx-2.2	30.1	2982.4

2.2.3. Investigation of a putative regulation by microRNAs

As outlined before, miRNAs play an important role during cancer development and progression (oncomiRs). In gliomas, respectively glioblastomas, several onocmiRs were identified previously (see paragraph 1.3.2.). Hence, if Nkx2.2 is really a tumor suppressor protein in glioma biology, one could speculate that it is potentially down-regulated by certain oncomiRs. To support this hypothesis, the 3'-UTR of Nkx2.2 was analyzed using microRNA.org and TargetScan 6.2 to search for predicted miRNA binding sites. Remarkably, the 3'-UTR contains a predicted target site for miRNAs, which have the same seed sequence and arise from the miR-17~92 cluster or its paralogs (Figure 2.20 A). Since miR-17 and miR-106b are specifically enriched in CD133-positive cells (see paragraph 1.3.2.), this thesis investigated more closely if Nkx2.2 is indeed a target for miR-17 and/or miR-106b.

To validate the predicted miR-17/-106b target site, the Nkx2.2 3'-UTR was fused to firefly luciferase. The construct was expressed from a reporter vector also coding for renilla luciferase (constant renilla activity was used for normalization of the firefly activity). As negative control, the seed sequence of the miR-17/-106b target site was mutated into a *Bam*HI restriction site. Furthermore, positive controls were generated by cloning the fully complementary sequences of miR-17 and miR-106b into the luciferase reporter vector. The target site validation was assayed by co-tansfecting stable T98G glioma cells with the dual luciferase reporter plasmid and 2'-O-methylated antisense inhibitors against miR-17 or miR-106b. These chemically modified RNA antisense oligonucleotides inhibit endogenous miRNAs in a very efficient way (*146*). Therefore, if the Nkx2.2 3'-UTR is regulated by miR-17 and/or miR-106b, the normalized firefly activity should be significantly higher in comparison to a control inhibitor (de-repression). Here, the inhibitor of the liver-specific miR-122 was used as control.

Figure 2.20 B and C show the specific inhibition of either miR-17 or mir-106b. In both cases, the normalized activity of the firefly luciferase fused to the wildtype Nkx2.2 3'-UTR shows no obvious difference compared to the firefly luciferase with the mutated 3'-UTR. This was also observed when both miRNAs were inhibited at once (Figure 2.20 D).

The assays were repeated several times, also using other cell lines such as LNT229 cells, resulting in basically the same outcome as shown in Figure 2.20 for one assay with T98G cells. Furthermore, the validation of the miR-17/-106b target site was also assayed in a different way by miR-17 and/or miR-106b overexpression using plasmids that encode for the corresponding miRNA precursors, or by co-transfection of a pre-annealed miR-17 and/or miR-106b duplex mimics. Also in these assays, the firefly luciferase with the Nkx2.2 3'-UTR was not affected significantly by elevated miR-17 or miR-106b concentrations, whereas the positive controls (fully complementary sequences of miR-17 and miR-106b fused to firefly luciferase) clearly responded upon the elevated concentrations of these miRNAs (strong reduction of the firefly luciferase activity) (data not shown).

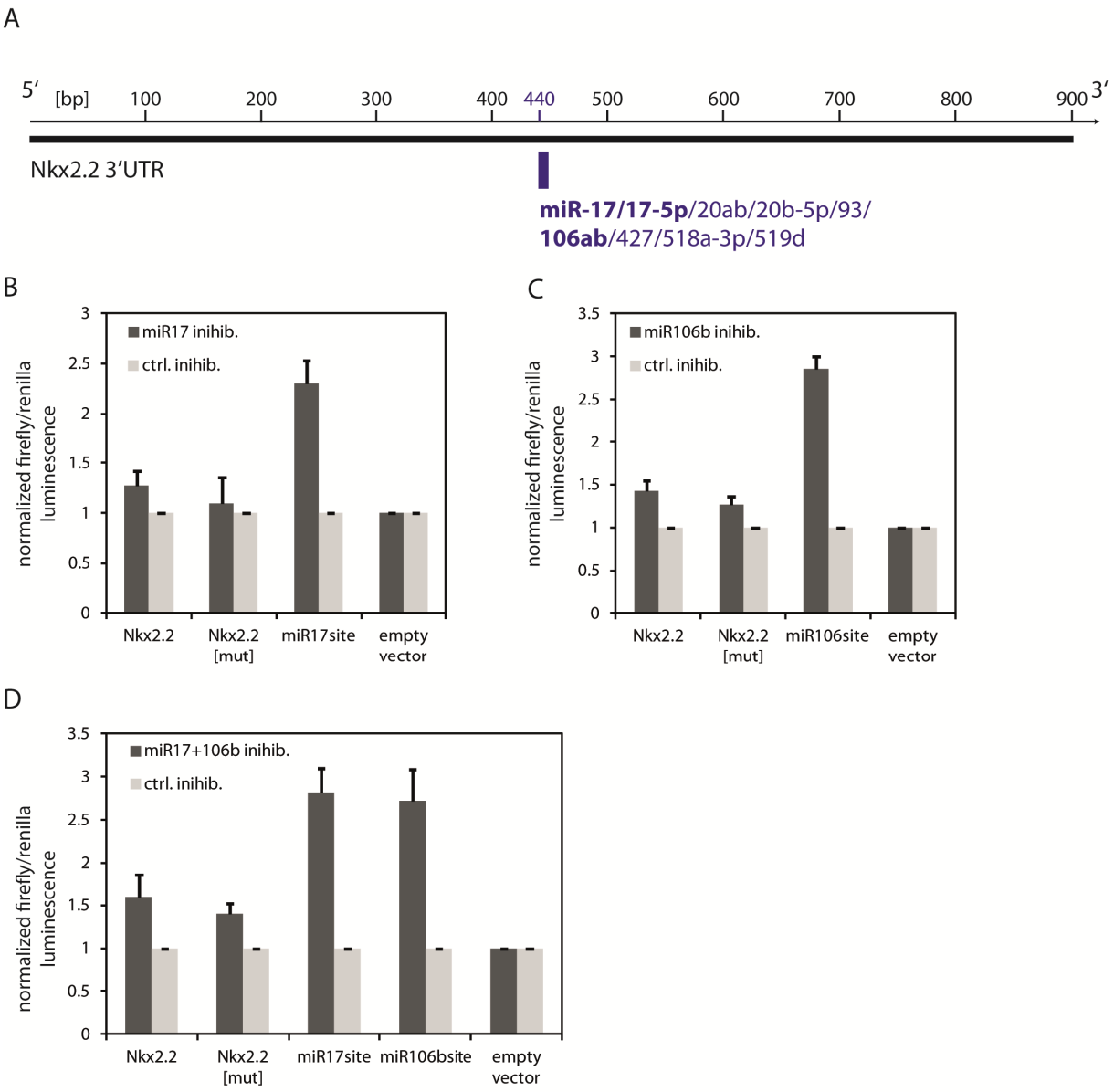

Figure 2.20: Nkx2.2 as a potential target for miR-17-5p and miR-106b. **A:** Nkx2.2 3'-UTR illustrated schematically. Analysis via miRNA.org TargetScan 6.2 revealed a target site for miR-17-5p and miR-106b within the 3'-UTR. **B to D:** Dual luciferase reporter assays using T98G cells. For the assays the following constructs fused to firefly luciferase were used: wildtype 3'-UTR of Nkx2.2 (Nkx2.2), miR-17/106b target site mutated Nkx2.2-3'-UTR (Nkx2.2[mut]), full complementary (artificial) target sites of miR-17 or miR-106b (miR-17 or miR106b site). The particular miRNAs were specifically depleted as indicated: miR-17-5p (**B**), miR-106b (**C**), and simultaneous inhibition of miR-17/106b (**D**); a liver-specific miR-122 inhibitor was used as control (ctrl.). For all assays no significant de-repression of the Nkx2.2-3'-UTR reporter was observed.

Taken together, the results of the different reporter assays for the validation of the predicted miR-17/-106b target site in the Nkx2.2 3'-UTR suggest that Nkx2.2 is presumably not regulated by miR-17 or miR-106b.

To further investigate the general regulation of the Nkx2.2 3'-UTR by miRNAs, a key factor of the miRNA-directed regulation mechanism, the Ago protein, was prevented from carrying out its function as mediator of silencing. This was achieved by overexpression of a 85 amino acid long peptide which binds Ago proteins with high affinity (Hauptmann *et al.*, unpublished data). This strong binding affinity of the peptide (termed "T6B") is due to the fact that T6B consists basically of an interaction motif of TNRC6B, which is part of the TNRC6B Ago binding region (*147*). Hence, the T6B competes with full-length endogenous TNRC6B for Ago binding. Because of the high concentration of T6B upon overexpression, most of the Ago proteins are bound by T6B and are thus prevented for interaction with endogenous TNRC6B (and probably other TNRC6 proteins) (Hauptmann *et al.*, unpublished data). It can be assumed that this makes miRNA-guided silencing virtually inoperable. Therefore, this peptide can be used to investigate a general miRNA-directed regulation of distinct transcripts.

For the dual luciferase assays using T6B, the expression plasmid coding for T6B with an N-terminal FLAG/HA-tag and a C-terminal GFP-tag was co-transfected into cells together with the reporter plasmids. In addition to reporter plasmid containing the wildtype Nkx2.2 3'-UTR, plasmids with the mutated Nkx2.2 3'-UTR (miR-17/-106b seed sequence mutated), the CAMTA1 3'-UTR, the HMGA2 3'-UTR, the mutated HMGA2 3'-UTR, and with the empty multiple cloning site were used as controls. Thereby, the mutated HMGA2 3'-UTR is characterized by the mutation of all seven let-7 target sites [according to (*148*)]. The normalized firefly activities of the corresponding constructs were analyzed in comparison to GFP overexpression. As a control, a mutated version of the peptide was co-transfected together with each of the reporter constructs. This mutant is characterized by lacking all tryptophan residues and can thus not interact with Ago proteins (Hauptmann *et al.*, unpublished data).

Figure 2.21 A (left panel) shows a "T6B-assay" carried out with HeLa cells. Here, firefly luciferase-CAMTA1 3'-UTR and firefly luciferase-HMGA2 3'-UTR clearly responded to T6B overexpression (compared to GFP). In contrast, the activity of the firefly luciferase fused to the Nkx2.2 3'-UTR showed no change upon overexpression of T6B. When the mutated T6B was overexpressed (Figure 2.21 A, right panel), no firefly luciferase construct was de-repressed, indicating that the assay was successful.

The assay was also repeated in stable T98G glioma cells (Figure 2.21 B) resulting in a similar outcome as observed for HeLa cells, although the de-repression of the firefly luciferase-CAMTA1-3'-UTR and firefly luciferase-HGMA2-3'-UTR constructs was not as strong as in the assays with HeLa cells.

Since the T6B-assays using the Nkx2.2 3'-UTR reporter construct resulted in no clear de-repression, the general question emerged whether Nkx2.2 is regulated by miRNAs at all. This is discussed more closely in paragraph 3.2.2.

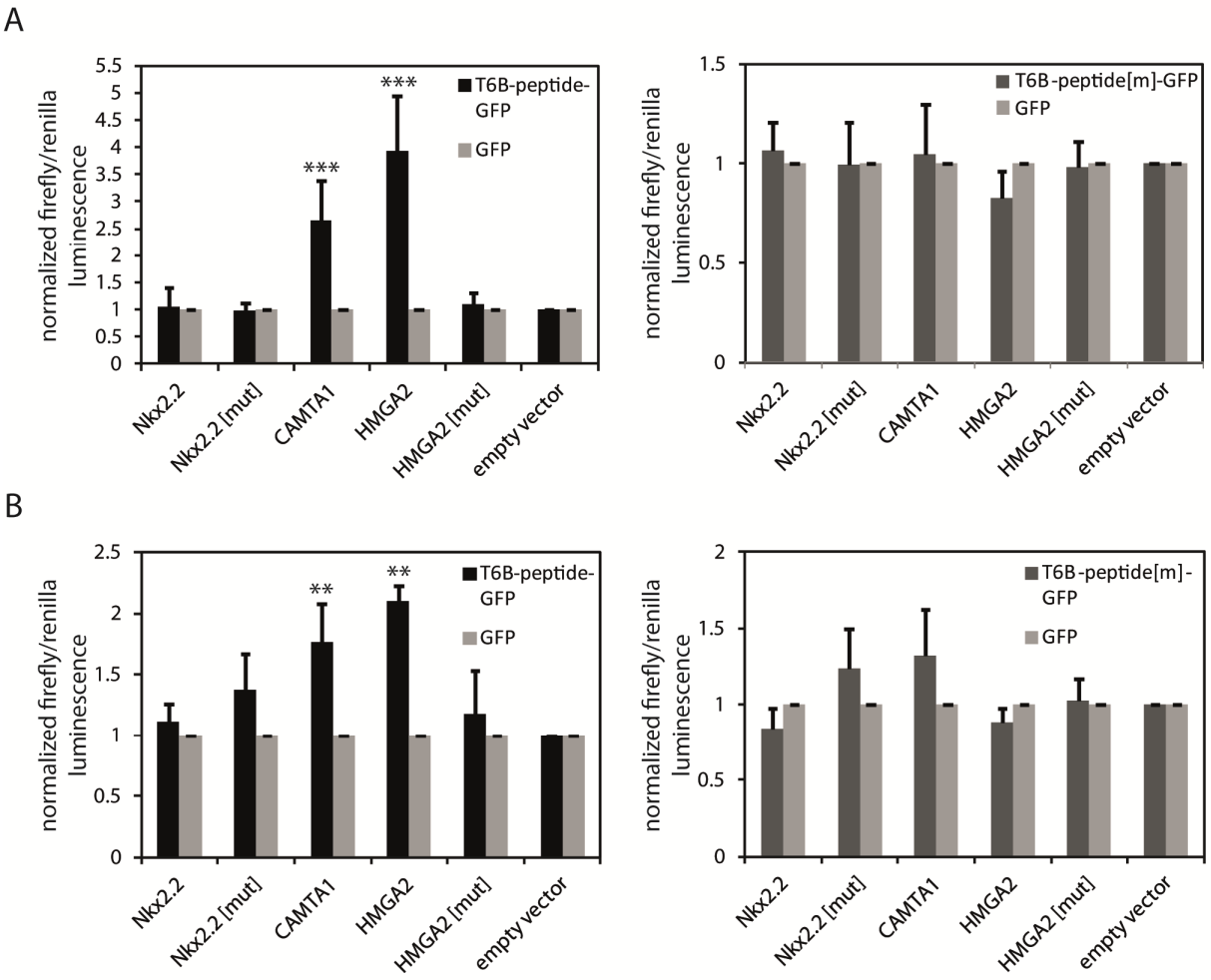

Figure 2.21: Investigation via dual luciferase reporter assays if Nk2.2 is generally regulated by miRNAs in HeLa and T98G cells. For the assays the following constructs fused to firefly luciferase were used: The wildtype 3'-UTR of Nkx2.2, CAMTA1, and HMGA2 as well as the mutated 3'-UTRs of Nkx2.2 (Nkx2.2[mut]; miR-17/106b target site mutated) and HMGA2 (HMGA2[mut]; all let-7 sites mutated). Additionally, the T6B peptide, which disrupts Ago function, or the mutated peptide (T6B-peptide[m]) were overexpressed, as indicated. **A:** Assay performed in HeLa cells. Overexpression of T6B caused a significant de-repression of the CAMTA1-3'-UTR as well as the HMGA2-3'-UTR but had basically no effect on the Nkx2.2-3'-UTR (left panel). In contrast, no de-repression at all was observed when the mutated T6B was overexpressed (right panel). **B:** The assay using T98G cells showed a similar outcome as the assay with HeLa cells. In **A** and **B** significance was assessed by two-sided Student's *t*-test (** $P < 0.01$, *** $P < 0.001$)

2.2.4. The effect of Nkx2.2 on glioma tumor biology

2.2.4.1. Nkx2.2 overexpression leads to decreased neurosphere formation of primary glioblastoma cells

As mentioned before, isolated primary glioblastoma cells show neurosphere-like growth when they are cultivated under stem cell conditions. Muraguchi *et al.* reported previously that Nkx2.2 overexpression led to significantly reduced neurosphere formation of mouse and human primary glioblastoma cells (*142*). In order to examine if this effect is reproducible for other human primary glioblastoma cell lines, Nkx2.2 was overexpressed in R11 and ZH161 primary glioblastoma cells. A negatively affected neurosphere formation upon Nkx2.2 overexpression of these cells would further support the role of Nkx2.2 as tumor suppressor for glioblastomas. Indeed, a reduced neurosphere formation due to Nkx2.2 overexpression was observed for both R11 and ZH161 cells (Figure 2.22, page 62). For R11 cells the combined results of two biological replicates is shown in Figure 2.22 A. Thereby, the significance of the effect caused by Nkx2.2 was not that strong (P = 0.07) as observed for ZH161 cells (Figure 2.22 B). Here, the diagramed result arises from four biological replicates and it shows a significantly reduced neurosphere formation in response to Nkx2.2 overexpression.

It was also investigated in this thesis if the deletion or the mutation of one critical residue of the Nkx2.2 homeobox binding domain has an effect on neurosphere formation. For the exchange of one single amino acid in the DNA binding domain, structural information preciously published for Nkx2.5 was used (*115*). As mentioned before, tyrosine 191 of Nkx2.5 is essential for sequence specific recognition of the NK-response element (NKE) by the homeobox binding domain (*115*). Since this domain is highly conserved among Nk-2 family members, the corresponding tyrosine of Nkx2.2 (Y181) was mutated to cystein (referred to as "Nkx2.2Y181C"). In theory, both the homeobox deletion mutant (referred to as "Nkx2.2ΔHD") and Nkx2.2Y181C should not be able to bind DNA. This disrupts most likely the function of these mutants to act as transcription factors. It was further hypothesized that thus these mutants probably lose the capability to trigger a tumor suppressive effect. Such loss-of-function mutants

would in turn lead to a neurosphere formation similar to the negative control when these constructs are overexpressed in primary glioblastoma cells. However, both Nkx2.2Y181C and Nkx2.2ΔHD were still able to reduce the number of spheres in comparison to the control (Figure 2.23, page 63). Here, it appears that the overexpression of the deletion mutant (Nkx2.2ΔHD) had a milder effect, while Nkx2.2Y181C and the wildtype strongly reduced the formation of neurosphere-like colonies. Yet, this effect was not significant compared to the wildtype (this is presumably also due to the fact that this result was gained from only two biological replicates).

Summing up, the effect of Nkx2.2 on neurosphere formation reported previously was confirmed in this thesis. This further supports the idea of Nkx2.2 as a tumor suppressor for glioblastomas. Regarding the mutants, one would expect a loss of function reflected by a neurosphere formation similar to the control. This was not the case, in particular for Nkx2.2Y181C. A possible explanation for this is discussed in paragraph 3.2.3.

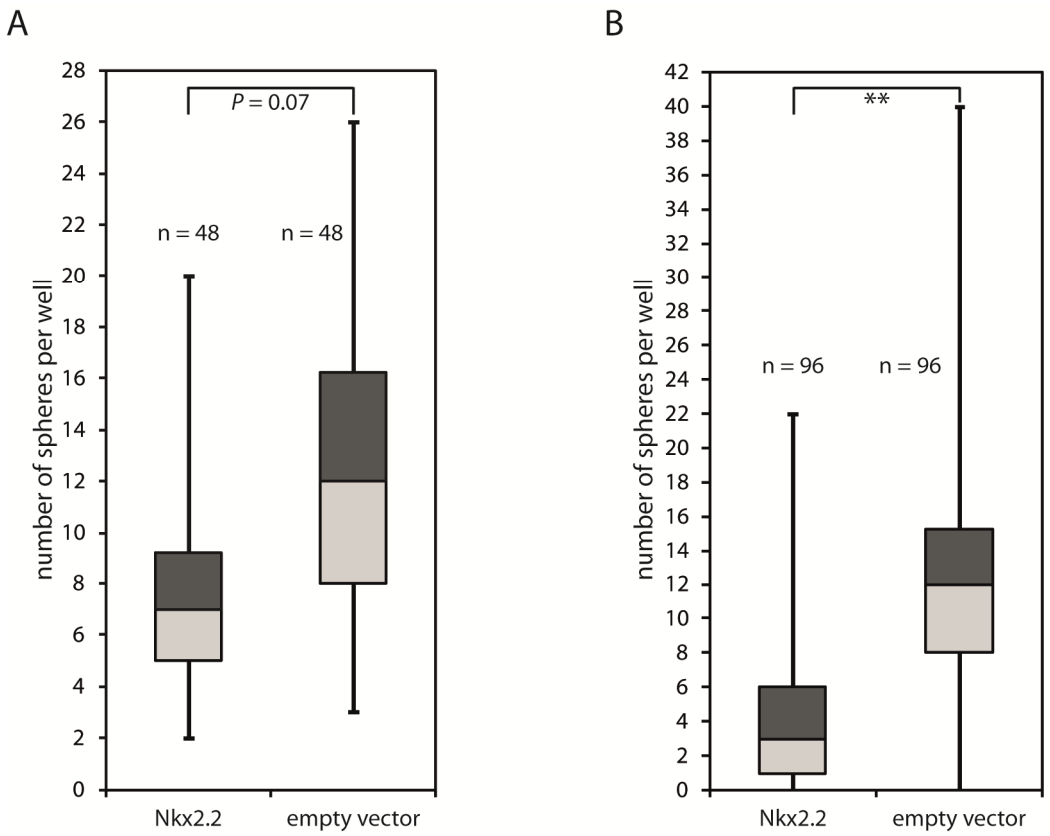

Figure 2.22: Nkx2.2 reduces the formation neurosphere-like colonies. Nkx2.2 was overexpressed in primary glioblastoma cells. **A:** Neurosphere assay using R11 cells. The box blot shows combined results from two biological replicates (n: total number of wells). **B:** Neurosphere formation of ZH161 was significantly repressed by Nkx2.2 overexpression. For the box blot results from four biological replicates were combined (n: total number of wells). In **A** and **B** significance was assessed by two-sided Student's *t*-test (** $P < 0.01$).

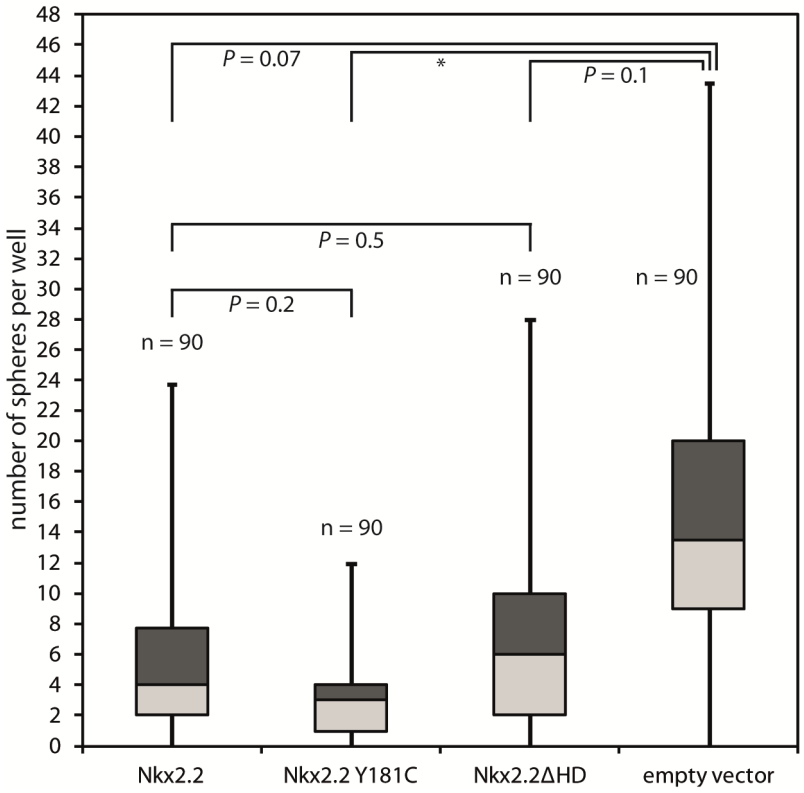

Figure 2.23: Effect of a mutated or deleted Nkx2.2 homeobox-binding domain on neurosphere formation of ZH161 cells. Overexpression of Nkx2.2Y181C (point mutation in the HD) and Nkx2.2ΔHD (deletion of the entire HD) still reduced the formation of neurosphere-like colonies (compared to the empty vector control). The box blot shows combined results from two biological replicates (n: total number of wells). Significance was assessed by two-sided Student's *t*-test (* $P < 0.05$).

2.2.4.2. Nkx2.2 expression correlates with glioma outcome

To further support the previous findings that suggest a role for Nkx2.2 as a tumor suppressor in glioblastomas, Nkx2.2 expression data from glioma patients were analyzed. These datasets were obtained from the Repository of Molecular Brain Neoplasia Data (REMBRANDT) database, which is provided by the U.S. National Cancer Institute. Nkx2.2 expression levels from patients diagnosed with all types of gliomas (low-grade as well as high-grade such as glioblastomas) were correlated to patient survival and plotted as Kaplan-Meier survival curve in Figure 2.24 A (page 65). Strikingly, patients characterized by a higher Nkx2.2 expression survived significantly longer than patients with low or intermediate expression. Moreover, data from patients

exclusively suffering from glioblastomas were also analyzed in terms of survival. Accordingly, also glioblastoma patients with up-regulated Nkx2.2 expression showed a longer survival. However, this higher survival rate is statistically not significant due to the low number of samples in this study (data not shown).

The REMBRANDT database provides also Affymetrix microarray data derived from patients with low-, medium-, or high-grade gliomas. These microarray data were used to analyze the mRNA expression level of Nkx2.2 in astrocytoma (low-grade glioma) and glioblastoma (high-grade glioma) in contrast to samples originating from non-tumor brain tissue. As diagrammed in Figure 2.24 B (left panel), Nkx2.2 shows no differences concerning its expression pattern for astrocytoma, glioblastoma or non-tumor tissue. For comparison, CAMTA1 expression is strongly decreased in astrocytoma and glioblastoma tumor samples (Figure 2.24 B, right panel). This expression pattern of CAMTA1 was observed and published before (*53*).

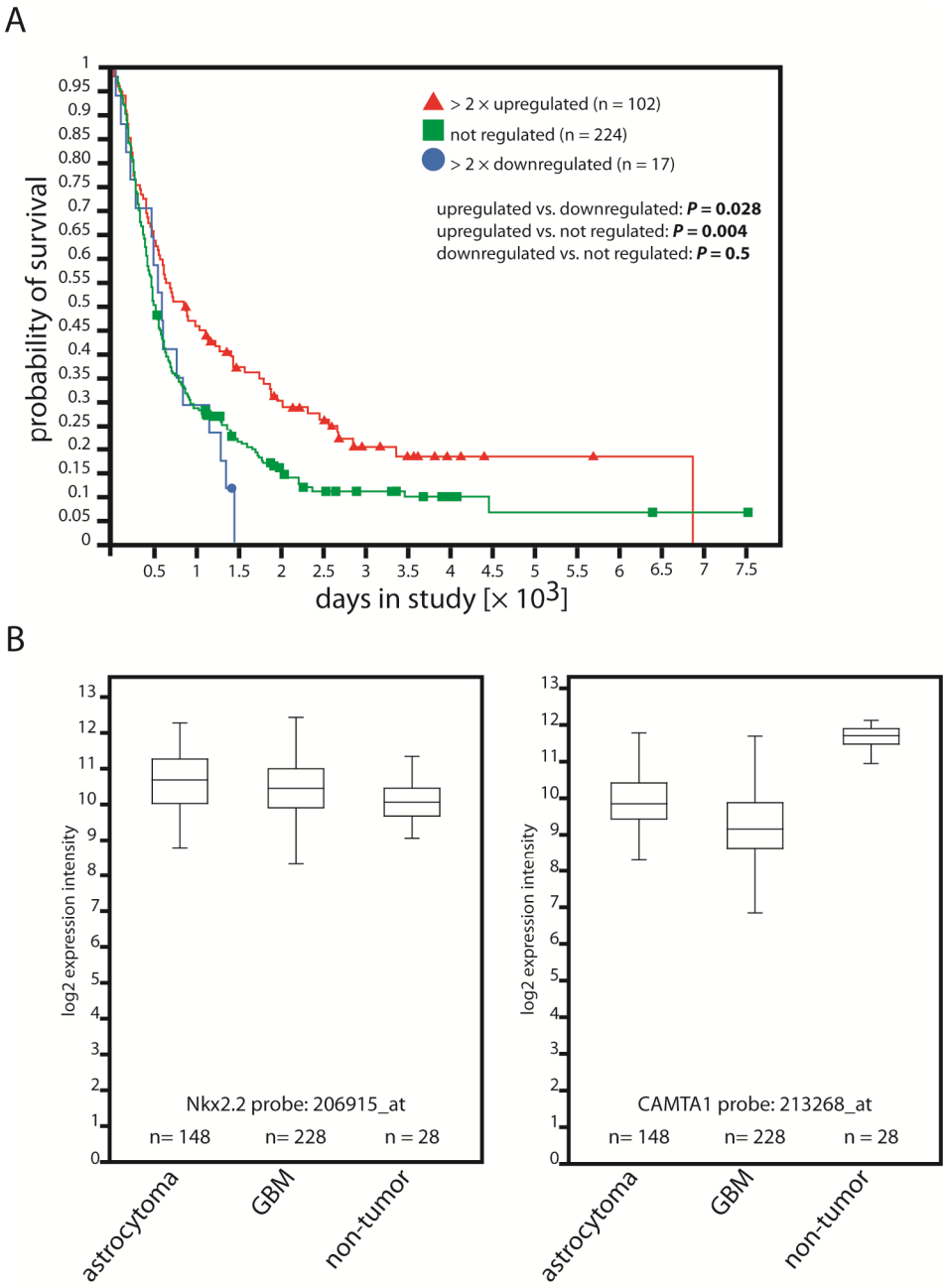

Figure 2.24: Nkx2.2 expression correlates with survival of glioma patients. A: Kaplan-Meier survival plot for patients (suffering from all types of gliomas) characterized by high (red curve), intermediate (green curve), or low (blue curve) Nkx2.2 expression. **B:** Nkx2.2 expression (left panel) in low- (astrocytomas) and high-grade gliomas (glioblastomas; GBM) in comparison to CAMTA1 expression (right panel) in low- and high-grade gliomas. In contrast to CAMTA1, Nkx2.2 showed similar expression levels in low- and high-grade gliomas as well as in normal brain tissue (non-tumor). Expression analysis was performed using the indicated Affymetrix probes on a U-133A microarray (n: number of samples). Data for **A** an **B** was obtained from the REMBRANDT database.

2.2.4.3. Nkx2.2 overexpression shows an antiproliferative effect on stable glioma cells

Since overexpression of Nkx2.2 showed a negative effect on neurosphere formation in this thesis and Nkx2.2 was suggested as a tumor suppressor candidate in glioblastomas before (*142*), it was also investigated if Nkx2.2 triggers a potential antiproliferative effect.

To examine the effect of Nkx2.2 overexpression on cell proliferation, stable LNT229 glioma cells were transfected and the assays were performed as described in paragraph 4.2.4.3. The effect of Nkx2.2 overexpression was observed in comparison to the overexpression of negative controls, namely the Nkx2.2 mutants Nkx2.2Y181C and Nkx2.2ΔHD as well as GFP. Cell proliferation was monitored for four subsequent days and an effective overexpression of wildtype Nkx2.2 and the mutants was confirmed by western blot at the end of the experiment [whereas an efficient expression of GFP was verified by fluorescence microscopy (data not shown)].

The results were reproduced in three independent experiments. Thereby, Nkx2.2 had a striking negative effect on cell proliferation compared to GFP (Figure 2.25 shows the result of one experiment). This is consistent with the neurosphere assays. Notably, in contrast to the neurosphere assays, the overexpression of Nkx2.2ΔHD showed a clear loss-of-function-phenotype reflected by a much higher cell proliferation compared to the wildtype protein (Figure 2.25 A). Although the phenotype caused by Nkx2.2Y181C was never as strong as observed for Nkx2.2ΔHD, the proliferation rate observed for this mutant was still higher than for the wildtype (Figure 2.25 A).

As described in the working model for this thesis (see paragraph 1.6.), it was assumed that Nkx2.2 is able to activate the *NPPA* gene in the same way as Nkx2.5 does in the heart. Moreover, since for ANP an antiproliferative effect was reported before (*143*), it was further hypothesized that the antiproliferative effect observed for Nkx2.2 was mediated by *NPPA* induction. To prove this assumption, total RNA was isolated after the proliferation-experiment shown in Figure 2.25 had been performed. Subsequently, the mRNA levels of NPPA and its main receptor NPR-A were quantified via qRT-PCR. An overexpression of Nkx2.2 led indeed to up-regulated mRNA levels of NPPA (compared to GFP overexpression), but not of NPR-A (Figure 2.25 C). However,

Nkx2.2Y181C resulted also in an elevated NPPA mRNA level although it is not as high as caused by overexpressing the wildtype. In contrast, the effect of the deletion mutant Nkx2.2ΔHD on NPPA mRNA level is only weak (Figure 2.25 C).

It was also investigated, if the CAMTA1 mRNA level was affected by the overexpression of Nkx2.2 wildtype or the mutants. This was not the case as the qRT-PCR quantification revealed (Figure 2.25 C).

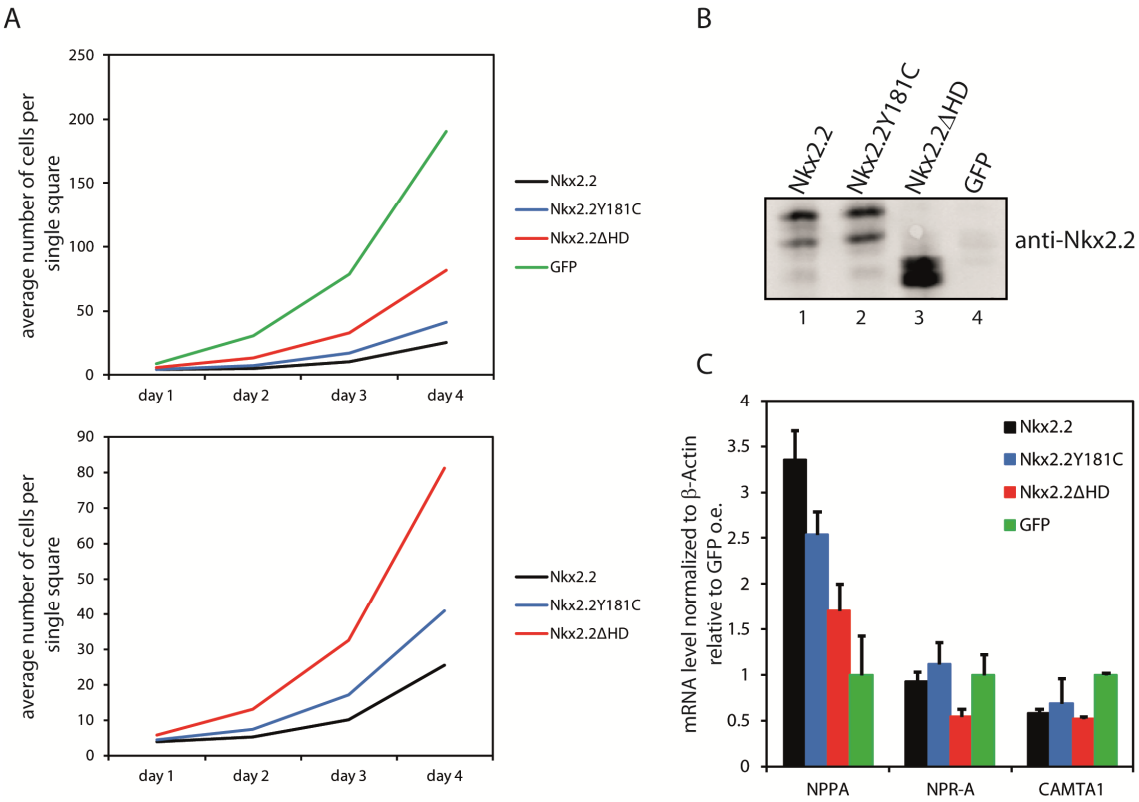

Figure 2.25: Nkx2.2 causes an antiproliferative effect and elevates the expression of NPPA. A: The indicated proteins were overexpressed in LNT229 cells and the cell proliferation was observed for four subsequent days. Nkx2.2 overexpression has a clear antiproliferative effect on LNT229 cells, in contrast to the Nkx2.2ΔHD mutant. Overexpression of Nkx2.2Y181C showed a less strong phenotype in comparison to Nkx2.2ΔHD. **B:** Overexpression was controlled by western blot analysis using a Nkx2.2 specific antibody (70 µg of each lysate was loaded). **C:** Nkx2.2 overexpression resulted in an increase of the NPPA mRNA-levels, but had no effect on the expression of the ANP receptor A (NPR-A) or CAMTA1.

2.2.5. NPPA as a potential Nkx2.2 target gene: Only Nkx2.2 with an intact homeobox binding domain induces the NPPA promoter

As already mentioned before, Nkx2.5 regulates the *NPPA* gene in the heart via binding to the NKE sites of the *NPPA* promoter as a homodimer (*115*). The same mode of action was assumed for Nkx2.2 in the brain.

In the previous paragraph it was shown that an Nkx2.2 overexpression leads to an elevated NPPA mRNA level. This result turns *NPPA* into a candidate as Nkx2.2 target gene. Therefore, it was investigated in this thesis if Nkx2.2 is able to induce the *NPPA* promoter. For this purpose, a firefly luciferase vector containing a 1.5 kb-long DNA fragment bearing the distal and proximal *NPPA* promoter region was used to validate the regulation of the *NPPA* promoter by Nkx2.2 using dual luciferase reporter assays. For this assays, HEK293-T cells were used for high transfection efficiency as well as for high firefly and renilla expression levels. Thereby, the reporter plasmid was co-transfected together with an Nkx2.2 expression vector and a renilla luciferase encoding plasmid for normalization.

Remarkably, Nkx2.2 overexpression leads to strongly increased firefly activity compared to the empty vector control (three-fold higher activity, cf. Figure 2.26). Moreover, it was also examined if the mutants Nkx2.2Y181C and Nkx2.2ΔHD (extensively described in the previous paragraph) can still induce the *NPPA* promoter. As clearly depicted in Figure 2.26, both mutants show no effect on firefly activity, which means they are not capable of regulating the *NPPA* promoter anymore.

In summary, this leads to the conclusion that an intact (wildtype-)HD of Nkx2.2 is necessary to induce the promoter of its potential target gene *NPPA*. In particular, the highly conserved tyrosine Y181 is obviously essential for this stimulation (as it is also the case for the corresponding tyrosine of Nkx2.5, see paragraph 1.5.1.). It was further thought that the induction of *NPPA* mainly triggers the tumor suppressive effect of Nkx2.2 (discussed in paragraph 3.2.3.).

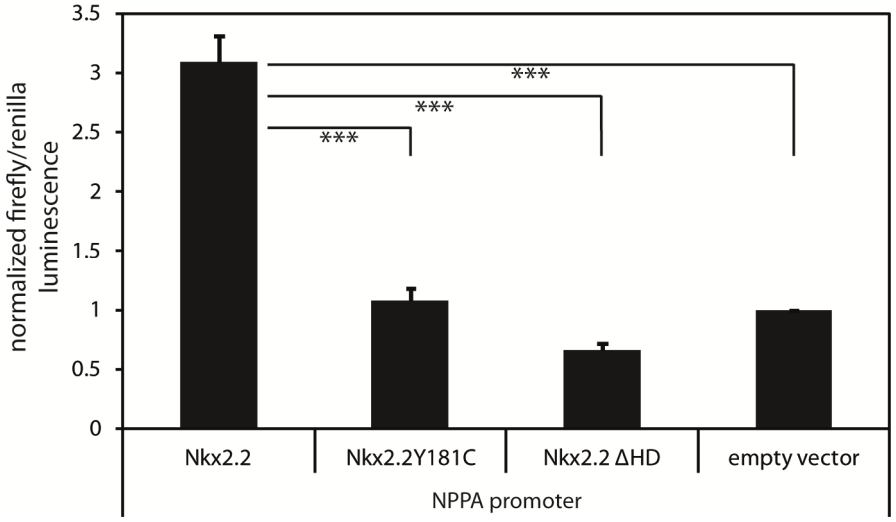

Figure 2.26: Nkx2.2 is able to induce the *NPPA* promoter. Promoter activation was examined via dual luciferase assays. The firefly luciferase reporter containing the *NPPA* promoter was co-expressed in HEK293-T cells with the indicated constructs. Only wildtype Nkx2.2 characterized by an intact HD caused an induction of the *NPPA* promoter. Significance was assessed by two-sided Student's *t*-test (*** $P < 0.001$).

3. Discussion

3.1. Characterization of CAMTA1

In this thesis, siRNAs and antibodies against CAMTA1 were generated and established as tools to study CAMTA1 in detail. The characterization of CAMTA1 involved the investigation of potential target genes and interaction partners. In this regard, an interaction between CAMTA1 and Nkx2.2 was investigated.

3.1.1. Establishment of an siRNA-mediated CAMTA1 knockdown and a potential function for alternative CAMTA1 transcripts

All siRNAs against CAMTA1 generated, led to a reduction of the CAMTA1 mRNA level. Thereby, siRNA1, 2, and 3 were the most efficient ones. The target sites for the particular siRNAs are distributed over the whole CAMTA1 mRNA. However, besides this main CAMTA1 transcript, which encodes for the full-length CAMTA1 protein, also several alternative transcripts are predicted. These, much shorter transcript variants, share either certain 5'-exons or 3'-exons with the main transcript (see also Figure 2.1. A), hereinafter termed 5'- or 3'-alternative transcripts. Additionally, most of the alternative transcripts carry unique exons. The siRNAs 1, 2, and 3, which caused the strongest decrease of the CAMTA1 mRNA level, should also target such 3'-alternative transcripts that include the respective exons 16, 17, and 20 of the main transcript (see also Figure 2.1. A).

Yet, it remains unclear if these alternative transcripts have any functional relevance. The alternative transcripts can probably emerge by alternative transcription or splicing events. Some of these transcript are predicted to encode for CAMTA1 isoforms

[according to www.uniprot.org (Q9Y6Y1) or to the UCSC genome browser]. Other transcript variants might be long non-coding RNAs since no coding sequence could be identified within these transcripts [e.g. CAMTA1 transcript variant 4 (NCBI accession number: NR_038934)].

The 3'-alternative transcripts containing also the last exon (exon 23) of the major transcript are of particular interest since this exon encodes for the CAMTA1-3'-UTR. The 3'-UTR of CAMTA1 bears several target sites for miR-9/9*, miR-17-5p, and miR-106b (*53*). Alternative transcripts involving this exon contain most likely the same functional miRNA target sites as the 3'-UTR of the main transcript. Assuming that such alternative CAMTA1 transcripts are indeed expressed, they could function as so-called "competitive endogenous RNAs" ("ceRNAs") for the above-mentioned miRNAs (and others). Such ceRNAs compete for the same set of miRNAs with other RNAs having the same miRNA target sites (*149*). For the tumor suppressor PTEN it was shown that a pseudogene called *PTENP1* is targeted by the same set of miRNAs since the 3'-UTRs of both transcripts are partly identical (*150*). In this regard, the 3'-UTR of *PTENP1* functions as a decoy for miRNAs that repress PTEN (*150*). By this de-repression mechanism of PTEN, the *PTENP1* 3'-UTR itself acts as a tumor suppressor (*150*). It has been suggested that almost any kind of RNA sharing common miRNA binding sites with another RNA can in principle function as a ceRNA (*149*). Hence, it is conceivable that some of the alternative CAMTA1 transcripts bearing the same 3'-UTR as the main mRNA act as decoy for the CAMTA1-targeting miRNAs. This would be interesting to investigate in the context of glioblastoma progression and, in particular, of glioblastoma CSCs genesis. One could speculate that these alternative transcripts might be less abundant in glioblastoma CSCs, which would, in turn, increase the repression of the CAMTA1 tumor suppressor by certain oncogenic miRNAs such as miR-9/9*.

3.1.2. Functionality of the polyclonal antibodies against CAMTA1

Two sets of antibodies against CAMTA1 were extensively tested regarding their functionality in western blot, immunoprecipitation, and immunofluorescence. In general, all antibodies can detect overexpressed mycCAMTA1 in western blot analyses. In contrast, it is rather difficult to determine if these antibodies can indeed detect endogenous CAMTA1 since basically no decrease of putative CAMTA1 bands was observed for the CAMTA1 knockdown samples. However, all knockdowns were proven to be effective on mRNA level via qRT-PCR. Therefore, one could speculate that either simply all antibodies cannot detect endogenous CAMTA1 in western blot analyses or that CAMTA1 is a very stable protein. The mRNA level generally reflects the real protein level only to a certain extent since protein stability also depends on post-translational modifications such as ubiquitination or SUMOylation. It could be that a relatively stable endogenous CAMTA1 protein pool exists which is not affected by an siRNA-mediated knockdown immediately (even when the cells were transfected with siRNAs twice, as performed for several CAMTA1 knockdowns in this thesis). However, the IF using the 1886 antibody (and probably also the IF with the purified SY6161 antibody) argues against this hypothesis since it shows a clear reduction of the detected nuclear signal in cells with knocked down CAMTA1.

Western blot, IF and IP are different experimental methods and an antibody which is useful for one of these applications is not likewise suitable for the other. In this regard, the 1886 antibody turned out to be the best antibody valuable for IFs. In contrast, the purified SY6161 antibody is probably more useful for immunoprecipitations of endogenous CAMTA1 since it precipitated CAMTA1 from HEK293-T, T98G, and LNT229 total cell lysates. Moreover, this antibody also detected enriched endogenous CAMTA1 in western blot analyses of IP samples. Furthermore, western blot analyses of HEK293-T and HeLa subcellular fractions using this antibody also revealed a band, which ran slightly lower than 180 kDa (the theoretical molecular weight of CAMTA1) and originated from the nuclear fractions of HEK293-T and HeLa cells. This is consistent with previously published western blot analyses of subcellular fractions of *Arabidopsis* aerial tissues, which showed clearly that atCAMTA1 was only present in the

nuclear fraction (*60*). The purified SY6161 antibody visualized also a band running slightly higher than 180 kDa which was present in the cytoplasmic and nuclear fractions of HEK293-T and HeLa cells. This band was also detected by the 1901 antibody with strong intensity in western blot analysis of subcellular HEK293-T fractions (and in western blot analyses of total lysates from other cell lines such as R11). It is possible that this band represents CAMTA1 which is post-translationally modified and thus is also associated with the cytoplasmic fraction. However, this is rather speculative and has to be further examined.

3.1.3. Interaction between CAMTA1 and Nkx2.2

It was shown in this thesis, that mycCAMTA1 clearly interacted with FH-Nkx2.2 when both proteins were simultaneously overexpressed in HEK293-T cells (Figure 2.14). This supports the hypothesis of an interaction between both proteins as pointed out in the working model (see paragraph 1.6.). To further identify an interaction motif, mycCAMTA1 was truncated. However, FH-Nkx2.2 was co-immunoprecipitated in basically all IPs with these constructs. For the interaction between CAMTA2 and Nkx2.5 it was shown that the interaction is mediated by the CG-1 domain and stabilized by the TAD of CAMTA2 (*61*). The corresponding region was deleted in the mycCAMTA1ΔN600 construct, but this construct still interacted with FH-Nkx2.2. Remarkably, the strongest signal observed for co-precipitated FH-Nkx2.2 was detected in western blot analysis for the co-IP by mycCAMTA1 M. In contrast, the weakest FH-Nkx2.2 signal was detected for co-IP by the mycCAMTA1 C (Figure 2.17). The mycCAMTA1 M construct consists essentially of the TIG domain only, whereas mycCAMTA1 C bears exclusively the ankyrin repeats, the CaMBD, and the IQ domain. The results of these interaction studies suggest that the TIG domain is possibly involved in the interaction between CAMTA1 and Nkx2.2 in contrast to the C-terminal CAMTA1 domains. This is further supported by previous reports for the TIG domain of NF-κB family members, which showed that this domain is also responsible for dimerization of these proteins (*71-74*). Furthermore, the TIG domain of CAMTA2

is important for the co-activation of the *NPPA* promoter in the heart and thus it was suggested that this domain is essential for the association of CAMTA2 with Nkx2.5 at the *NPPA* promoter (*61*).

However, the CAMTA1 and Nkx2.2 interaction mapping experiments must be interpreted with caution. These truncated, tagged constructs are rather artificial and it is unpredictable how these will fold within the cells. It is possible that truncated CAMTA1 variants expose certain residues or motifs which are not accessible for protein-protein interaction in the native protein. This could cause false positive co-IP results. To overcome this problem, separated units of CAMTA1 with known folding could be used for further interaction experiments. For example, the folding of the TIG domain (*71, 72*) or ankyrin repeats (*75, 78, 151*) was revealed previously. Moreover, for complementation of these interaction studies it should also be considered to include mutated versions and/or folding units of Nkx2.2. Point mutations or deletions in the particular Nkx2.2 domains affecting the potential interaction between Nkx2.2 and CAMTA1 would be interesting to examine.

Furthermore, the interaction of the endogenous proteins was investigated. These studies using LNT229 cells revealed that CAMTA1 and Nkx2.2 could not be co-immunoprecipitated for the lysates of these cells, regardless of which protein was immunoprecipitated. Several reasons for this result are conceivable: It could be possible that both transcription factors associate only with chromatin in a certain state. Interestingly, Song *et al.* pulled down a complex of (*in vitro* translated) CAMTA2 and GST-Nkx2.5 with a DNA-oligonucleotide containing the NK-response element (NKE) (*61*). This indicates that DNA might be necessary for the formation of a stable interaction between both proteins. Moreover, the interaction could be dependent on additional interaction factors which are either lost during IP or are less abundant in these LNT229 cells. Latter is indeed possible since these cells are glioma-derived cells in which the interaction between CAMTA1 and Nkx2.2 could be directly or indirectly disrupted to suppress antiproliferative effects. Nonetheless, the interaction studies were performed with these cells since LNT229 cells showed a strong nuclear signal for Nkx2.2 (see also paragraph 3.2.1.).

3.2. Characterization of Nkx2.2

Besides its potential interaction with CAMTA1, Nkx2.2 was further characterized regarding its subcellular localization in glioblastoma cells, the identification of other interaction partners, and the possible regulation by miRNAs. Moreover, this thesis provides further evidences that Nkx2.2 acts as a tumor suppressor for glioblastomas. The tumor suppressive function of Nkx2.2 and its relevance for other gliomas is more closely discussed in the last paragraph of this chapter.

3.2.1. Nuclear localization of Nkx2.2 and identification of interaction partners

Nuclear localization of Nkx2.2

Nkx2.2 is clearly localized in the nucleus of LNT229 glioma cells. This is in line with the role of Nkx2.2 as a transcription factor that localizes via its internal NLS into the nucleus (*144*). The localization of Nkx2.2 was also investigated for another glioma-derived cell line, T98G. In these cells Nkx2.2 was also detected exclusively in the nucleus, but this signal was very faint in contrast to the strong nuclear Nkx2.2 signal observed for LNT229 cells (data not shown). It needs to be further investigated, if the different expression of Nkx2.2 is due to a different linage origin of these cell lines. As discussed below, Nkx2.2 expression indeed varies between certain types of gliomas.

Search for Nkx2.2 interaction partners

To gain further insights into the cellular network, into which Nkx2.2 is probably integrated, it was intended to identify Nkx2.2 interaction partners via biochemically complex isolation, followed by mass spectrometry. However, the mass-spectrometric analysis of FH-Nkx2.2 (co-)immunoprecipitates revealed no reasonable candidate for Nkx2.2 interaction which could be further investigated (see appendix, page 151). Furthermore, neither known Nkx2.2 interaction partners nor the potential interaction partner CAMTA1 were identified in this mass spectrometry analysis. Regarding the identified proteins, it was thought that these proteins were non-specifically co-

precipitated (e.g. by an unspecific binding to the used anti-FLAG agarose). Hence, the washing conditions and/or the elution procedure probably need to be further optimized for this IP. Furthermore, co-IPs using nuclear extracts might be valuable for a more selective identification of Nkx2.2-specific interaction partners.

Nevertheless, the mass spectrometric analysis showed that Nkx2.3 was co-immunoprecipitated. Thereby, the identified peptides for Nkx2.3 were clearly distinguishable, which excludes the possibility that this result was a mass spectrometric artifact. The co-IP of Nkx2.3 is not surprising since it was reported previously that Nk-2 class protein can form heterodimers. For Nkx2.5 a heterodimerization with other Nk-2 class proteins such as Nkx2.6 and Nkx2.3 was reported before (*152*). Therefore, the identified Nkx2.3 probably resulted from heterodimerization of exogenous, overexpressed FH-Nkx2.2 and endogenous Nkx2.3 of HEK293-T cells.

3.2.2. Is Nkx2.2 regulated by miRNAs?

A computational analysis of the 3'-UTR of Nkx2.2 revealed a binding site for miR-17-5p and miR-106b, related miRNAs which have an identical seed sequence (see Figure 2.20 A and Figure 3.1). These miRNAs arise from paralogous miRNA-clusters: miR-17~92 and miR-106b~25 (*50*). As already mentioned, both miRNAs are specifically enriched in CD133-positive glioblastoma cancer stem cells (*53*). Hence, it was hypothesized in this thesis that Nkx2.2 is potentially repressed by these miRNAs in glioblastoma CSCs and that this negative regulation is in turn important for the maintenance of these cancer stem cells, as it was previously reported for CAMTA1 by Schraivogel *et al.* (*53*).

However, the validation of the miR-17-5p/miR-106b target site in the Nkx2.2 3'-UTR via dual-luciferase assay was negative since a specific inhibition of endogenous miR-17-5p, miR-106b, or both showed no de-repression of the firefly-Nkx2.2 3'-UTR reporter construct in T98G stable glioblastoma cells. Although the assay was performed in various other cell lines, a clear de-repression effect was never observed upon depletion of these particular miRNAs. *Vice versa,* an exogenous elevation of miR-17-5p and/or miR-

106b concentrations showed for the Nkx2.2. 3'-UTR reporter construct no decrease of the firefly-luciferase activities, in contrast to the positive controls (data not shown). Taken together, these results indicate that the 3'-UTR of Nkx2.2 is neither targeted by miR-17-5p nor by miR-106b.

Thus, the question was raised whether Nkx2.2 is regulated by miRNAs at all. To address this, the function of Ago proteins as key mediators of miRNA-induced gene silencing was disrupted by overexpression of a short peptide derived from TNRC6B ("T6B"). This leads to a de-repression of the reporter constructs, when they are co-expressed with T6B.

Remarkably, it was shown that the two firefly-reporter constructs bearing the CAMTA1 3'-UTR or the HMGA2 3'-UTR are both clearly de-repressed when T6B is overexpressed. The regulation of the CAMTA1 mRNA by miR-9/9* (and potentially also by miR-17-5p) was shown by Schraivogel *et al.* (*53*) and also the repression of HMGA2 by the miRNA let-7 was demonstrated previously (*148, 153*). The effectiveness of this reporter assay was on the one hand controlled by the use of a reporter construct where all let-7 sites of the HMGA2 3'-UTR were mutated. On the other hand, a mutated T6B peptide, which does not bind Ago was overexpressed. Strikingly, in both cases basically no de-repression of the reporter constructs was observed.

In contrast to the CAMTA1 or HMGA2 3'-UTR, the effect of the overexpressed peptide on the Nkx2.2-3'-UTR reporter construct was only weak, but not significant. This would imply that Nkx2.2 is not regulated by miRNAs. However, although the performed T6B peptide-assay seems to be very effective, it allows only to address the effect of endogenously expressed miRNAs of the used cell lines. In this thesis, the T6B peptide-assay was carried out with HeLa (and T98G cells). Both miR-17-5p and miR-106b, which have a predicted target site within the Nkx2.2 3'-UTR are overexpressed in HeLa cells (*154*). Hence, if these miRNAs target Nkx2.2, a de-repression of the Nkx2.2-3'-UTR reporter construct should be observed in the T6B peptide-assay with HeLa cells, which was not the case.

Interestingly, further examination of the Nkx2.2-3'-UTR by TargetScan 6.2 for additional miRNA binding sites also revealed potential binding sites for miR-26a and for miR-182 (Figure 3.1). These two miRNAs play also a role in glioblastoma progression. MiR-26a was already introduced in paragraph 1.3.2. as an oncogenic miRNA targeting the tumor suppressor PTEN (*48*). Thus, the predicted binding site also in the Nkx2.2 3'-UTR turns this miRNA to an interesting candidate for Nk2.2 regulation. An oncogenic function in glioblastomas was also reported for miR-182. This miRNA is abundant in high-grade glioblastomas and targets CYLD deubiquitinase, which is a negative regulator of the NF-κB signaling pathway (*155, 156*). In glioblastomas, this particular pathway is important for mediating the (de-regulated) EGFR signaling (*157*).

It was reported previously that miR-26a and miRNA-182 are highly expressed in HeLa as well as T98G cells (*154, 155, 158, 159*). Therefore, these particular miRNAs were presumably already included by the T6B assays performed with HeLa and T98G cells in this thesis. Still, the Nkx2.2-3'-UTR reporter was only slightly affected by the T6B overexpression in T98G cells and showed no tendency of a de-repression in HeLa, as already mentioned. However, to interpret the influence of certain miRNAs in the T6B peptide-assay, it is also important to consider that miRNA expression profiles may vary due to culture conditions or passage number of the used cell lines. Hence, the expression of particular miRNAs under assay conditions has to be experimentally assessed (e.g. by northern blot analysis).

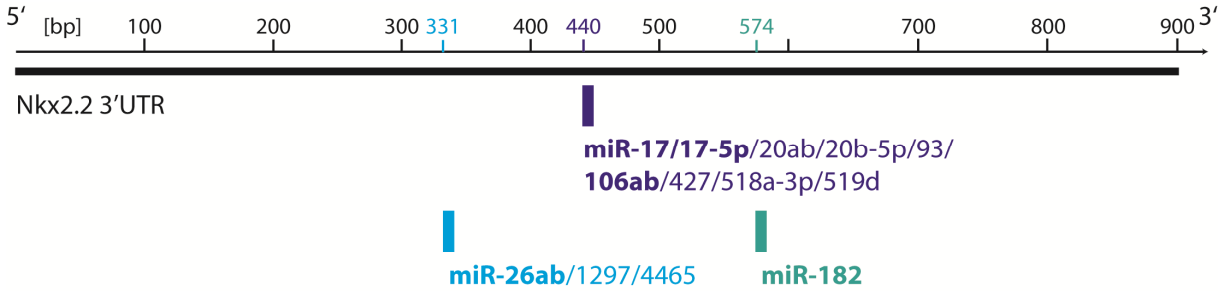

Figure 3.1: The 3'-UTR of Nkx2.2 has additional binding sites for miR-26a and miR-182. Both miRNAs act as oncogenes for glioblastomas. Illustration based on analysis via TargetScan 6.2.

To conclude, the results of the T6B peptide assay must be construed carefully. On the one hand this reporter assay is efficient, but on the other hand it is to some extent artificial and provides no information about the identities of the targeting miRNAs. Moreover, due to the overexpression of the reporter, a potential regulation by endogenously low expressed miRNAs can hardly be detected by de-repression reporter assays.

An alternative, more informative and sensitive approach to investigate a potential regulation of Nkx2.2 by miRNAs is the CLIP (cross-linking immunoprecipitation) method, in particular PAR-CLIP (photoactivatable-ribonucleoside-enhanced CLIP). For PAR-CLIP, nascent RNA molecules like mRNAs are labeled by photoactivatable ribonucleosides such as 4-thiouridine (4-SU) (*160, 161*). Thereafter, RNA-binding proteins such as Ago are crosslinked to the 4-SU labeled transcripts by UV-light. The crosslinked complexes are subsequently immunoprecipitated by Ago-specific antibodies, the RNA is recovered and used for the generation of cDNA libraries, which can be analyzed by deep sequencing. At the crosslinked site, a characteristic thymine to cytosine mutation can be observed frequently (*160, 161*). Finally, the sequencing reads can be aligned to a known sequence, in this case the Nkx2.2 3'-UTR. This method reflects the native status of a 3'-UTR of interest more accurately. It would be an alternative possibility to validate predicted miRNA binding sites in the Nkx2.2-3'-UTR and to identify new sites beyond these. However, this method is technically challenging and cost-intensive.

3.2.3. Function of Nkx2.2 as a tumor suppressor for gliomas

Nkx2.2 causes an antiproliferative effect

As shown in the results, the overexpression of Nkx2.2 had a clear antiproliferative effect on LNT229 glioma cells. This further supports the assumption of Nkx2.2 as a tumor suppressor for glioblastomas. An intact HD of Nkx2.2 is obviously necessary to cause the observed antiproliferative effect, although the phenotype of the Nkx2.2Y181C mutant was not as strong as that of the Nkx2.2ΔHD, which lacks the entire HD. The

phenotype for the latter mutant is not surprising since it is most likely unable to bind DNA and can therefore not cause a transcriptional response. Furthermore, the HD of Nkx2.2 carries two nuclear localization signals, both of which are necessary for an efficient localization of Nkx2.2 into the nucleus (*144*). Therefore, the Nkx2.2ΔHD deletion mutant should not even enter the nucleus. In contrast, the Nkx2.2Y181C mutant can probably still localize to the nucleus since the two NLS are likely not affected by this point mutation. Yet, the highly conserved tyrosine Y181 of Nkx2.2 is presumably responsible for specific NKE recognition, as it was shown for the corresponding tyrosine of Nkx2.5 (*115*). Therefore, it was suggested that the transcriptional regulation of the Nkx2.2Y181C mutant is disrupted.

However, for Nkx2.5 it is known that it binds as a homodimer to DNA (*115, 152*). This dimerization involves the HD and is also mediated by the C-terminus of Nkx2.5 (*152*). Thereby, two conserved residues at the C-terminal end of the HD, K194 and R195, are essential for dimerization (*152*). Consistently, the Y181C mutation in HD of Nkx2.2 would most likely not impair a potential dimerization of Nkx2.2 because it does not affect the critical residues (K184 and R184 in Nkx2.2). Hence, it is conceivable that a dimerization can occur not only between two Nkx2.2Y181C mutants, but also between the mutant and endogenous Nkx2.2. This heterodimer is possibly capable to interact with NKE sites of target genes due to the intact HD of the endogenous protein. Moreover, other factors, which are required for target activation could still be recruited by this heterodimer. All in all, this might cause a transcriptional response, which would give a plausible explanation for the weaker phenotype observed for Nkx2.2Y181C in comparison to the deletion mutant. Furthermore, for Nkx2.2 an additional recognition sequence was reported (5'-GAGT-3') (*111*). It remains unknown if the mutation of the tyrosine, which is critical for the NKE binding also affects the recognition of this alternative target site.

Interestingly, the antiproliferative effect of Nkx2.2 was recently also observed upon Nkx2.2 overexpression in mouse oligodendrocytes: The elevated Nkx2.2 levels significantly decreased cell proliferation of oligodendrocyte precursors in the developing spinal cord, but did not affect survival of these cells (*133*).

It would be of further interest to investigate how the other Nkx2.2 domains contribute to the observed antiproliferative phenotype. Therefore, the effect of mutations/deletions in the Nk-SD (which was suggested to be an interaction platform), in the TAD, and in the transcriptional repression domain (TD) should be examined. Latter would be of particular interest since several studies reported that Nkx2.2 acts as transcriptional repressor as well (*131, 133, 135, 136, 141*). Consistently, it has been suggested that the antiproliferative effect of Nkx2.2 on oligodendrocyte precursors is due to direct repression of *Pdgfra* (Pdgf receptor α), which impairs Pdgf signaling (*133*).
However, in this thesis it was assumed that the antiproliferative phenotype of Nkx2.2 is caused by transcriptional activation, in particular by activation its potential target gene *NPPA* (cf. the working model in paragraph 1.6.).

NPPA as a target gene of Nkx2.2

Notably, an overexpression of Nkx2.2 in LNT229 glioma cells caused an elevation of the mRNA level of NPPA (Figure 2.25 C). Furthermore, a strong induction of the *NPPA* promoter by wildtype Nkx2.2 was demonstrated via dual luciferase assays in HEK293-T cells (Figure 2.26). In contrast, the Nkx2.2ΔHD deletion mutant and Nkx2.2Y181C did not activate the *NPPA* promoter anymore. For the deletion mutant this result is not surprising. However, for the Nkx2.2Y181C mutant is was speculated above that it possibly still can dimerize with endogenous Nkx2.2 and thus affect Nkx2.2 targets to some extent. This was not observed in the luciferase reporter assays in HEK293-T cells, but is possibly reflected by the qRT-PCR quantification for NPPA mRNA levels upon Nkx2.2Y181C overexpression in LNT229 cells. The latter revealed that this mutant also elevated the NPPA mRNA levels, but less strong than the wildtype protein and in contrast to the deletion mutant. This is consistent with the observed weaker antiproliferative phenotype of this mutant compared to the deletion mutant.
Nevertheless, this thesis further supports the hypothesis that *NPPA* is a potential target gene for Nkx2.2. As already mentioned before, *NPPA* encodes for the precursor of the atrial natriuretic peptide (ANP), which is a secreted peptide hormone (*124, 162*). ANP

is an essential hormone for the regulation of renal NaCl reabsorbtion. It is produced and secreted by the myoendocrine cells of the heart (*124, 162*). However, ANP acts not only as an endocrine hormone but is also an important autocrine/paracrine factor for heart (*124*) as well as for brain development and function (*163-166*). In particular, the expression of ANP and ANP receptors was also detected in various types of mammalian glia cells and it was suggested that ANP is relevant for glia cell biology (*166*).

Interestingly, it was shown previously that ANP has an antiproliferative effect on mammalian astrocytes *in vitro* (*167*) and also on various types of human cancer cells like colon adenocarcinoma (*168*), prostate carcinoma (*169*), small-lung cancer (*170*), pancreatic cancer (*171*) as well as glioblastoma cells (*143*). ANP signaling is mainly transmitted via the receptor NPR-A, which is embedded in the plasma membrane and is characterized by an external ANP-binding and an internal guanylate cyclase domain. The activation of NPR-A results in the catalytic conversion of GTP to cyclic GMP (cGMP) by the intrinsic guanylate cyclase domain (*162, 172*). Cyclic GMP is a second messenger, which induces a signaling cascade involving the inhibition of certain signaling pathways within in the cell (*172*). In this regard, cGMP efficiently inhibits kinases of the Ras-MEK1/2-ERK1/2-signaling pathway, as previously shown for prostate cancer (*173-175*). Signaling via this pathway is also increased by overexpressed EGFR during the progression of glioblastomas (*17*). Besides the inhibition of the Ras-MEK1/2-ERK1/2-signaling pathway, ANP signaling via NPR-A and cGMP represses various other signaling pathways (or the crosstalk between certain pathways) which are often de-regulated in cancer, for example AKT- or STAT3-signaling (*172*). Interestingly, STAT3 was reported previously to be an important factor which maintains the stem cell abilities of glioblastoma CSCs (*176*). Therefore, it is conceivable that ANP-signaling also has a negative effect on these cancer stem cells.

In this thesis, an increase of the NPR-A mRNA level upon Nkx2.2 overexpression in LNT229 cells was not observed. However, it was shown by Schraivogel *et al.* that CAMTA1 overexpression in LNT229 caused a drastic elevation of the NPR-A expression (*53*). Moreover, this overexpression increased also the NPPA mRNA levels (*53*) to a similar extent as measured in this thesis for Nkx2.2 overexpression. This

suggests a collaborative network between both proteins in which they interact to activate NPPA and CAMTA1 additionally leads to an increased expression of the ANP receptor. Such a collaboration is possibly required for efficient ANP signaling to cause a tumor suppressive effect and needs to be further investigated.

Nkx2.2 in cancer biology: A two-sided protein?

The data of this thesis confirm the previous results of Muraguchi *et al.* showing that Nkx2.2 can significantly repress the formation of neurosphere-like clones when it is overexpressed in primary glioblastoma cells. However, the mutants Nkx2.2Y181C and Nkx2.2ΔHD also reduced the neurosphere formation of ZH161 cells to some extent (Figure 2.23). Thereby, Nkx2.2ΔHD reduced neurosphere-like colonies less than the wildtype and the Nkx2.2Y181C mutant. Since this result reflects only two biological replicates, it is not significant and does not allow a final conclusion. Hence, the neurosphere assays including these Nkx2.2 mutants need to be continued to get a statistically more reliable result. As for the proliferation assay, one would expect no phenotype for the Nkx2.2ΔHD since it cannot (most likely) localize to the nucleus, bind DNA, and should therefore not cause any transcriptional response. In contrast, the Nkx2.2Y181C mutant possibly still causes a reduction of neurosphere formation, which might arise from the same effect already discussed for the proliferation assays.

The idea of Nkx2.2 as tumor suppressor in glioma biology was further supported by the analysis of patient survival data obtained from the REMBRANDT database. Strikingly, this analysis revealed a significantly higher survival rate for glioma patients with increased Nkx2.2 expression (Figure 2.24 A).

However, the relevance for Nkx2.2 regarding glioma progression remains to be discussed and further investigated. As already mentioned in the introduction (see paragraph 1.2.), Verhaak *et al.* classified glioblastomas into four distinct subtypes by their specific expression profiles (classical, mesenchymal, proneural, and neural) (*18*). Remarkably, Verhaak *et al.* further reported a high gene expression of *Nkx2.2* (as well as *Olig2*) for the proneural subtype, which is mainly characterized by an amplification of *Pdgfra* (*18*). Moreover, it was shown that most secondary glioblastomas are of the

proneural subtype (*18*). Secondary glioblastoma arise from lower-grade gliomas such as astrocytomas or oligodendrogliomas. On the other side, it is known that most glioblastomas are primary glioblastomas, i.e. they emerge *de novo*. Interestingly, Muraguchi *et al.* examined also the expression of Nkx2.2 in high-grade gliomas (glioblastomas) *versus* lower-grade gliomas (anaplastic astrocytomas and anaplastic oligodendrogliomas) via immunostaining: Whereas Nkx2.2 was clearly expressed in lower-grade gliomas, it was not detectable in most of the glioblastoma samples (*142*). However, analysis of microarray data obtained from the REMBRANDT database revealed no significant difference in Nkx2.2 expression between astrocytomas, glioblastomas and normal brain tissue (Figure 2.24 B). Additionally, Nkx2.2 expression was previously reported to be higher in grade II and III oligodendrogliomas than in astrocytomas or glioblastomas (*177*).

Taken together, one could speculate that there is a connection between the malignancy of gliomas on the one hand and Nkx2.2 expression on the other hand. Expression of Nkx2.2 could indicate a lower malignancy of the glioma since it is obviously expressed in lower-grade gliomas (or secondary glioblastomas that emerged from lower-grade gliomas). In contrast, Nkx2.2 is weakly expressed in high-grade, primary glioblastomas. Furthermore, it was shown previously that primary glioblastoma also contain significantly more CSCs, in particular CD133-positive cells, than secondary glioblastomas (*26*). Therefore, it is not unlikely that Nkx2.2 expression has an negative effect on the genesis of CSCs. The results of this thesis showing that Nkx2.2 can suppress the formation neurosphere-like colonies and of Muraguchi *et al.* support this hypothesis. A direct effect of Nkx2.2 on the CD-133 population would be interesting to investigate in further experiments.

Remarkably, Nkx2.2 also suppresses the expression of *Pdgfra* via direct regulation of its promoter (*133*). This is essential during oligodendrocyte development. However, de-regulated *Pdgfra* signaling is also frequently associated with glioblastoma progression (*16, 17*). As pointed out above, the proneural subtype is characterized by *Pdgfra* amplification and elevated Nkx2.2 expression. The higher Nkx2.2 expression observed for this subtype is probably due to the origin of these glioblastomas: Proneural

glioblastomas are often also classified as secondary glioblastomas. These arise presumably from a lower-grade glioma in which Nkx2.2 is expressed at higher levels, e.g. an oligodendroglioma. It is further possible that in lower-grade gliomas Nkx2.2 counteracts Pdgfra expression by direct repression. This could be beneficial for the lower malignancy and an interruption of this repression promotes probably the progression of a secondary, proneural glioblastoma. Consistently, this would further support the correlation between Nkx2.2 expression and glioma malignancy.

This thesis showed further evidence that the transcriptional activator Nkx2.2 has tumor suppressive abilities, at least for glioblastoma. In contrast, it was also reported that Nkx2.2 is necessary for oncogenic transformation in Ewing's sarcoma, a highly aggressive bone-associated tumor. In this type of tumor, Nkx2.2 is up-regulated by the EWS/FLI fusion protein which frequently occurs in Ewing's sarcoma (*178*). Furthermore, Nkx2.2 functions as a transcription repressor in this kind of tumor for which its TN domain (transcriptional repression domain) is essential (besides the HD and Nk-2 SD) (*179*). Thereby, this repression is probably caused by the recruitment of histone deacetylases (*179*), most likely in a similar manner as Nkx2.2 represses *MBP* or *Sirt2* during oligodendrocyte development (*135, 136*) (see also paragraph 1.5.2.).
Since Nkx2.2 carries both a transcriptional activation and repression domain, it is not surprising that it can act in two ways. The prevailing response depends most likely on the cellular context and, in this regard, on the Nkx2.2 interactome.
Besides, it is common for an Nk-2 class protein that it can act both as a tumor suppressor and as an oncogene. Nkx2.1 was previously reported to be a tumor suppressor (*180, 181*) as well as an oncogene (*182*) during lung cancer progression (summarized in (*183*)). Lung cancer is very heterogeneous and it has been suggested that Nkx2.1 can act in these two ways depending on the cellular origin.

Taken together, Nk-2 class proteins are indeed two-sided proteins. This is reflected by the presence of functional repression and activation domains and their oppositional roles during cancer progression. The role of Nk-2 class proteins in cancer development shows exemplary that cancer biology is extremely complex and diverse – not only for tumors

emerging from different tissues, but even for tumors occurring in the same organ. Hence, for the development of new therapy approaches, in particular of personalized therapies, it is important to know from which cellular linage one particular tumor originates and how this is reflected by the specific alterations in the genome, transcriptome, and interactome of certain key molecules, so called "biomarkers". Consequently, the identification and characterization of such biomarkers is highly relevant for personalized cancer medicine and patient-adapted therapies become more and more important due to the increasing understanding of the molecular-pathological diversity of many cancer types including glioblastomas. During the recent years, biomarkers for the various glioblastoma subtypes have been studied extensively, aiming to identify potential therapeutic targets for this highly malignant cancer type (*17, 18, 184*). In this context, a further characterization of the Nkx2.2 cellular interaction network will be beneficial to develop targeted treatment strategies. A current draft of this network is described in the following paragraph.

3.3. Expanding the working model

This thesis further supports the concept of an interaction between the two transcription factors CAMTA1 and Nkx2.2, which was hypothesized for tumor suppression of glioblastomas. Furthermore, this thesis and previous findings of Schraivogel *et al.* reveals *NPPA* as a potential target for CAMTA1/Nkx2.2. Analogous to the collaboration of CAMTA2 and Nkx2.5 in the heart, it is likely that CAMTA1 co-activates the *NPPA* promoter together with Nkx2.2 as well. In turn, the induction of *NPPA* is probably responsible for the antiproliferative effect caused by these tumor suppressors. This is supported by the previously reported observation that ANP signaling via its main receptor NPR-A negatively affects proliferation of various types of cancer cells. Moreover, this expanded model, which is illustrated in Figure 3.2, might be an important pathway to suppress the formation of high-malignant glioblastoma CSCs. Certain de-regulated factors such as miR-9/9* counteract this pathway which in turn promotes cancer progression and the maintenance of glioblastoma CSCs. However, several aspects of this model still need to be proven experimentally, in particular those regarding the impact on glioblastoma CSCs.

Nevertheless, this model reflects likely cellular mechanisms, which are important for a further understanding of cancer biology in general and glioblastoma CSCs biology in particular.

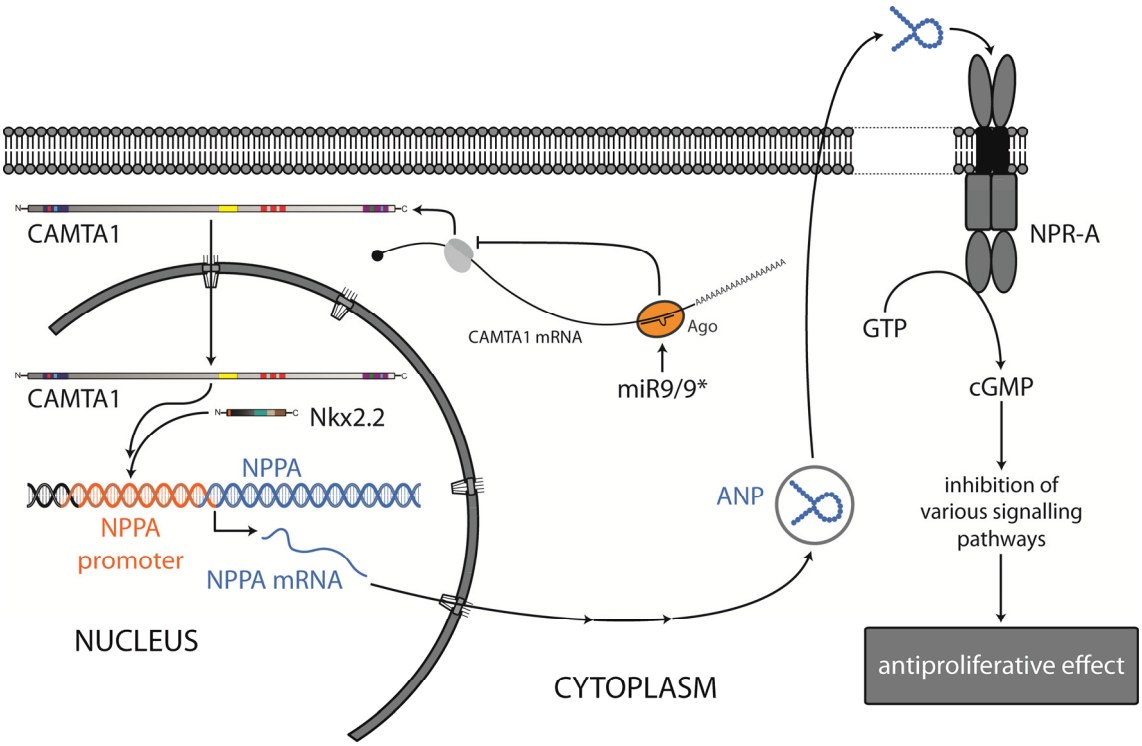

Figure 3.2: Expanded working model. The activation of NPPA by a cooperation of CAMTA1 and Nkx2.2 leads to a secretion of ANP. This peptide hormone acts in autocrine/paracrine manner to stimulate signaling via its receptor NPR-A. Activation of NPR-A causes in turn the conversion of GTP to cGMP, a secondary messenger which inhibits various intracellular signaling pathways. This inhibition finally leads to an antiproliferative effect on cancer cells.

4. Material and Methods

4.1. Materials

4.1.1. Consumables and Chemicals

If not indicated else wise, all used chemicals were purchased from Carl Roth (Karlsruhe, Germany), Merck (Darmstadt, Germany), AppliChem GmbH (Darmstadt, Germany), Sigma-Aldrich (Steinheim, Germany), Roche Diagnostics (Penzberg, Germany), GE Healthcare (Buckinghamshire, UK), Bio-Rad (Hercules, USA) Calbiochem-Behring (La Jolla, USA), Thermo Fischer Scientific (Waltham, USA), and USB Corporation (Cleveland, USA) at the highest degree of purity.

Nucleotides, double stranded DNA-ladders, and molecular weight markers were procured from Thermo Fischer Scientific.

Kits and the applications for which they were used are stated in Table 4.1.

Table 4.1: Used kits listed with the corresponding application.

kit	company	application
Amaxa® Cell Line Nucleofector® Kit R	Lonza (Cologne, Germany)	transfection of human LNT229 cells
Amaxa® Mouse Neural Stem Cell Nucleofector® Kit	Lonza	transfection of human primary R11 cells
First-Strand cDNA Synthesis Kit	Thermo Fischer Scientific	cDNA synthesis
iScript™ cDNA Synthesis Kit	Bio-Rad	cDNA synthesis
NucleoBond®-Xtra-Midi	MACHEREY-NAGEL (Düren, Germany)	plasmid purification, large scale
NucleoSpin®-Extract	MACHEREY-NAGEL	DNA purification from agarose gel slices, PCRs reactions or other enzymatic reactions
NucleoSpin®-Plasmid	MACHEREY-NAGEL	plasmid purification, small scale
NucleoSpin®-RNA	MACHEREY-NAGEL	RNA purification
pGEM®-T Easy vector system	Promega (Fitchburg, USA)	molecular cloning

4.1.2. Buffers

For each method the composition of the respective buffer(s) is specified and listed there.

4.1.3. Enzymes

Restriction enzymes were obtained either from Thermo Fischer Scientific or New England Biolabs (Ipswich, USA). For each construct generated in this thesis, the corresponding restriction enzymes used for molecular cloning is listed in Table 4.4, paragraph 4.1.6.

All other enzymes were purchased from Thermo Fischer Scientific, unless mentioned otherwise.

4.1.4. DNA-oligonucleotides

All used DNA-oligonucleotides were synthesized by Metabion (Martinsried, Germany). DNA-oligonucleotides used for quantitative real-time PCR are listed in Table 4.2, for molecular cloning and sequencing in Table 4.3 (pages 94 to 96).

Table 4.2: DNA-oligonucleotides used as primers for qRT-PCR. The particular NCBI accession numbers of the targets, the targeted exons, and the amplicon lengths (AL) are stated as indicated. [fwd.: forward primer (p), rev.: reverse primer]

designation	sequence (5‘ to 3‘)	target (NCBI accession number)	exon	AL [bp]
CAMTA1 p1 fwd.	GAGAGGCACCGCTGGAACACTAATGAG	CAMTA1 (NM_015215.2)	3	125
CAMTA1 p1 rev.	GAGTATCATTGAGCCATTCTGTGGTCTTG	CAMTA1	5	
CAMTA1 p2 fwd.	AGGTGGTTAGCCATTCTTCG	CAMTA1	3	146
CAMTA1 p2 rev.	TGTCTGCCGAAATGTTCAAG	CAMTA1	4	
CAMTA1 p3 fwd.	CTGCTGTGCTCATCCAAAAG	CAMTA1	20	140
CAMTA1 p3 rev.	TTTTCGAGCAGCTTGATCCT	CAMTA1	21	
GAPDH fwd.	TGGTATCGTGGAAGGACTCATGAC	GAPDH (NM_002046.5)	7	189
GAPDH rev.	ATGCCAGTGAGCTTCCCGTTCAGC	GAPDH	8	
Nkx2.2 fwd.	GCCCGAGCCAGCCAAGAGG	Nkx2.2 (NM_002509.3)	1	159
Nkx2.2 rev.	GCCAGACCGTGCAGGGAGTA	Nkx2.2	2	
NPPA fwd.	CAGGATGGACAGGATTGGA	NPPA (NM_006172.3)	2	64
NPPA rev.	TCTTCAGTACCGGAAGCTGTT	NPPA	3	
NPR-A fwd.	TCGAAACCACCAAACTCCTC	NPR-A (NM_000906)	20	147
NPR-A rev.	AGTGGTGGGACTGAAGATGC	NPR-A	21	
β-Actin fwd.	GGACTTCGAGCAAGAGATGG	β-Actin (NM_001101.3)	2	138
β-Actin rev.	AGGAAGGAAGGCTGGAAGAG	β-Actin	2	

Table 4.3: DNA-oligonucleotides used for molecular cloning and sequencing. The particular primer melting temperatures (T_m), sites for restriction enzymes (RE), and corresponding applications are stated as indicated (fwd.: forward primer, rev.: reverse primer, S.: sense, AS.: antisense).

designation	sequence (5‘ to 3‘)	T_m [°C]	application (RE)
CAMTA1 AscI rev.	ATACGGCGCGCCTCAAGTTCCTTGGCCTTTTTCAATTCTTTCACTCC	81.5	cloning (*Asc*I)
CAMTA1 C-term. FseI fwd.	ATATGGCCGGCCATGTGGGCGAAGTCCAAGCACTTG	80	cloning (*Fse*I)
CAMTA1 C-term. fwd.	TGGGCGAAGTCCAAGCACTTGATCC	69.1	cloning
CAMTA1 FseI fwd.	ATATGGCCGGCCATGTGGCGCGCGGAGGGGAAATG	82.4	cloning(*Fse*I)
CAMTA1 M AscI rev.	ATACGGCGCGCCTCAGCAGGCTCGGCTCATCATC	81.3	cloning (*Asc*I)
CAMTA1 M FseI fwd.	ATATGGCCGGCCATGCAGACGGGCCACAGCCC	81.5	cloning (*Fse*I)
CAMTA1 N-term. 600 rev.	GCTGAAGCTGGACGTGTAGTCCTTG	69.1	cloning
CAMTA1 seq. 1215 fwd.	GTGTTCATGTCAGAGGTCACC	61.3	sequencing
CAMTA1 seq. 1861 fwd.	GAGCTTCTTCCTGCAGGACG	62.5	sequencing
CAMTA1 seq. 2508 fwd.	CCTGCAGCTGAGCAGCTCG	63.8	sequencing
CAMTA1 seq. 3185 fwd.	GCACTTGATCCACTCAAAGAC	59.4	sequencing
CAMTA1 seq. 3805 fwd.	CCACTGCACTGAGTCTGGAAG	63.3	sequencing
CAMTA1 seq. 4316 fwd.	CATTAGCAGTACAATGAGCTG	57.4	sequencing
CAMTA1 seq. 537 fwd.	GACATCGTCCTGGTGCACTAC	63.3	sequencing
CAMTA1-F3 BamHI TEV fwd.	CCAGGATCCGAAAACCTGTATTTTCAGGGAGTGTCTACAGTACAGGTGACTGG	70.6	cloning (*Bam*HI); introducing TEV protease cleavage site
CAMTA1-F3 SalI rev.	ATATGTCGACTCAACTGACGGGAGAGCCAAC	73.6	cloning (*Sal*I)
CAMTA1 ΔN FseI fwd.	ATATGGCCGGCCATGGGCAAGCCTTGCGGCCCCATC	83.5	cloning (*Fse*I)
CAMTA1 ΔN600 FseI fwd.	ATATGGCCGGCCATGCAGACGGGCCACAGCCC	81.5	cloning (*Fse*I)

Table continued on next page

designation	sequence (5‘ to 3‘)	T_m [°C]	application (RE)
CAMTA ΔC AscI rev.	ATACGGCGCGCCTCAGAAAGTCTTTGAGTGGATCAAGTGCTTG	80.8	cloning (*AscI*)
CMV promoter seq. fwd.	CGCAAATGGGCGGTAGGCGTG	67	sequencing
M13 seq. fwd.	TGTAAAACGACGGCCAGT	53.8	sequencing
M13 seq. rev.	CAGGAAACAGCTATGACCATG	59.4	sequencing
miR106b target site AS	CCTGGAGTGCGTAGGTCTAATTAAAGTGCTGACAGTGCAGATGGCTTAAACAAGGTGGCGATA	-	Cloning, full complementary miR-106b target site (5': *Spe*I; 3': *Sac*I)
miR-106b target site S	CTAGTATCGCCACCTTGTTTAAGCCATCTGCACTGTCAGCACTTTAATTAGACCTACGCACTCCAGGAGCT	-	cloning, full complementary miR-106b target site (5': *Spe*I; 3': *Sac*I)
miR-17 target site S	CTAGTATCGCCACCTTGTTTAAGCCCTACCTGCACTGTAAGCACTTTGATTAGACCTACGCACTCCAGGAGCT	-	cloning, full complementary miR-17 target site (5': *Spe*I; 3': *Sac*I)
miR-17 target site AS	CCTGGAGTGCGTAGGTCTAATCAAAGTGCTTACAGTGCAGGTAGGGCTTAAACAAGGTGGCGATA	-	cloning, full complementary miR-106b target site (5': *Spe*I; 3': *Sac*I)
Nkx2.2 3'UTR fwd.	AGTACAACGCCCAGTACAG	57.3	cloning (nested PCR)
Nkx2.2 3'UTR NaeI rev.	ACACGCCGGCTTTTAAACACAGGATTTTTATTAAAATTC	71.5	cloning (*NaeI*)
Nkx2.2 3'UTR rev.	TTTTAAACACAGGATTTTTATTAAAATTC	57.7	cloning (nested PCR)
Nkx2.2 3'UTR SpeI fwd	ATATACTAGTGCGCCGCCCCAACGAGAC	73	cloning (*SpeI*)

Table continued on next page

designation	sequence (5‘ to 3‘)	T_m [°C]	application (RE)
Nkx2.2 3'UTR[mut] fwd.	AAAGCAAGTGGAGAAGGATCCAAAAATACAGAGAATTTC	72.6	cloning; site-directed mutagenesis
Nkx2.2 3'UTR[mut] rev.	GAAATTCTCTGTATTTTTGGATCCTTCTCCACTTGCTTT	72.6	cloning; site-directed mutagenesis
Nkx2.2 BamHI fwd.	ATACGGATCCATGTCGCTGACCAACACAAAGAC	74	cloning (*Bam*HI)
Nkx2.2 BamHI rev.	ATACGGATCCTCACCAAGTCCACTGCTG	72	cloning (*Bam*HI)
Nkx2.2 C-term. fwd.	GCCGAGAAAGGTATGGAGGTG	63.3	cloning
Nkx2.2 EcoRV fwd.	ATACGATATCATGTCGCTGACCAACACAAAGAC	71	cloning (*Eco*RV)
Nkx2.2 NotI fwd.	ATATGCGGCCGCATGTCGCTGACCAACACAAAG	76.4	cloning (*Not*I)
Nkx2.2 N-term. rev.	CTTGCCGGCGTCCCC	57	cloning
Nkx2.2 Y181C [mut] fwd.	TTCCAGAACCACCGCTGCAAGATGAAGCGCGCC	78.9	cloning; site-directed mutagenesis
Nkx2.2 Y181C [mut] rev.	GGCGCGCTTCATCTTGCAGCGGTGGTTCTGGAA	78.9	cloning; site-directed mutagenesis
pGEX seq. fwd.	GGGCTGGCAAGCCACGTTTGGTG	70	sequencing
pGEX seq. rev.	GGAGCTGCATGTGTCAGAG	59.5	sequencing
pIRES/VP5 seq. rev.	CCCAACAGCTGGCCCTCGCAGA	69.6	sequencing
T7 promoter seq. fwd.	TAATACGACTCACTATAGGG	54	sequencing

4.1.5. RNA-oligonucleotides

The used RNA-oligonucleotides were synthesized either at the Max-Planck Institute for Biochemistry (Martinsried, Germany) or by Metabion and are listed in Table 4.4.

Table 4.4: RNA-oligonucleotides. The particular oligonucleotides are stated with their corresponding targets in the case of siRNAs and miRNA inhibitors (S: sense, AS: antisense, r: ribose, d: desoxyribose, 2'-OMe: 2'-O-methylated).

designation	S/AS	sequence (5‘ to 3‘)	target (exon)	comment; application
CAMTA1 si1	S	r(CUACCGAAGUUAUAAGAAAU)dT	CAMTA1 (20)	siRNA; RNAi
CAMTA1 si1	AS	r(UUUCUUAUAACUUCGGUAGU)dT	CAMTA1 (20)	siRNA; RNAi
CAMTA1 si2	S	r(CCAAAUAUCAGGAAGCAAAU)dT	CAMTA1 (16)	siRNA; RNAi
CAMTA1 si2	AS	r(UUUGCUUCCUGAUAUUUGGC)dT	CAMTA1 (16)	siRNA; RNAi
CAMTA1 si3	S	r(CCAAAUAUCAGGAAGCAAAU)dT	CAMTA1 (16)	siRNA; RNAi
CAMTA1 si3	AS	r(AAAUUCUCCUGCUUGAUUCG)dT	CAMTA1 (16)	siRNA; RNAi
CAMTA1 si4	S	r(CCCGACUGUUUCCUUAAUAUU)	CAMTA1 (16)	siRNA; RNAi
CAMTA1 si4	AS	r(UAUUAAGGAAACAGUCGGGUU)	CAMTA1 (16)	siRNA; RNAi
CAMTA1 si5	S	r(GCCGAAAUGUUCAAGUUUA)dTdT	CAMTA1 (16)	siRNA; RNAi
CAMTA1 si5	AS	r(UAAACUUGAACAUUUCGGC)dTdT	CAMTA1 (16)	siRNA; RNAi
siNkx2.2	S	r(CGCCGUGUUUACAGAAUGU)dTdT	Nkx2.2	siRNA; RNAi
siNkx2.2	AS	r(ACAUUCUGUAAACACGGCG)dTdT	Nkx2.2	siRNA; RNAi
UNBIAS	S	r(UUGUCUUGCAUUCGACUAAU)dT	no target	ctrl. siRNA; RNAi
UNBIAS	AS	r(UUAGUCGAAUGCAAGACAAU)dT	no target	ctrl. siRNA; RNAi
miR-17-5p	S	r(CAAAGUGCUUACAGUGCAGGUAG)dT	-	hsa-miR-17-5p mimic; miR binding site validation
miR-17-5p	AS	r(UACCUGCACUGUAAGCACUUUGU)dT	-	hsa-miR-17-5p mimic; miR binding site validation

Table continued on next page

designation	S/AS	sequence (5‘ to 3‘)	target (exon)	comment; application
miR-106b	S	r(AAAAGUGCUUACAGUGCAGGUAG)dT	-	hsa-miR-106b mimic; miR binding site validation
miR-106b	AS	r(UACCUGCACUGUAAGCACUUUUU)dT	-	hsa-miR-106b mimic; miR binding site validation
miR-122a	S	r(AACGCCAUUAUCACACUAAAUA)dT	-	hsa-miR-122 mimic; miR binding site validation
miR-122a	AS	r(UGGAGUGUGACAAUGGUGUUUG)dT	-	hsa-miR-122 mimic; miR binding site validation
miR-17-5p inihb.	AS	r[2'-OMe](ACUACCUGCACUGUAAGCACUUUG)dT	hsa-miR-17-5p	inhibition of human miR-17-5p; miR binding site validation
miR-106b inhib.	AS	r[2'-OMe](AUCUGCACUGUCAGCACUUUA)dT	hsa-mir106b	inhibition of human miR-106b; miR binding site validation
miR-122a inhib.	AS	r[2'-OMe](ACAAACACCAUUGUCACACUCCA)dT	hsa-miR122a	inhibition of human liver specific miR-122; miR binding site validation

4.1.6. Plasmids

Table 4.5 contains all plasmids and constructs that were already available at the beginning of this thesis in the department Biochemistry I (University of Regensburg). All used plasmids contain the sequence encoding for the ampicillin resistance gene.

Table 4.5: Used plasmids. The here listed plasmids were available at Biochemistry I, University of Regensburg. For each plasmid the particular promoter(s) [upstream of insert(s)], inserts, sequences for protein tags (if encoded), and applications are stated as indicated.

designation	promoter	insert (NCBI accession number)	sequence for protein tag	application/comment
pCS2	CMV	empty	N-terminal 6 × myc tag	eukaryotic expression vector
pCS2-Ago2	CMV	Argonaute 2	6 × myc tag	over expression of myc-Ago2
pCS2-Dicer	CMV	Dicer	6 × myc tag	over expression of myc-Dicer
pCS2-TOE1	CMV	Toe 1	6 × myc tag	over expression of myc-Toe1
pCS2-XP5	CMV	Exportin 5	6 × myc tag	over expression of myc-Exportin5
pGEM®-T easy	T7	-	-	sub-cloning vector
pGEX-6p1	tac	empty	N-terminal GST tag	bacterial expression vector
pGL3 basic	-	firefly luciferase	-	luciferase assay (promoter regulation)
pGL3-NPPA-P	NPPA	firefly luciferase	-	luciferase assay (promoter regulation)
pIRES-CAMTA1	CMV	CAMTA1 (NM_015215.2)	-	over expression of wild type CAMTA1 in human cell lines
pIRES-CAMTA1ΔN	CMV	CAMTA1ΔN aa 1 to 188 deleted	-	over expression of CAMTA1ΔN (N-terminal deletion mutant)
pIRESpuro-3	CMV	empty	-	eukaryotic expression vector
pMIR-CAMTA1-3'UTR	HSV-TK (firefly) SV40 (renilla)	firefly+CAMTA1-3'UTR; renilla	-	luciferase assay (miRNA binding site validation)
pMIR-HMGA2-3'UTR	HSV-TK (firefly) SV40 (renilla)	firefly+HMGA2-3'UTR; renilla	-	luciferase assay (miRNA binding site validation)
pMIR-HMGA2-3'UTR[mut]	HSV-TK (firefly) SV40 (renilla)	firefly+HMGA2-3'UTR mutated; renilla	-	luciferase assay (miRNA binding site validation)
pMIR-RNL-TK	HSV-TK (firefly) SV40 (renilla)	firefly/renilla luciferase	-	luciferase assay (miRNA binding site validation)
pRL-TK	HSV-TK	renilla luciferase	-	luciferase assay (promoter regulation)
pSUPER-miR-106b	H1-RNA gene	precursor hsa-miR-106b	-	luciferase assay (miRNA binding site validation)
pSUPER-miR-17-5p	H1-RNA gene	precursor hsa-miR-17-5p	-	luciferase assay (miRNA binding site validation)
VP5	CMV	empty	N-terminal FLAG-HA	eukaryotic expression vector
VP5-GFP	CMV	GFP	N-terminal FLAG-HA tag	transfection and IP control
VP5-T6B[mut] -GFP	CMV	mutated T6B peptide	N-terminal FLAG-HA-tag; C-terminal GFP-tag	luciferase assay (miRNA binding site validation)
VP5-T6B-GFP	CMV	T6B peptide	N-terminal FLAG-HA-tag; C-terminal GFP-tag	luciferase assay (miRNA binding site validation)

All constructs, generated in this thesis are listed in Table 4.6. Here, also the respective cloning strategy and restriction enzymes for every particular construct are specified.

Table 4.6: Cloned constructs. For the particular constructs the corresponding inserts and cloning strategy is specified as indicated.

designation	insert (NCBI accession number)	cloned via
pIRES-Nkx2.2	Nkx2.2 (NM_002509.3)	EcoRV/*Bam*HI
pIRES-Nkx2.2Y181C	Nkx2.2 mutant (Y181 mutated to C)	*Eco*RV/*Bam*HI
pIRES-Nkx2.2ΔHD	Nkx2.2 deletion mutant (ΔHD)	*Eco*RV/*Bam*HI; blunt end fusion of N-and C-terminus
VP5-Nkx2.2	Nkx2.2	*Not*I/*Bam*HI
pCS2-CAMTA1	CAMTA1 (NM_015215.2)	*Asc*I/*Fse*I
pCS2-CAMTA1ΔN	CAMTA1 deletion mutant (Δaa 1-188)	*Asc*I/*Fse*I
pCS2-CAMTA1ΔN600	CAMTA1 deletion mutant (Δaa 1-600)	*Asc*I/*Fse*I
pCS2-CAMTA1 N+C	CAMTA1 deletion mutant (Δaa 600-1054)	*Asc*I/*Fse*I; blunt end fusion of N-and C-terminus
pCS2-CAMTA1 M	CAMTA1 deletion mutant (Δaa 1-600 and 1054-1673)	*Asc*I/*Fse*I
pCS2-CAMTA1 ΔC	CAMTA1 deletion mutant (Δaa 1064-1673)	*Asc*I/*Fse*I
pCS2-CAMTA1 C	CAMTA1 deletion mutant (Δaa 1-1054)	*Asc*I/*Fse*I
pMIR-Nkx2.2 3'-UTR	3'-UTR of Nkx2.2	*Spe*I/*Nae*I
pMIR-Nkx2.2 3'-UTR[mut]	3'-UTR of Nkx2.2; miR-17/106b site mutated	*Spe*I/*Nae*I
pMIR-miR17site	full complementary, artificial miR-17-5p target site	*Spe*I/*Sac*I
pMIR-miR106bsite	full complementary, artificial miR-106b target site	*Spe*I/*Sac*I
pGEX-CAMTA1-F3	CAMTA1 fragment (aa 1330-1480)	*Bam*HI/*Sal*I

4.1.7. Antibodies

Antibodies used for western blot (see paragraph 4.2.3.7.), immunofluorescences (see paragraph 4.2.3.11.) as primary antibodies and/or immunoprecipitations (see paragraph 4.2.3.2.), are itemized in Table 4.8 (see next page).

4.1.8. Bacterial strains and bacterial growth medium

Table 4.7 contains a list of bacterial *Escherichia coli* (*E. coli*) strains used for this thesis together with their features. Bacteria were inoculated and cultivated at 37°C in LB-medium composed of:

NaCl	1 % (w/v)
yeast extract	0.5 % (w/v)
bacto-tryptone	1 % (w/v)
pH = 7.2 - 7.5	

Table 4.7: Bacterial strains.

strain	features
Rosetta	F^- dcm ompT lon $hsdS_B$ (r_B^- m_B^-) gal λ(DE3) pRARE (Cam^R)
XL1-blue	F^- recA1 endA1 gyrA96 thi-1 hsdR17 supE44 relA1 lac F'[proAB $lacI^qZ$_M15 Tn10 (Tet^R)]

Table 4.8: Used antibodies. The particular antibodies are listed with their amounts used for the corresponding methods: western blot (WB), immunofluorescence (IF), and immunoprecipitation (IP); (purf.: purified).

designation	working solution/amount			IgG origin (mono- or polyclonal)	obtained from
	for WB	for IF	for IP		
anti-HA	1:1,000 in TBS-T + 2% (w/v) milk	-	-	mouse (monoclonal)	Covance (Princeton, USA)
anti-c-myc	1:500 in TBS-T + 2% (w/v) milk	1:60 in IF blocking solution	2.5 - 5 µg	rabbit (polyclonal)	Sigma-Aldrich
anti-α-Tubulin	1:5,000 in TBS-T + 2% (w/v) milk	-	-	mouse (monoclonal)	Sigma-Aldrich
anti-laminA/C	1:1,000 in TBS-T + 2% (w/v) milk	-	-	rabbit (polyclonal)	Santa Cruz biotechnology Inc. (Dallas, USA)
anti-CAMTA1 1886 serum	1:200 in TBS-T + 2% (w/v) milk	1:100 in IF blocking solution	0.1 - 0.2 % (v/v) of an IP preparation	rabbit (polyclonal)	Biochemistry I, University of Regensburg
anti-CAMTA1 1901 serum	1:200 in TBS-T + 2% (w/v) milk	1:100 in IF blocking solution	0.1 - 0.2 % (v/v) of an IP preparation	rabbit (polyclonal)	Biochemistry I, University of Regensburg
anti-CAMTA1 SY6160 serum/purified	1:100 in TBS-T + 2% (w/v) milk	1:100 in IF blocking solution	10 µg (purf. serum)	rabbit (polyclonal)	Eurogentec (Liège, Belgium), generated in this thesis
anti-CAMTA1 SY6161 serum/purified	1:100 in TBS-T + 2% (w/v) milk	1:100 in IF blocking solution	10 µg (purf. serum)	rabbit (polyclonal)	Eurogentec, generated in this thesis
anti-Nkx2.2 74.5A5	1:3 in TBS-T	1:10 in IF blocking solution	10 µg	mouse (monoclonal, hybridoma clone)	Developmental Studies Hybridoma Bank (University of Iowa, Iowa City, USA)

4.1.9. Human cell lines

All used human cell lines are listed in Table 4.9. The primary glioblastoma cell line R11 was previously described in (*53*). The ZH161 cell line was obtained from the University Hospital Zurich (Department of Neurology, Prof. Michael Weller).

Table 4.9: Human cell lines.

cell line	specification
HEK293-T	embryonic kidney cells
HeLa	cervical cancer cells
HeLa-S3 suspension culture	cervical cancer cells
LNT229	stable glioma cells
T98G	stable glioma cells
R11	primary glioblastoma cells
ZH161	primary glioblastoma cells

4.1.10. Software and databases

Often used software and databases are stated in Table 4.10 (see next page).

Table 4.10: Software and databases.

software/database	application	company
CFX-Manager	qPCR	Bio-Rad
Leica LAS-AF	confocal laser scanning microscopy	Leica (Wetzlar, Germany)
Protein-Scape	mass spectrometry raw data analysis	Bruker Daltonics (Billerica, USA)
Odyssey application software 3.0	western blot scanning	Licor
iQ 2.1	qPCR	Bio-Rad
http://www.ebi.ac.uk/	bioinformatic tools	
http://www.expasy.org/	bioinformatic tools	
http://www.ncbi.nlm.nih.gov/	general database	
http://genome.ucsc.edu/	database, mouse and human genome browser	
http://www.uniprot.org/	protein database	
http://www.proteinatlas.org/	protein database (SWISS-PROT)	
http://www.mirbase.org/	miRNA database	
http://www.targetscan.org/	TargetScan 6.2.; miRNA binding sites prediction for 3'-UTRs	
http://www.microrna.org/	miRNA binding sites prediction for 3'-UTRs	
http://mirtarbase.mbc.nctu.edu.tw/	database for experimentally validated miRNA-target interactions	
http://sirna.wi.mit.edu/	siRNA design	
https://caintegrator.nci.nih.gov/rembrandt/	molecular pathologic database for gliomas (REMBRANDT database)	

4.1.11. Devices

Frequently used devices and their application are listed in Table 4.11.

Table 4.11: Frequently used devices.

device	company	application
ÄKTA purifier	GE Healthcare	fast protein liquid chromatography
Branson Sonifier 450	Branson (Danbury, USA)	cell sonication
C1000 thermal cycler/CFX96 Real time System	Bio-Rad	qRT-PCR
GeneAmp PCR Sytems 9700	Applied Biosystems	PCR
iCycler/MyiQ	Bio-Rad	qRT-PCR
Leica TCS SP8	Leica	confocal laser scanning microcopy (immunofluorescence)
Mastercycler gradient	Eppendorf (Hamburg, Germany)	PCR
Mithras LB 940 Luminometer	Berthold technologies (Bad Wildbad, Germany)	luciferase assays
Nanodrop® spectrophotometer ND-100	Thermo Fischer Scientific	determination of DNA-, RNA or protein concentrations
Nucleofector®-Device II	Lonza	transfection of human cells
Odyssey IR Imager	Licor	western blot
peqSTAR Thermocycler	Peqlab (Erlangen, Germany)	PCR
Thermal cycler 2720	Applied Biosystems (Delaware, USA)	PCR
Zeiss Axiovert 200M	Zeiss (Oberkochen, Germany)	phase contrast fluorescence microscopy (immunofluorescence)
Zeiss Axiovert 35	Zeiss	phase contrast fluorescence microscopy (human cell culture)

4.2. Methods

4.2.1. Working with DNA

4.2.1.1. Polymerase chain reaction

Polymerase chain reaction (PCR)

Gene amplification for molecular cloning via PCR was performed using the Phusion® high-fidelity DNA-polymerase. The used types of templates and their particular quantities for a single PCR (total reaction volume was always 50 µl) are specified in Table 4.12. DMSO was added to a final concentration of 3 % (v/v) for every PCR. The final concentration of the other components (buffer, nucleotides, forward and reverse primer) conformed to the manufacturer's instructions (Thermo Fischer Scientific). The general PCR program is indicated hereinafter:

step	temperature	time
1	98°C	10 s
2	98°C	10 s
3	annealing temperature; 2-3°C below the T_m of the particular primer	30 s
4	72°C	30 s per kb
5	72°C	10 min
6	4°C	∞

Whereupon, step two to four is the amplification cycle. Normally, the total number of cycles was 35. If a particular primer contained a longer non-complementary part, the initial amplification was performed for five cycles at an annealing temperature corresponding to the complementary part. This initial amplification was then followed by the main amplification (30 cycles) at the annealing temperature corresponding to the whole primer. In the case of an annealing temperature above the elongation temperature of the polymerase, the annealing was performed at 72°C.

For subsequent applications every PCR was purified via agarose-gel electrophoresis using gels with a agarose concentration of 0.8 to 2 % (w/v). After the electrophoresis

run (at 120 V for 30 to 45 minutes) the DNA fragments were extracted from ethidium bromide-stained gels via the NucleoSpin®-Extract kit.

Table 4.12: Templates used for PCR.

type of template	amount used for PCR
Human Brain, whole Marathon-Ready™ cDNA, conc. 0,1 ng/µl (Clontech, Mountain View, USA)	4 % (v/v) of a PCR reaction
human cDNA (1:10 diluted), generated as stated in 4.2.2.2.	4 - 10 % (v/v) of a PCR reaction
human genomic DNA	250 - 500 ng
plasmid DNA	50 - 100 ng
PCR product	1 - 4 % (v/v) of a PCR reaction

PCR-directed mutagenesis

The primers for the PCR-directed mutagenesis were designed in a way that the non-complementary, mutated single nucleotide or sequence was flanked by 15 to 20 complementary nucleotides. For the PCR reaction 1 µM (final concentration) of each primer and 50 ng template (plasmid DNA) were used. The PCR was performed using the Phusion®-Polymerase, with an annealing temperature of 58°C and a total cycle-number of 15.

The PCR was then purified (NucleoSpin®-Extract kit) and used for a DpnI-digestion (30 µl total reaction volume). The DpnI-digestion results in a degradation of methylated, not mutated plasmids (originating from bacterial amplification) and was performed for 2 to 6 hours at 37°C, followed by enzyme inactivation at 80°C for 5 minutes. The whole digestion reaction was then used for transformation of 120 µl XL1-blue bacteria suspension according to the below mentioned method (see paragraph 4.2.1.2.). Effective mutagenesis was finally confirmed by sequencing as described in the next paragraph.

4.2.1.2. Molecular cloning and sequencing

Molecular cloning via restriction enzymes generating cohesive ends

Gel-purified PCR products (generated by primers bearing the required restriction sites) and destination vectors were digested with the required restriction enzymes for 2 to 4 hours at 37°C. For the preparative digestion, up to 2 µg DNA and up to 7 % (v/v) enzyme in a total reaction volume of 30 µl were used. To prevent re-ligation, vectors were then also dephosphorylated using Alkaline-Phosphatase FastAP®.

The ligation of the insert with the destination-vector was performed using 25 up to 70 ng vector and a stoichiometric ratio vector/insert of 1:2. The total reaction volume of a ligation was always 10 µl containing 10 % T4-DNA ligase (5 U/µl). Ligation reactions were incubated 2 to 3 hours at room temperature or over night at 16°C.

The entire ligation reaction was then used for transformation of 60 µl chemically competent XL1-blue bacteria suspension. The transformation was carried out using the calciumphosphate-heat shock method, described in (*185*). Afterwards the bacteria were plated out on LB-Agar plates composed of LB-medium containing 1.5 % (w/v) agar and the required amount of antibiotic for selection (e.g. 0.1 mg/ml ampicillin).

Screening for efficient cloning was carried out for each putative positive clone by inoculating 5 ml LB-medium (containing antibiotic), small-scale plasmid isolation (NucleoSpin®-Plasmid), and finally small-scale (10 µl total reaction volume) test digestion with restriction enzymes.

Plasmids of clones identified as potential successful cloned were sequenced as described below. In such a way verified constructs were then purified in large scale using the NucleoBond®-Xtra-Midi kit.

Molecular cloning using pGEM®-T easy as sub-cloning vector

For cloning of DNA-fragments generated by PCR into pGEM®-T easy vectors, the PCR-products had to be A-tailed first (due to the T-overhangs of the linear pGEM®-T easy vector at the multiple cloning site). This was performed in a reaction (10 µl total reaction volume) with recombinant DNA-Polymerase from *Thermus aquaticus* (0.25 U/µl final concentration) and dATP (0.2 mM final concentration) at 72°C for 30

minutes. After purification of the A-tailed product (NucleoSpin®-Extract kit) the ligation with the pGEM®-T easy vector was performed according to the manufacturer's instructions. Subsequently, 10 µl of the ligation was used for transformation of 60 µl XL1-blue bacteria suspension. After transformation, the bacteria were finally plated out on LB-plates containing ampicillin as well as 40 µl X-gal (20 mg/ml) and 4 µl IPTG (1 M) for blue-white-screening of positive clones (pGEM®-T easy vectors carry the *lacZ* gene at the multiple cloning site).

Molecular cloning via blunt ends

PCRs using the Phusion® polymerase result in DNA fragments bearing *per se* blunt ends. These fragments had to be phosphorylated for the ligation with the destination vector. Phosphorylation via T4-Polynucleotide-Kinase of blunt end inserts and ligation were carried out in one reaction, because the used kinase is also active in the used ligation buffer. The ratio vector/insert of 1:4 was for the ligation of blunt ends. First the inserts were phosphorylated in reaction volume of 10 µl (with 10 % (v/v) kinase and 1 µl ligation buffer) at 37°C for 30 minutes, then the reaction was stopped at 75°C for 10 minutes. Finally, the reaction was filled up with 1 µl ligation buffer, 25 to 70 ng linearized vector, 2 µl PEG 4000 solution [50 % (w/v)], 1 µl ligase, and water to a total end volume of 20 µl. The subsequent steps were then carried out in the same manner as already described for cohesive end cloning strategy.

For some constructs, two inserts bearing sticky ends as well as blunt ends were fused via the blunt ends and ligated with the linearized vector by the sticky ends in one single ligation reaction. This kind of ligation was carried out like the "normal" blunt end ligation. This was for example the case for cloning the constructs "pCS2-CAMTA1-N+C" and "pIRES-Nkx2.2ΔHD".

Molecular cloning using single stranded oligonucleotides

Artificial, single stranded oligonucleotides needed to be annealed and phosphorylated first before the ligation step was performed. This was the case for the generation of artificial, full-complementary binding sites for miRNA-17-5p and miR-106b fused to

the coding sequence of firefly luciferase. The annealing was performed in the same way as described for the annealing of two complementary siRNA-oligonucleotides (see paragraph 4.2.2.3.). The ligation including phosphorylation was carried out as before mentioned for blunt end cloning. Here, the molar ratio insert/vector was 1:2. The subsequent steps were then the same as for the other cloning strategies.

Sequencing

All constructs generated in this thesis were confirmed by Sanger-sequencing carried out by GATC (Cologne, Germany) or Macrogen Europe (Amsterdam, Netherlands).

4.2.1.3. Quantitative real-time polymerase chain reaction (qRT-PCR)

The real-time quantification of DNA-amplicons during PCR was performed in using fluorescent dyes which bind specifically double-stranded DNA molecules. The basic principle of this qRT-PCR method is described in (*186-188*).

For qRT-PCR, the iCylcer equipped with the MyiQ real-time detection system (Bio-Rad) or the C1000 thermal cycler CFX98™ Real Time System (Bio-Rad) were used. The qRT-PCR reaction was performed using the MESA GREEN qPCR mastermix (Eurogentec) for the MyiQ cycler and the SSoFast™ EvaGreen™ Supermix (Bio-Rad) for the CFX98™ Real Time System. The templates for qRT-PCR were generated by cDNA synthesis (see paragraph 4.2.2.2.) and were used for the reaction as a 1:10 dilution (in nuclease-free water). One single qRT-PCR reaction contained 5 µl diluted cDNA as template, forward and reverse qRT-PCR primers (each with a final concentration of 50 to 200 nM), and 10 µl two-times concentrated qRT-PCR mastermix, filled up to a total reaction volume of 20 µl with nuclease-free water.

Every reaction was performed in technical triplicates. The qRT-PCR programs for the two different mastermixes is specified hereinafter.

	MESA GREEN		EvaGreen™	
Step	temperature	time	temperature	time
1	95°C	3 min	98°C	1 min
2	95°C	10 s	98°C	5 s
3	60°C	30 s	60°C	10-15 s

The amplification was completed within 40 cycles (step two and three). For every qRT-PCR reaction a melt peak analysis was performed after the amplification phase in order to check the quality of the respective amplicons.

Data for qRT-PCRs were evaluated using the "ddC_t-method" with GAPDH or β-actin as reference mRNAs. The ddC_t-method is described in (*188*). For every qRT-PCR the mean of the triplicate C_t values was used to calculate the corresponding ddC_t value. The calculation of the error bars was carried out as described in (*188*).

4.2.2. Working with RNA

4.2.2.1. Isolation of RNA from cultured cells

The isolation and purification of total RNA from cultured cells was performed using the NucleoSpin®-RNA kit according to the manufacturer's instructions. The standard procedure for this kit includes also an DNase I digestion to remove residual DNA contaminations.

4.2.2.2. Reverse Transcription

For the synthesis of cDNA, 200 ng up to 2 µg total RNA was used as templates. The synthesis was performed using either the iScript™ or the First-Strand cDNA synthesis kit, in both cases according to the instructions of the manufactures. For the First-Strand cDNA synthesis always random DNA-hexamers were used as primers.

After cDNA synthesis, the reaction was diluted 1:10 in nuclease-free water and used for downstream applications such as molecular cloning and/or qRT-PCR.

4.2.2.3. Annealing of siRNA-oligonucleotides for RNA interference

SiRNAs for a siRNA-mediated gene knockdown were designed using the siRNA selection program of http://sirna.wi.mit.edu/. The single-stranded full-complementary siRNA-oligonucleotides had to be annealed first. The duplex was then transfected into cultured cells (see paragraph 4.2.4.2.). The annealing of complementary siRNA-strands was performed in siRNA-annealing buffer (specified hereinafter) at 95°C for one minute, followed by incubation at 37°C for one hour (at constant shaking).

annealing buffer	
magnesium acetate	2 mM
potassium acetate	100 mM
HEPES	30 mM
pH = 7.4	

The concentrations of the single-stranded oligonucleotides was determined before and the amounts taken for the annealing resulted in a solution containing 20 or 40 μM double-stranded RNA-oligonucleotide.

The efficiency of the annealing reaction was verified by agarose-gel electrophoresis using gels with agarose concentrations of 4 % (w/v), followed by ethidium bromide staining.

4.2.3. Working with proteins

4.2.3.1. Preparation of whole cell protein lysates

For the preparation of whole cell lysates, cultured human cells were first harvested at a confluence of 80 to 95 %. Transfected cells overexpressing the protein(s) of interest were harvested 48 hours after transfection (see paragraph 4.2.4.2.). After removal of the cultivation medium, cells were pelletized (500 g, five minutes, 4°C) and washed twice with PBS, composed of as stated hereinafter.

PBS	
NaCl	140 mM
KCl	2.7 mM
Na_2HPO_4 (× 2 H_2O)	10 mM
KH_2PO_4	1.8 mM
pH = 7.5	

The washed cell pellet was then resuspended in a lysis buffer which was suitable for the respective downstream application.

Lysis using nuclear lysis buffer

For an effective lysis of the whole cell including the nucleus a lysis buffer was used containing the detergents SDS and sodium deoxycholate. The exact composition of this nuclear lysis buffer was:

TRIS	50 mM
EDTA	10 mM
SDS	1 % (w/v)
sodium deoxycholate	0.1 % (w/v)
AEBSF	2 mM
pH = 8	

Before lysis, the nuclear lysis buffer was supplemented with DNase I (final concentration of 5 U/ml). Cells were then resuspended in the appropriate volume of nuclear lysis buffer (e.g. 500 µl lysis buffer for an amount of 90 % confluent cells from a 10 cm-cell culture dish) and incubated for 20 minutes at room temperature. Afterwards cells were sonicated for 10 to 20 seconds on a Branson Sonifier 450. Finally, lysates were cleared by centrifugation at 20,000 g for 20 minutes and 4°C. The cleared lysate (supernatant) was then used for western blot analysis.

Lysis for immunoprecipitation

Two different procedures were performed to lyse cells for IPs (see paragraph 4.2.3.2.) of nuclear proteins such as CAMTA1 and Nkx2.2.

One method includes the usage of a lysis buffer containing sodium deoxycholate for nuclear lysis. This lysis buffer (referred to as "IP-lysis buffer 1") was composed of:

NaCl	140 mM
KCl	2.7 mM
Na_2HPO_4 (× 2 H_2O)	10 mM
KH_2PO_4	1.8 mM
sodium deoxycholate	0.25 % (w/v)
NP-40	1 % (v/v)
DTT	1 mM
AEBSF	1 mM
pH = 7.5	

Harvested cells were lysed by resuspending the cell pellet in the appropriate volume of IP-lysis buffer 1 (e.g. 1 ml lysis buffer for an amount of 90 % confluent cells from a 15 cm-cell culture dish). The suspension was then incubated for 15 to 20 minutes at 4°C and cleared afterwards by centrifugation (20,000 g for 20 min and 4°C). The supernatant was finally used as input for IP.

For the second IP-lysis method, a hypotonic lysis buffer (stated as "IP-lysis buffer 2") containing no monovalent salt (except of NaF at a very low concentration) was used:

TRIS	50 mM
EDTA	5 mM
NaF	5 mM
NP-40	0.2 % (v/v)
DTT	1 mM
AEBSF	1 mM
pH = 7.5	

For lysis, harvested cells were incubated for 20 minutes at 4°C and constant rotation with the appropriate volume of IP-lysis buffer 2 (e.g. 1 ml for one 15 cm-cell culture dish). This hypotonic treatment leads to an osmotic swelling and breaking of the cells. After this first incubation, NaCl was added to final concentration of 150 mM to extract nuclear proteins. The lysate was then incubated again for 20 minutes at 4°C and

constant rotation. Finally, the lysate was shortly sonified (10 to 20 seconds) and centrifuged (20,000 g for 20 min and 4°C). The supernatant was used as input for IP.

4.2.3.2. Immunoprecipitation

The inputs for IPs were prepared as described in the previous paragraph. After taken a certain amount as an input-sample (normally 0.5 to 2 % of the input), the protein of interest was immunoprecipitated by adding the input to 40 - 50 µl beads (amount for a single IP), which were pre-coupled to a protein-specific antibody. The list of antibodies as well as their amount used for coupling is stated in Table 4.7. (see paragraph 4.1.7.). The choice of the beads (protein A- or protein G-Sepharose™ beads; both purchased from GE Healthcare) complied with the species origin of the particular antibody IgG. Rabbit-IgGs were coupled to protein A- or G-Sepharose™ and murine IgGs to protein G-Sepharose™ beads. Accordingly, either normal rabbit IgG (Santa Cruz) or beads only (in the case of using antibodies from mouse) were used as IP-controls. The antibody coupling was performed in PBS over night at 4°C and constant rotation, after washing the beads once with PBS-T (PBS containing 0.1 % (v/v) Tween-20) and once with PBS (each time: 3,000 g and 4°C for 2 minutes). For the IP of FLAG-tagged proteins, 40 - 50 µl slurry of ANTI-FLAG® M2 affinity agarose (Sigma-Aldrich) was used (washed twice with PBS-T before).

The IP reaction was performed for 3 to 5 hours at 4°C while rotating. Afterwards, beads were spun down (at 3,000 g and 4°C for 2 minutes) and washed four times with IP-wash buffer, composed of:

NaCl	300 mM
TRIS	50 mM
MgCl2 (× 6 H_2O)	5 mM
NaF	1 mM
NP-40	0.01 % (v/v)
pH = 7.5	

Finally, the proteins were eluted from beads after a last washing step with PBS. The elution was performed by adding an equivalent volume of two-times concentrated

Laemmli sample buffer [composition described in (*189*)] to the beads, followed by boiling at 95°C for five minutes. The IP-eluate was cleared from beads by short centrifugation and then used for downstream applications such as western blot analysis (see paragraph 4.2.3.7.) or mass spectrometry (see paragraph 4.2.3.8.).

4.2.3.3. Generation of nuclear extracts

Nuclear extracts from HeLa-S3 suspension culture cells

For nuclear extracts from HeLa-S3 suspension culture, cells were cultivated (see paragraph 4.2.4.1.) until they had reached a confluence of one billion cells per liter culture volume. The extraction was performed as described previously by Dignam *et al.* (*190*) with some adjustments.

First, cells were harvested by centrifugation (500 g, room temperature) and subsequently washed once with PBS. The further extraction steps were performed at 4°C. Next, pelletized cells were washed once (1,000 g for 5 minutes) with 5 × pellet volume hypotonic Roeder A buffer, composed of:

HEPES	10 mM
KCl	10 mM
MgCl2 (× 6 H_2O)	1.5 mM
DTT	0.5 mM
AEBSF	0.5 mM
pH = 7.9	

The cells were then incubated with 3 × pellet volume Roeder A buffer for 15 minutes for osmotic swelling. Afterwards, this suspension was transferred to an glass homogenizer. Breaking of the cells was archived by moving the pestle at least ten times up and down and was confirmed by Trypan-blue exclusion staining. Subsequently, fractionating of the cell cytoplasm was performed by centrifugation at 3000 g for ten minutes. The supernatant (raw cytoplasmic fraction) was further purified by adding 0.1 pellet volume Roeder B buffer (composition specified below) and another centrifugation step at 100,000 g for 60 minutes. This yielded the cleared cytoplasmic fraction (supernatant after removal of the lipid layer). After taken the raw cytoplasmic fraction,

the remaining cell debris was washed two times with 5 × pellet volume Roeder A buffer (each time: 1,000 g for 5 minutes) and the pellet was subsequently resuspended in 3 ml per 10^9 cells hypertonic Roeder C buffer composed of as indicated below. The nuclei were broke by transferring the suspension into a homogenizer and douncing ten times. This crude nuclear extract was then further incubated for 30 minutes while stirring, followed by centrifugation at 25,000 g for 20 minutes. The supernatant which is the soluble nuclear fraction was kept until further analysis and the pellet was resuspended in 3 ml per 10^9 cells Roeder C. Finally, this suspension was sonified on a Branson Sonifier 450 (four times 20 seconds) and cleared by centrifugation at 25,000 g for 20 minutes. The resulting supernatant was kept as nuclear insoluble fraction for further analysis. The purity of the cytoplasmic/nuclear fractionation was controlled by western blot analyses (see paragraph 4.2.3.7.) using antibodies against lamin A/C and α-Tubulin.

Roeder B		Roeder C	
HEPES	300 mM	HEPES	20 mM
KCl	1.4 mM	KCl	100 mM
MgCl2 (× 6 H_2O)	30 mM	MgCl2 (× 6 H_2O)	1.5 mM
DTT	0.5 mM	EDTA	0.2 mM
AEBSF	0.5 mM	glycerol	20 % (v/v)
		DTT	0.5 mM
		AEBSF	0.5 mM
pH = 7.9		pH = 7.9	

Nuclear extracts from HEK293-T cells

The preparation of nuclear extracts from adherent growing HEK293-T cells was performed at a cell confluence of 80 %. First, cells were harvested by centrifugation at 500 g and room temperature for five minutes, followed by washing once with PBS. The pelletized cells were then resuspended in 5 ml/g cell pellet TB buffer, composed of as stated hereinafter.

TB buffer	
HEPES	20 mM
potassium acetate	110 mM
magnesium acetate (× 4 H_2O)	2 mM
EGTA	1 mM
DTT	1 mM
AEBSF	1 mM
pH = 7.3	

Cells were then subsequently lysed by adding 10 ml/g cell pellet digitonin (100 µg/ml stock solution). Digitonin treatment was performed at 4°C until approximately 90 % of the cells were lysed (checked by Trypan-blue exclusion staining). Next, the cell debris was spun down at 1,000 g for 5 minutes at 4°C. The supernatant yielded then the cleared cytoplasmic extract. The pellet was further purified by washing three times with 10 ml/g cell pellet TB buffer containing 0.3 % (v/v) NP-40 (at each washing step the suspension was vortexed thoroughly for 10 seconds). After the last washing step, the pellet was resuspended in 5 ml TB buffer per g cell pellet. This crude nuclear extract was finally sonified on a Branson Sonifier 450 (four times 20 seconds) and cleared by centrifugation at 20,000 g for 20 minutes at 4°C. The resulting supernatant (cleared nuclear extract) was kept for further analysis. The purity of the cytoplasmic/nuclear fractionation was confirmed by western blot detection (see paragraph 4.2.3.7.) of lamin A/C and α-Tubulin.

4.2.3.4. Determination of protein concentrations

Total protein concentrations in lysates were determined on the Nanodrop® spectrophotometer at a wavelength of 280 nm, if the nuclear lysis buffer was used. In all other cases, measurement of total protein concentrations was performed using the Bradford protein assay, described in (*191*). For the assay, Roti®-Quant (Carl Roth) was used according to the manufacturer's instructions with dissolved BSA (in serial dilutions) as calibrating protein.

4.2.3.5. SDS-polyacrylamide gel electrophoresis

Separation of proteins by their molecular weight using denaturating SDS-polyacrylamide gel electrophoresis (SDS-PAGE) was performed as described by Laemmli (*189*).

The composition of the stacking and separating gel is specified hereinafter.

stacking gel		separating gel	
TRIS	125 mM	TRIS	380 mM
SDS	0.1 % (w/v)	SDS	0.1 % (w/v)
TEMED	0.15 % (v/v)	TEMED	0.1 % (v/v)
APS	0.05 % (w/v)	APS	0.05 % (w/v)
acrylamide/bis solution (37.5:1)	5 % (v/v)	acrylamide/bis solution (37.5:1)	10 % (v/v)
pH = 6.8		pH = 8.8	

Unless stated otherwise, separating gels with an acrylamide concentration of 10 % were used.

Before loading, samples for SDS-PAGE were mixed with Laemmli buffer and boiled at 95°C for 5 minutes (except of IP-eluates since they were already boiled during the elution step, see paragraph 4.2.3.2.). Protein separation was performed at a constant current of 50 mA using a running buffer composed of:

TRIS base	25 mM
glycine	192 mM
SDS	0.1 % (w/v)

4.2.3.6. Coomassie and silver staining of SDS-polyacrylamide gels

Coomassie staining

Coomassie staining of SDS-PAGE gels was performed over night at room temperature with Coomassie staining solution, composed of:

acetic acid	10 % (v/v)
ethanol	30 % (v/v)
Coomassie R250	0.25 % (w/v)

For destaining (at room temperature until protein bands were clearly visible) the following solution was used:

acetic acid	10 % (v/v)
ethanol	30 % (v/v)

Silver staining

Sliver staining of protein gels was performed according to Blum *et al.* (*192*) with some adaptations.

Gels were first fixed with 50 % (v/v) methanol and 12 % (v/v) acetic acid for 1.5 hours at room temperature. This was followed by washing once with 50 % (v/v) and once with 30 % ethanol (each time: for 10 to 30 minutes at room temperature). Gels were then treated for one minute with 0.02 % (w/v) sodium thiosulfate and afterwards rinsed three times with water. Subsequently, gels were incubated for 20 minutes at room temperature with a 0.1 % (w/v) silver nitrate solution, rinsed two times with water, and finally developed with freshly prepared 6 % (w/v) sodium carbonate solution containing 0.074 % (v/v) formaldehyde and 400 µg/l sodium thiosulfate. The developing reaction was stopped with 5 % (v/v) acetic acid (for 5 minutes at room temperature) when the protein bands of interest were clearly visible. However, developing was not longer performed than 10 minutes.

4.2.3.7. Western blot

Semi-dry transfer

For the semi-dry transfer of proteins from a SDS-PAGE gel to a nitrocellulose blotting membrane (Amersham™ Protean™, GE Healthcare), the following transfer buffer was used:

TRIS	25 mM
glycine	192 mM
methanol	20 % (v/v)
pH = 8.6	

The transfer was performed using semi-dry transfer chambers purchased from Bio-Rad. On the bottom electrode (anode) of the chamber four Whatman®-papers (Biometra, Göttingen, Germany), soaked with transfer buffer, were first positioned. The membrane was placed on the Whatman®-papers, followed by the gel (both incubated shortly with transfer buffer). To complete the "transfer-sandwich", the gel was covered by again four soaked Whatman®-papers.
The semi-dry blot was carried out at constant current of 2 mA per square centimeter Whatman®-paper and for approximately 1 minute per kDa molecular weight corresponding to the protein of interest.

Wet blot transfer

A wet blot was performed to transfer proteins with a high molecular weight such as CAMTA1. The wet blot transfer was carried out using the Trans-blot® Cell wet blot chamber (Bio-Rad) and a transfer buffer, composed of:

TRIS	25 mM
glycine	192 mM
pH = 8.3	

The set-up of the "transfer-sandwich" was in principle the same as described for the semi-dry blot. Wet blot transfer was performed over night at 4°C and constant voltage of 30 V.

Further procedure after transfer

After the transfer, membranes were incubated for one hour at room temperature or over night at 4°C with 5 % (w/v) milk in TBS-T as blocking solution. TBS-T was composed of:

NaCl	150 mM
TRIS	10 mM
Tween-20	0.1 % (v/v)
pH = 8.0	

Subsequent to the blocking step, membranes were incubated with a primary antibody solution listed in Table 4.7 (see paragraph 4.1.7.) for at least one hour at room temperature or over night at 4°C. Primary antibodies were diluted in TBS-T containing 2 % (w/v) milk and 0.02 % (v/v) sodium azid, except of the anti-Nkx2.2 hybridoma supernatant, which was diluted in TBS-T with sodium azid only. In the case of using the Nkx2.2 antibody, the membrane was washed twice with TBS-T after blocking.
After incubation with primary antibody, the membrane was washed three times with TBS-T (each time 5 minutes while shaking). Subsequently, the secondary antibody solution was deployed on the membrane. The used secondary antibodies are coupled to fluorescent dyes and were all purchased by Licor. Depending on the species origin of the primary antibody either anti-Mouse-IgG-IRDye®-800CW/-680 or anti-Rabbit-IgG-IRDye®-800CW/-680 were used as 1:10,000 dilutions in TBS-T (containing 2 % (w/v) milk and 0.02 % (v/v) sodium azid). The incubation with the secondary antibody was performed for one hour at room temperature (light-protected), followed by washing three times with TBS-T. Finally, protein and marker bands were visualized at the Odyssey IR Imager (Licor).

4.2.3.8. Mass spectrometry

Protein bands for mass spectrometry analysis were cut out from silver stained gels and transferred to 2 ml-Eppendorf cups. From these gel slices proteins were extracted, purified, and digested with trypsin. This procedure and identification of proteins via analytical mass spectrometry were carried out in collaboration with the group of Prof. Rainer Deutzmann (Department Biochemistry I, University of Regensburg). The raw data gained from mass spectrometry were interpreted by the Protein-Scape software (Bruker Daltonics) using the Mascot search engine (v2.3.02) to identify proteins. Thereby, SWISS-PROT database search was carried out for identification. Detected proteins were tabularly ordered according to their particular Mascot protein score (from high to low values). For further analysis the list of identified proteins was cleared from contaminations such as keratin, which were caused obviously by sample preparation.

4.2.3.9. Purification of recombinant expressed GST-tagged proteins via fast protein liquid chromatography

Large scale purification of recombinant expressed human GST-tagged proteins was performed via fast protein liquid chromatography (FPLC) on an ÄKTA purifier (GE Healthcare). Thereby, "large scale" means more than one liter of expression culture.

First, for the bacterial expression of human proteins, chemically competent bacteria of the Rosetta *E. coli* strain were transformed (by heat shock) with a pGEX-6p1 plasmid encoding for the protein of interest and an N-terminal GST-tag. The Rosetta stain is characterized by bearing an additional plasmid coding for chloramphenicol resistance and human tRNAs which are rarely used in *E. coli*.

On the day of expression, a large volume (e.g. 4 l) of LB medium containing final concentrations of 100 µg/ml ampicillin (pGEX-6p1) and 50 µg/ml chloramphenicol was inoculated 1:50 by a pre-culture (cultivated over night at 37°C). Bacterial growing was then continued at 37°C until the culture had reached an OD_{600} around 0.6. Afterwards, the culture was incubated for 30 to 60 minutes at the optimal temperature for protein expression (e.g. 25 °C) until OD_{600} was between 0.6 and 0.9. Next, protein expression was induced by adding IPTG to a final concentration of 1 mM. After induction, the incubation at the expression temperature was continued for the optimal expression time (e.g. 5 hours). The optimal expression temperature and time was determined before by small scale (up to 100 ml culture volume) expression tests.

After expression, bacteria were harvested (5,000 g for 15 minutes at 4°C) and resuspended in bacterial lysis buffer (20 ml per liter culture volume), composed of:

NaCl	500 mM
TRIS	50 mM
$MgCl_2$	5 mM
AEBSF	1 mM
pH = 7.5	

Before use, Benzonase® Endonuclease (Merck; 10 U/ml final concentration) and lysozym (1 mg/ml final concentration) were added to the lysis buffer. To lyse the cells, bacteria were sonified with a Branson Sonifier 450 (pulses at an intensity 7 to 8 for 3 × 3

minutes). The raw bacterial lysate was subsequently centrifuged at 30,000 g for 30 minutes at 4°C and cleared by filtration. The lysate was then loaded on a glutathione Sepharose™ column (GSTrap FF, GE Healthcare) using the ÄKTA FPLC system to purify the overexpressed GST-tagged protein. After washing the column with 10 column volume of bacterial lysis buffer, GST-tagged proteins were eluted from the column using bacterial lysis buffer at pH of 8.0 supplemented with 3 mg/ml reduced glutathione. Finally, fractions containing the GST fusion protein with the highest amounts (peak fractions) were pooled together.

As mentioned above, for the purification of GST-CAMTA1-F3 an anion exchange chromatography was necessary as a further purification step. Thereby, pooled fractions containing GST-CAMTA1-F3 were first concentrated to a total volume of 10 ml. Afterwards, this concentrated protein solution was desalted by chromatography (HiPrep 26/10 Desalting, GE Healthcare) using a low salt buffer (50 mM NaCl, 20 mM TRIS), which had a pH value 2.5 units above the theoretical pI of GST-CAMTA1-F3 (4.94), i.e. pH of 7.5. This buffer was also used to equilibrate the ion exchange column (RESOURCE™ Q, GE Healthcare). The fractions of the desalted protein were pooled and loaded on the ion exchange column. After washing with 1 to 2 column volume of the above mentioned low salt puffer, GST-CAMTA1-F3 was eluted with a high salt elution buffer (500 mM NaCl, 20 mM TRIS, pH 7.5). Fractions containing the fusion protein at highest degree of purity (confirmed by SDS-PAGE) were pooled and further concentrated. The protein concentration was then determined with a photometer at 280 nm. Finally, the protein solution was stored at -80°C after adding glycerol (5 % (v/v) final concentration) and fast-freezing with liquid nitrogen.

4.2.3.10. Generation and purification of polyclonal antibodies

The polyclonal antibody sera anti-CAMTA1 SY6160 and anti-CAMTA1 SY6161 were generated by immunization of rabbits at Eurogentec using GST-CAMTA1-F3 as antigen.

For purification of polyclonal antibody sera via affinity chromatography, the corresponding antigen was covalently coupled to a cyanogen bromide-Sepharose4™

matrix (CNBr-activated-Sepharose4™ Fast Flow, GE Healthcare). For one coupling reaction 300 mg of activated Sepharose4™ was incubated with hydrogen chloride (1 mM) for 30 minutes at 4°C (for swelling). The swollen matrix was then transferred into a 15 ml-Poly Prep chromatography column (Bio-Rad). This was followed by adjusting the pH of the matrix to 8.3 with coupling buffer, composed of:

NaCl	0.5 M
$NaHCO_3$	192 mM
pH = 8.3	

Before the antigen peptide solution was loaded on the matrix, the antigen was dialyzed against 1 l coupling buffer over night at 4°C (Dialysis Tubing Visking, cellulose, 10 -14 kDa molecular weight cutoff, Roth). The matrix was then incubated with the antigen over night at 4°C while rotating for coupling.

Afterwards, the matrix was washed with 5 × matrix volume coupling buffer and subsequently resuspended in 5 × matrix volume ethanolamine (1 M, pH 8), followed by two hours incubation at room temperature for blocking. Then, the matrix was washed alternately with wash buffer 1 (pH 3 to 4) and wash buffer 2 (pH 8 to 9), eight times in total beginning with wash buffer 1 (each time: one column volume buffer). The exact composition of wash buffer 1 and 2 was:

wash buffer 1		wash buffer 2	
sodium acetate	100 mM	TRIS	100 mM
NaCl	500 mM	NaCl	500 mM
pH = 3 to 4		pH = 8 to 9	

After a final washing step with PBS, the antibody serum was deployed on the antigen-coupled matrix for purification and incubated over night at 4°C while rotating. Finally, after washing twice with PBS (each time: one column volume), the purified antibody solution was eluted by 10 ml glycine at a pH of 2.3. The eluate was fractionated as 1 ml-fractions. At the end, the pH value of each fraction was adjusted to a not acidic level with 100 µl/fraction TRIS (1 M, pH 8.8). To store the purified antibody solution,

glycerol (5 % (v/v) final concentration) was added to each fraction, followed by fast-freezing with liquid nitrogen.

4.2.3.11. Immunofluorescence

For IFs, cells were cultivated in 24-well cell culture plates on microscopy cover slips (circular, 12 mm diameter) until they had reached a confluence between 50 and 80 %. After removing the cultivation medium, cells were washed once with [pre-warmed (37°C)] PBS, followed by fixation with (pre-warmed) PBS containing 4 % (w/v) paraformaldehyde at 37°C for ten minutes. Fixation was then stopped by replacing PBS-paraformaldehyde with (pre-warmed) PBS containing 100 mM glycine. After incubation at 37°C for 5 minutes, cover slips were washed twice with (pre-warmed, 37°C) PBS. Afterwards, the cells were permeabilized for 15 minutes at room temperature using PBS with 0.2 % (v/v) Triton X-100. This was followed by washing twice with blocking solution composed of PBS containing 0.05 % (v/v) Triton X-100 and 1 % (w/v) BSA. Subsequently, cells were incubated for one hour at room temperature with blocking solution. Then, primary antibody solutions were deployed on the cover slips. Primary antibodies used for IF are sated in Table 4.7 (see paragraph 4.1.7.). All antibodies used in IF were diluted in blocking solution (see also Table 4.7 for the particular amounts used for IF of the respective antibodies). Cells were incubated for one to two hours at room temperature with primary antibodies, followed by washing four-times with blocking solution. Afterwards, secondary antibodies conjugated to fluorescent dyes were deployed on the cells for one hour (at room temperature and protected from light). According to the species origin of the primary antibody IgG, either Alexa Fluor® 555 Goat Anti-Rabbit IgG (H+L) or Alexa Fluor® 555 Goat Anti-Mouse IgG (H+L) secondary antibodies were used, diluted 1:400 in blocking solution. Both secondary antibodies were purchased from Life Technologies (Carlsbad, USA). After incubation with secondary antibodies, the cover slips were washed once with blocking solution, three times with PBS, and at last with water. Finally, one drop of ProLong® Gold Antifade Mountant with DAPI (Life

Technologies) for each cover slip was deployed on a microscopy slide, before the cover slips were transferred to these slides (with the cell covered surface down to the mounting solution). The usage of this solution for mounting resulted also in DAPI-staining of nuclei. After transferring the slips, the prepared slides were dried for at least 24 hours (light-protected, at 4°C) before IFs were visualized. Thereby, either the Axiovert 200M fluorescence microscope (Zeiss) or the TCS SP8 confocal laser scanning microscope (Leica) was used.

4.2.4. Human cell culture

4.2.4.1. Cultivation of human cell lines

All cell lines listed in Table 4.9 were cultivated at 37°C in an atmosphere with 95 % humidity and a CO_2-content of 5 %.

For the cultivation of HEK293-T, HeLa, and stable glioma cell lines (LNT229 and T98G) Dulbecco's Modified Eagle's Medium (DMEM) was used containing 10 % (v/v) FBS and 1 % (v/v) Penicillin/Streptomycin stock solution. DMEM, FBS, and Penicillin/Streptomycin were all purchased from Sigma-Aldrich. These adherent growing cell lines were passaged normally three times a week using Trypsin-EDTA (Sigma-Aldrich).

For the cultivation of HeLa-S3 suspension culture cells Joklik's Medium was used, which was composed of:

Minimum essential medium Joklik's modified (Sigma-Aldrich)	11.02 g/l
$NaHCO_3$	2 g/l
L-glutamine (Sigma-Aldrich)	0.29 g/l
MEM non-essential amino acids (Life Technologies)	1 % (v/v)
Penicillin/Streptomycin stock solution	1 % (v/v)
FBS	5 % (v/v)
pH = 7	

The cells were cultivated (up to one liter culture volume) in glass flasks while constant stirring. These suspension cells were normally passaged every third day by inoculating fresh cultivation medium with a certain amount of cells resulting in confluence of 400,000 to 600,000 cells/ml.

The R11 primary glioblastoma cell line was cultivated in neural stem cell medium as previously described in (*53*). This medium was also used for the cultivation of the primary glioblastoma cell line ZH161. R11 cells were passaged every four to five days, ZH161 every seven to ten days, by detaching with a pipette.

4.2.4.2. Transfection

Transfection using calcium phosphate precipitation

This method was used for transfection of HEK293-T cells cultivated in 15 cm-cell culture dishes. Transfection was performed at a confluence of 15 to 25 % and at least six hours after the last passage via trypsinization. For the transfection of one single 15-cm cell culture dish, a DNA/$CaCl_2$ solution with a total volume of 1.13 ml was prepared first. This solution contained 10 up to 20 µg total plasmid DNA diluted in (sterile) water and a final concentration of 243 mM $CaCl_2$. Afterwards 1.13 ml of two-times concentrated HBS was added drop by drop while constant shaking. HBS was composed of:

NaCl	137 mM
Na_2HPO_4 (× 2 H_2O)	0.75 mM
HEPES	27.3 mM
pH = 7.1	

Before the transfection solution was deployed on the cultivated cells, the solution was incubated for 5 to 10 minutes at room temperature to ensure the efficient formation of calcium-DNA complexes.

Transfected HEK293-T cells were harvested for further downstream applications 48 hours after transfection.

Transfection via lipofection

Either Lipofectamine™ 2000 or Lipofectamine™ RNAiMAX was used for lipofection of cells with plasmid-DNA and/or RNA-oligonucleotides. Both reagents were purchased from Life Technologies. Transfection with plasmid-DNA together with RNA or with plasmid-DNA only was performed via Lipofectamine™ 2000, whereas transfection for RNAi with pre-annealed siRNA-strands (see paragraph 4.2.2.3.) was achieved by Lipofectamine™ RNAiMAX. In both cases the transfection procedure was carried out according to the manufacturer's instructions. For the transfection, cells were cultivated in medium without antibiotics. DNA and RNA as well as the lipofection reagents were diluted with Opti-MEM® (Life Technologies).

The transfection for a gen-specific knockdown with Lipofectamine™ RNAiMAX was always carried out in 6-well cultivation plates. The total concentration of siRNAs was 40 nM per well. Transfections using Lipofectamine™ 2000 were performed in 6-well and 48-well plates. The amount of transfected DNA/RNA is stated in the corresponding downstream application.

Cultivation medium was changed 24 hours after lipofection and the transfected cells were used for downstream applications after a further cultivation period of 24 hours.

Transfection via Nucleofection®

Nucleofection® uses electroporation and transfection reagents with nuclear localization signals for an efficient transfection. In this thesis, LNT229 and R11 cells were transfected by this method. Thereby, the Amaxa® Cell Line Nucleofector® Kit R was used for the transfection of LNT229 cells, whereas R11 cells were transfected with the Amaxa® Mouse Neural Stem Cell Nucleofector® Kit. Both kits were purchased from Lonza. The electroporation was carried out for both kits at the Nucleofector®-Device II (Lonza).

Both kits use in principle the same transfection protocol. For one single transfection 3×10^6 cells (cultivated in antibiotics-free medium) and 5 µg total plasmid-DNA were used. The transfection was carried out according to the manufacturer's instructions.

After the electroporation step cells were seeded in 10 cm-cell culture dishes and cultivated for at least 24 hours until they were used for further downstream applications.

4.2.4.3. Proliferation assays

In this thesis, the effects of Nkx2.2 and Nkx2.2 mutants on cell proliferation of stable glioma LNT229 cells were examined. For this assay, LNT229 cells were first transfected with eukaryotic expression vectors encoding for the particular proteins by the above mentioned Nucleofection® method. One day after transfection, 40,000 cells (per one single transfection) were seeded into µDish Grid-500 (35 mm) counting plates (ibidi, Planegg, Germany) and further cultivated. These plates contain a microscopic grid for counting on the bottom surface (4 × 10 × 10 squares with 500 × 500 μm^2). One day after seeding, cells in an area of 6 × 6 squares were counted (per transfection). On the three subsequent days, the number of cells in this area was further quantified to determine the cell proliferation rate. For analysis, the mean number of cells per square (in the counting area) was calculated for every day of counting.

4.2.4.4. Neurosphere assays using primary glioblastoma cell lines

To investigate the effects of Nkx2.2 and Nkx2.2 mutants on the neurosphere-forming capability of primary glioblastoma cells, R11 and ZH161 were transfected with plasmids coding for the particular proteins. The transfection of R11 cells was performed by Nucleofection® as described in 4.2.4.3., whereas ZH161 cells were transfected in 6-well plates with Lipofectamine™ 2000. Thereby, an amount between 300,000 and 500,000 cells was transfected with 4 µg plasmid-DNA for one single transfection. One to two days after transfection R11 or ZH161 cells were singularized and counted (using a Neubauer hemocytometer). Afterwards, 1,000 cells were transferred into every second well of a 96-well cell culture plate. These plated cells were further diluted 1:10 in cultivation medium and seeded into the remaining wells of the plates. Plated cells were then further cultivated until the formation of neurosphere-like clones was observed in those wells containing the diluted cells. This was normally the case seven days after

transfection of R11 cells or approximately 14 days after transfection of ZH161. Neurosphere-like clones were quantified for every well, followed by calculating the mean number of clones per well. For analysis, results from several biological replicates were used. Significance was assessed by two-sided Student's *t*-test for unequal sample variance. *P*-values less than 0.05 were considered as significant.

4.2.5. Dual luciferase reporter assays

4.2.5.1. Validation of promoter regulation by transcription factors

For investigation of potential promoter regulation by transcription factors such as Nkx2.2, the pGL3/pRL luciferase reporter vectors (Promega) were used. Thereby, the pGL3-basic vector encodes for firefly luciferase with a multiple cloning site located upstream of the luciferase open reading frame to clone the promoter of interest in front of the luciferase. For normalization of the firefly activity, the pRL-TK vector coding for renilla luciferase (under control of the constitutively active HSV-TK promoter) was co-transfected. The third co-transfected plasmid was a pIRES-expression vector encoding e.g. for wildtype Nkx2.2. The co-transfections were preformed as biological quadruplicates using Lipofectamine™ 2000. They were carried out in 48-well plates with 50,000 HEK293-T cells and 240 ng total plasmid-DNA per well (80 ng of each type of vector). One day after transfection cultivation medium was changed. Finally, cell lysis and measurement of the luciferase activities was performed 48 hours after transfection. For the lysis, cultivation medium was replaced by 100 µl/well passive lysis buffer (Promega). Cells were then incubated with lysis buffer for 20 minutes on room temperature while shaking. Firefly and renilla activities were determined separately on a Mithras LB 940 Luminometer (Berthold technologies) by transferring for each measurement 20 µl lysate from each well to special 96-well plates characterized by a high reflectivity for an efficient luminescence measurement (BRANDplates® pureGrade™, Brand, Wertheim, Germany). The respective buffers in which firefly or renilla luciferase were active were composed of as stated hereinafter.

firefly luciferase buffer		renilla luciferase buffer	
Na_2EDTA	0,1 mM	Na_2EDTA	2.2 mM
$MgSO_4$ (× 7 H_2O)	5.34 mM	K_3PO_4	220 mM
tricine	20 mM	BSA	0.44 mg/ml
ATP	530 µM	NaCl	1.1 M
coenzyme A	270 µM	NaN_3	1.3 mM
D-luciferin	470 µM	coleenterazin	1.43 nM
DTT	33.3 mM		
pH = 8.0		pH = 5.1	

The ratios of firefly to renilla activity were calculated after the separate measurements. For analysis, the average ratio was assessed for each quadruplicate. The mean values were then double-normalized: first to the corresponding average ratio of the pIRES empty vector control and second to the corresponding average ratios of pGL3-basic empty vector samples. Significance was assessed from biological replicates using two-sided Student's *t*-test for unequal sample variance. *P*-values less than 0.05 were considered as significant.

4.2.5.2. Validation of miRNA binding sites in 3'-UTRs

To validate *in silico* identified potential miRNA binding sites in the 3'-UTR of Nkx2.2, pMIR-RNL-TK dual luciferase reporter vectors were used. These vectors [previously described in (*146*)] are characterized by a multiple cloning site at the 3'-end of the firefly luciferase coding sequence. Cloning of a 3'-UTR in these vectors leads to a fusion of the firefly luciferase with this 3'-UTR. Moreover, these vectors contain the sequence encoding for renilla luciferase to normalize the firefly activity.

For investigation of miRNA regulation either endogenous miRNAs were inhibited by transfection of miRNA-specific 2'-O-methylated antisense oligonucleotides or concentrations of certain miRNAs were increased by transfection of duplex mimics or pSUPER plasmids. Furthermore, general miRNA-regulation was examined by the overexpression of the T6B peptide. In all cases transfections were performed with Lipofectamine™ 2000 using 48-well plates. In each well an amount of 50,000 cells were plated. Per well, either 80 nM final concentration 2'-O-methylated inhibitors, 10 to 20

nM duplex mimic, or 200 ng pSUPER plasmid were co-transfected with 120 to 150 ng reporter vector. The assays using the T6B peptide were performed by co-transfection of 125 ng per well of the peptide expression vector (VP5-T6B-GFP) with 125 ng per well reporter vector. All transfections were carried out in biological quadruplicates.

The further procedure and the readout were in principle the same as described in the paragraph before (4.2.5.1). Analysis was here also performed by double normalization of the average ratio values with the corresponding values of the controls. Thereby, the following controls were used: pMIR-RNL-TK empty vector and the miR-122 inhibitor for the assays with miRNA-specific inhibitors, pMIR-RNL-TK empty and the pSUPER empty vectors in the case of assays with pSUPER vectors. Negative controls for the T6B peptide assay were the empty reporter vector and the VP5-GFP expression vector.

4.2.6. Analysis of molecular-pathological data from glioma patients

Data for the analyses of patient survival and gene expression in gliomas was obtained from the REMBRANDT database (*193, 194*), as mentioned above. Further information can be found at https://caintegrator.nci.nih.gov/rembrandt/.

5. References

1. D. Hanahan, R. A. Weinberg, Hallmarks of cancer: the next generation. *Cell* **144**, 646 (Mar 4, 2011).
2. N. A. Lobo, Y. Shimono, D. Qian, M. F. Clarke, The biology of cancer stem cells. *Annu Rev Cell Dev Biol* **23**, 675 (2007).
3. T. Lapidot *et al.*, A cell initiating human acute myeloid leukaemia after transplantation into SCID mice. *Nature* **367**, 645 (Feb 17, 1994).
4. D. Bonnet, J. E. Dick, Human acute myeloid leukemia is organized as a hierarchy that originates from a primitive hematopoietic cell. *Nature medicine* **3**, 730 (Jul, 1997).
5. M. Al-Hajj, M. S. Wicha, A. Benito-Hernandez, S. J. Morrison, M. F. Clarke, Prospective identification of tumorigenic breast cancer cells. *Proc Natl Acad Sci U S A* **100**, 3983 (Apr 1, 2003).
6. S. K. Singh *et al.*, Identification of a cancer stem cell in human brain tumors. *Cancer Res* **63**, 5821 (Sep 15, 2003).
7. S. K. Singh *et al.*, Identification of human brain tumour initiating cells. *Nature* **432**, 396 (Nov 18, 2004).
8. N. Uchida *et al.*, Direct isolation of human central nervous system stem cells. *Proc Natl Acad Sci U S A* **97**, 14720 (Dec 19, 2000).
9. C. Li *et al.*, Identification of pancreatic cancer stem cells. *Cancer Res* **67**, 1030 (Feb 1, 2007).
10. C. A. O'Brien, A. Pollett, S. Gallinger, J. E. Dick, A human colon cancer cell capable of initiating tumour growth in immunodeficient mice. *Nature* **445**, 106 (Jan 4, 2007).
11. A. Eramo *et al.*, Identification and expansion of the tumorigenic lung cancer stem cell population. *Cell death and differentiation* **15**, 504 (Mar, 2008).
12. I. Bussing, F. J. Slack, H. Grosshans, let-7 microRNAs in development, stem cells and cancer. *Trends Mol Med* **14**, 400 (Sep, 2008).

13. F. Rangwala, A. Omenetti, A. M. Diehl, Cancer stem cells: repair gone awry? *Journal of oncology* **2011**, 465343 (2011).
14. D. N. Louis *et al.*, The 2007 WHO classification of tumours of the central nervous system. *Acta neuropathologica* **114**, 97 (Aug, 2007).
15. P. Y. Wen, S. Kesari, Malignant gliomas in adults. *N Engl J Med* **359**, 492 (Jul 31, 2008).
16. J. T. Huse, E. C. Holland, Targeting brain cancer: advances in the molecular pathology of malignant glioma and medulloblastoma. *Nat Rev Cancer* **10**, 319 (May, 2010).
17. J. I. Bastien, K. A. McNeill, H. A. Fine, Molecular characterizations of glioblastoma, targeted therapy, and clinical results to date. *Cancer* **121**, 502 (Feb 15, 2015).
18. R. G. Verhaak *et al.*, Integrated genomic analysis identifies clinically relevant subtypes of glioblastoma characterized by abnormalities in PDGFRA, IDH1, EGFR, and NF1. *Cancer cell* **17**, 98 (Jan 19, 2010).
19. H. Ohgaki, P. Kleihues, Genetic pathways to primary and secondary glioblastoma. *The American journal of pathology* **170**, 1445 (May, 2007).
20. R. Stupp *et al.*, Radiotherapy plus concomitant and adjuvant temozolomide for glioblastoma. *N Engl J Med* **352**, 987 (Mar 10, 2005).
21. S. Gil-Perotin *et al.*, Loss of p53 induces changes in the behavior of subventricular zone cells: implication for the genesis of glial tumors. *J Neurosci* **26**, 1107 (Jan 25, 2006).
22. S. Bao *et al.*, Glioma stem cells promote radioresistance by preferential activation of the DNA damage response. *Nature* **444**, 756 (Dec 7, 2006).
23. F. Pistollato *et al.*, Intratumoral hypoxic gradient drives stem cells distribution and MGMT expression in glioblastoma. *Stem Cells* **28**, 851 (May, 2010).
24. J. Chen *et al.*, A restricted cell population propagates glioblastoma growth after chemotherapy. *Nature* **488**, 522 (Aug 23, 2012).
25. S. Bao *et al.*, Stem cell-like glioma cells promote tumor angiogenesis through vascular endothelial growth factor. *Cancer Res* **66**, 7843 (Aug 15, 2006).
26. D. Beier *et al.*, CD133(+) and CD133(-) glioblastoma-derived cancer stem cells show differential growth characteristics and molecular profiles. *Cancer Res* **67**, 4010 (May 1, 2007).

27. M. J. Son, K. Woolard, D. H. Nam, J. Lee, H. A. Fine, SSEA-1 is an enrichment marker for tumor-initiating cells in human glioblastoma. *Cell Stem Cell* **4**, 440 (May 8, 2009).

28. T. Strojnik, G. V. Rosland, P. O. Sakariassen, R. Kavalar, T. Lah, Neural stem cell markers, nestin and musashi proteins, in the progression of human glioma: correlation of nestin with prognosis of patient survival. *Surg Neurol* **68**, 133 (Aug, 2007).

29. D. Beier *et al.*, CD133 expression and cancer stem cells predict prognosis in high-grade oligodendroglial tumors. *Brain Pathol* **18**, 370 (Jul, 2008).

30. H. S. Gunther *et al.*, Glioblastoma-derived stem cell-enriched cultures form distinct subgroups according to molecular and phenotypic criteria. *Oncogene* **27**, 2897 (May 1, 2008).

31. G. Meister, T. Tuschl, Mechanisms of gene silencing by double-stranded RNA. *Nature* **431**, 343 (Sep 16, 2004).

32. D. P. Bartel, MicroRNAs: target recognition and regulatory functions. *Cell* **136**, 215 (Jan 23, 2009).

33. R. W. Carthew, E. J. Sontheimer, Origins and Mechanisms of miRNAs and siRNAs. *Cell* **136**, 642 (Feb 20, 2009).

34. A. Esquela-Kerscher, F. J. Slack, Oncomirs - microRNAs with a role in cancer. *Nat Rev Cancer* **6**, 259 (Apr, 2006).

35. T. A. Farazi, J. I. Spitzer, P. Morozov, T. Tuschl, miRNAs in human cancer. *J Pathol* **223**, 102 (Jan, 2011).

36. Y. Lee *et al.*, MicroRNA genes are transcribed by RNA polymerase II. *The EMBO journal* **23**, 4051 (Oct 13, 2004).

37. Y. Lee *et al.*, The nuclear RNase III Drosha initiates microRNA processing. *Nature* **425**, 415 (Sep 25, 2003).

38. R. I. Gregory *et al.*, The Microprocessor complex mediates the genesis of microRNAs. *Nature* **432**, 235 (Nov 11, 2004).

39. A. M. Denli, B. B. Tops, R. H. Plasterk, R. F. Ketting, G. J. Hannon, Processing of primary microRNAs by the Microprocessor complex. *Nature* **432**, 231 (Nov 11, 2004).

40. R. Yi, Y. Qin, I. G. Macara, B. R. Cullen, Exportin-5 mediates the nuclear export of pre-microRNAs and short hairpin RNAs. *Genes & development* **17**, 3011 (Dec 15, 2003).

41. E. Lund, S. Guttinger, A. Calado, J. E. Dahlberg, U. Kutay, Nuclear export of microRNA precursors. *Science* **303**, 95 (Jan 2, 2004).
42. V. N. Kim, MicroRNA precursors in motion: exportin-5 mediates their nuclear export. *Trends Cell Biol* **14**, 156 (Apr, 2004).
43. T. P. Chendrimada *et al.*, TRBP recruits the Dicer complex to Ago2 for microRNA processing and gene silencing. *Nature* **436**, 740 (Aug 4, 2005).
44. H. Zhang, F. A. Kolb, L. Jaskiewicz, E. Westhof, W. Filipowicz, Single processing center models for human Dicer and bacterial RNase III. *Cell* **118**, 57 (Jul 9, 2004).
45. A. Dueck, G. Meister, Assembly and function of small RNA - argonaute protein complexes. *Biological chemistry* **395**, 611 (Jun, 2014).
46. M. R. Fabian, N. Sonenberg, W. Filipowicz, Regulation of mRNA translation and stability by microRNAs. *Annual review of biochemistry* **79**, 351 (2010).
47. E. Huntzinger, E. Izaurralde, Gene silencing by microRNAs: contributions of translational repression and mRNA decay. *Nature reviews. Genetics* **12**, 99 (Feb, 2011).
48. J. T. Huse *et al.*, The PTEN-regulating microRNA miR-26a is amplified in high-grade glioma and facilitates gliomagenesis in vivo. *Genes Dev* **23**, 1327 (Jun 1, 2009).
49. A. Rodriguez, S. Griffiths-Jones, J. L. Ashurst, A. Bradley, Identification of mammalian microRNA host genes and transcription units. *Genome research* **14**, 1902 (Oct, 2004).
50. V. Olive, I. Jiang, L. He, mir-17-92, a cluster of miRNAs in the midst of the cancer network. *The international journal of biochemistry & cell biology* **42**, 1348 (Aug, 2010).
51. B. Malzkorn *et al.*, Identification and functional characterization of microRNAs involved in the malignant progression of gliomas. *Brain Pathol* **20**, 539 (May, 2010).
52. A. Ernst *et al.*, De-repression of CTGF via the miR-17-92 cluster upon differentiation of human glioblastoma spheroid cultures. *Oncogene* **29**, 3411 (Jun 10, 2010).
53. D. Schraivogel *et al.*, CAMTA1 is a novel tumour suppressor regulated by miR-9/9* in glioblastoma stem cells. *EMBO J* **30**, 4309 (Oct 19, 2011).

54. A. N. Packer, Y. Xing, S. Q. Harper, L. Jones, B. L. Davidson, The bifunctional microRNA miR-9/miR-9* regulates REST and CoREST and is downregulated in Huntington's disease. *J Neurosci* **28**, 14341 (Dec 31, 2008).

55. C. Delaloy *et al.*, MicroRNA-9 coordinates proliferation and migration of human embryonic stem cell-derived neural progenitors. *Cell Stem Cell* **6**, 323 (Apr 2, 2010).

56. D. Nass *et al.*, MiR-92b and miR-9/9* are specifically expressed in brain primary tumors and can be used to differentiate primary from metastatic brain tumors. *Brain Pathol* **19**, 375 (Jul, 2009).

57. L. Ma *et al.*, miR-9, a MYC/MYCN-activated microRNA, regulates E-cadherin and cancer metastasis. *Nat Cell Biol* **12**, 247 (Mar, 2010).

58. T. Yang, B. W. Poovaiah, An early ethylene up-regulated gene encoding a calmodulin-binding protein involved in plant senescence and death. *J Biol Chem* **275**, 38467 (Dec 8, 2000).

59. T. Yang, B. W. Poovaiah, A calmodulin-binding/CGCG box DNA-binding protein family involved in multiple signaling pathways in plants. *J Biol Chem* **277**, 45049 (Nov 22, 2002).

60. N. Bouche, A. Scharlat, W. Snedden, D. Bouchez, H. Fromm, A novel family of calmodulin-binding transcription activators in multicellular organisms. *J Biol Chem* **277**, 21851 (Jun 14, 2002).

61. K. Song *et al.*, The transcriptional coactivator CAMTA2 stimulates cardiac growth by opposing class II histone deacetylases. *Cell* **125**, 453 (May 5, 2006).

62. A. Finkler, R. Ashery-Padan, H. Fromm, CAMTAs: calmodulin-binding transcription activators from plants to human. *FEBS Lett* **581**, 3893 (Aug 21, 2007).

63. O. da Costa e Silva, CG-1, a parsley light-induced DNA-binding protein. *Plant molecular biology* **25**, 921 (Aug, 1994).

64. A. Finkler, B. Kaplan, H. Fromm, Ca-Responsive cis-Elements in Plants. *Plant signaling & behavior* **2**, 17 (Jan, 2007).

65. C. J. Doherty, H. A. Van Buskirk, S. J. Myers, M. F. Thomashow, Roles for Arabidopsis CAMTA transcription factors in cold-regulated gene expression and freezing tolerance. *The Plant cell* **21**, 972 (Mar, 2009).

66. G. Benn *et al.*, A key general stress response motif is regulated non-uniformly by CAMTA transcription factors. *The Plant journal : for cell and molecular biology* **80**, 82 (Oct, 2014).
67. B. Kaplan *et al.*, Rapid transcriptome changes induced by cytosolic Ca2+ transients reveal ABRE-related sequences as Ca2+-responsive cis elements in Arabidopsis. *The Plant cell* **18**, 2733 (Oct, 2006).
68. J. Han *et al.*, The fly CAMTA transcription factor potentiates deactivation of rhodopsin, a G protein-coupled light receptor. *Cell* **127**, 847 (Nov 17, 2006).
69. P. Gong, J. Han, K. Reddig, H. S. Li, A potential dimerization region of dCAMTA is critical for termination of fly visual response. *J Biol Chem* **282**, 21253 (Jul 20, 2007).
70. C. Long *et al.*, Ataxia and Purkinje cell degeneration in mice lacking the CAMTA1 transcription factor. *Proc Natl Acad Sci U S A* **111**, 11521 (Aug 5, 2014).
71. G. Ghosh, G. van Duyne, S. Ghosh, P. B. Sigler, Structure of NF-kappa B p50 homodimer bound to a kappa B site. *Nature* **373**, 303 (Jan 26, 1995).
72. C. W. Muller, F. A. Rey, M. Sodeoka, G. L. Verdine, S. C. Harrison, Structure of the NF-kappa B p50 homodimer bound to DNA. *Nature* **373**, 311 (Jan 26, 1995).
73. L. Aravind, E. V. Koonin, Gleaning non-trivial structural, functional and evolutionary information about proteins by iterative database searches. *J Mol Biol* **287**, 1023 (Apr 16, 1999).
74. S. Ghosh, M. J. May, E. B. Kopp, NF-kappa B and Rel proteins: evolutionarily conserved mediators of immune responses. *Annual review of immunology* **16**, 225 (1998).
75. L. K. Mosavi, T. J. Cammett, D. C. Desrosiers, Z. Y. Peng, The ankyrin repeat as molecular architecture for protein recognition. *Protein science : a publication of the Protein Society* **13**, 1435 (Jun, 2004).
76. J. Li, A. Mahajan, M. D. Tsai, Ankyrin repeat: a unique motif mediating protein-protein interactions. *Biochemistry* **45**, 15168 (Dec 26, 2006).
77. A. M. Rubtsov, O. D. Lopina, Ankyrins. *FEBS Lett* **482**, 1 (Sep 29, 2000).
78. S. G. Sedgwick, S. J. Smerdon, The ankyrin repeat: a diversity of interactions on a common structural framework. *Trends Biochem Sci* **24**, 311 (Aug, 1999).

79. A. R. Rhoads, F. Friedberg, Sequence motifs for calmodulin recognition. *FASEB J* **11**, 331 (Apr, 1997).
80. M. Bahler, A. Rhoads, Calmodulin signaling via the IQ motif. *FEBS Lett* **513**, 107 (Feb 20, 2002).
81. B. Muller-Borer *et al.*, Calcium dependent CAMTA1 in adult stem cell commitment to a myocardial lineage. *PloS one* **7**, e38454 (2012).
82. N. Pandey *et al.*, CAMTA 1 regulates drought responses in Arabidopsis thaliana. *BMC genomics* **14**, 216 (2013).
83. Y. Kim, S. Park, S. J. Gilmour, M. F. Thomashow, Roles of CAMTA transcription factors and salicylic acid in configuring the low-temperature transcriptome and freezing tolerance of Arabidopsis. *The Plant journal : for cell and molecular biology* **75**, 364 (Aug, 2013).
84. Y. Galon *et al.*, Calmodulin-binding transcription activator (CAMTA) 3 mediates biotic defense responses in Arabidopsis. *FEBS Lett* **582**, 943 (Mar 19, 2008).
85. Y. Galon *et al.*, Calmodulin-binding transcription activator 1 mediates auxin signaling and responds to stresses in Arabidopsis. *Planta* **232**, 165 (Jun, 2010).
86. J. A. Hill *et al.*, Cardiac hypertrophy is not a required compensatory response to short-term pressure overload. *Circulation* **101**, 2863 (Jun 20, 2000).
87. C. L. Zhang *et al.*, Class II histone deacetylases act as signal-responsive repressors of cardiac hypertrophy. *Cell* **110**, 479 (Aug 23, 2002).
88. T. Nagase *et al.*, Prediction of the coding sequences of unidentified human genes. XII. The complete sequences of 100 new cDNA clones from brain which code for large proteins in vitro. *DNA Res* **5**, 355 (Dec 31, 1998).
89. V. Barbashina, P. Salazar, E. C. Holland, M. K. Rosenblum, M. Ladanyi, Allelic losses at 1p36 and 19q13 in gliomas: correlation with histologic classification, definition of a 150-kb minimal deleted region on 1p36, and evaluation of CAMTA1 as a candidate tumor suppressor gene. *Clin Cancer Res* **11**, 1119 (Feb 1, 2005).
90. M. J. Huentelman *et al.*, Calmodulin-binding transcription activator 1 (CAMTA1) alleles predispose human episodic memory performance. *Human molecular genetics* **16**, 1469 (Jun 15, 2007).

91. J. Thevenon *et al.*, Intragenic CAMTA1 rearrangements cause non-progressive congenital ataxia with or without intellectual disability. *Journal of medical genetics* **49**, 400 (Jun, 2012).
92. M. Shinawi, R. Coorg, J. S. Shimony, D. K. Grange, H. Al-Kateb, Intragenic CAMTA1 deletions are associated with a spectrum of neurobehavioral phenotypes. *Clinical genetics*, (Apr 17, 2014).
93. Y. Zhou, X. Zhang, A. Klibanski, MEG3 noncoding RNA: a tumor suppressor. *Journal of molecular endocrinology* **48**, R45 (Jun, 2012).
94. P. S. White *et al.*, A region of consistent deletion in neuroblastoma maps within human chromosome 1p36.2-36.3. *Proc Natl Acad Sci U S A* **92**, 5520 (Jun 6, 1995).
95. M. Katoh, Identification and characterization of FLJ10737 and CAMTA1 genes on the commonly deleted region of neuroblastoma at human chromosome 1p36.31-p36.23. *Int J Oncol* **23**, 1219 (Oct, 2003).
96. K. Nakatani *et al.*, Cell cycle-dependent transcriptional regulation of calmodulin-binding transcription activator 1 in neuroblastoma cells. *Int J Oncol* **24**, 1407 (Jun, 2004).
97. P. S. White *et al.*, Definition and characterization of a region of 1p36.3 consistently deleted in neuroblastoma. *Oncogene* **24**, 2684 (Apr 14, 2005).
98. E. F. Attiyeh *et al.*, Chromosome 1p and 11q deletions and outcome in neuroblastoma. *N Engl J Med* **353**, 2243 (Nov 24, 2005).
99. K. O. Henrich *et al.*, Reduced expression of CAMTA1 correlates with adverse outcome in neuroblastoma patients. *Clin Cancer Res* **12**, 131 (Jan 1, 2006).
100. K. O. Henrich *et al.*, Allelic variants of CAMTA1 and FLJ10737 within a commonly deleted region at 1p36 in neuroblastoma. *Eur J Cancer* **43**, 607 (Feb, 2007).
101. E. R. Okawa *et al.*, Expression and sequence analysis of candidates for the 1p36.31 tumor suppressor gene deleted in neuroblastomas. *Oncogene* **27**, 803 (Jan 31, 2008).
102. A. Mukasa *et al.*, Selective expression of a subset of neuronal genes in oligodendroglioma with chromosome 1p loss. *Brain Pathol* **14**, 34 (Jan, 2004).
103. K. Ichimura *et al.*, 1p36 is a preferential target of chromosome 1 deletions in astrocytic tumours and homozygously deleted in a subset of glioblastomas. *Oncogene* **27**, 2097 (Mar 27, 2008).

104. K. O. Henrich *et al.*, CAMTA1, a 1p36 tumor suppressor candidate, inhibits growth and activates differentiation programs in neuroblastoma cells. *Cancer Res* **71**, 3142 (Apr 15, 2011).

105. R. P. Harvey, NK-2 homeobox genes and heart development. *Dev Biol* **178**, 203 (Sep 15, 1996).

106. M. N. Stanfel, K. A. Moses, R. J. Schwartz, W. E. Zimmer, Regulation of organ development by the NKX-homeodomain factors: an NKX code. *Cell Mol Biol (Noisy-le-grand)* **Suppl 51**, OL785 (2005).

107. C. Y. Chen, R. J. Schwartz, Identification of novel DNA binding targets and regulatory domains of a murine tinman homeodomain factor, nkx-2.5. *J Biol Chem* **270**, 15628 (Jun 30, 1995).

108. D. Durocher, C. Y. Chen, A. Ardati, R. J. Schwartz, M. Nemer, The atrial natriuretic factor promoter is a downstream target for Nkx-2.5 in the myocardium. *Molecular and cellular biology* **16**, 4648 (Sep, 1996).

109. I. Shiojima *et al.*, Context-dependent transcriptional cooperation mediated by cardiac transcription factors Csx/Nkx-2.5 and GATA-4. *J Biol Chem* **274**, 8231 (Mar 19, 1999).

110. H. Watada, R. G. Mirmira, J. Kalamaras, M. S. German, Intramolecular control of transcriptional activity by the NK2-specific domain in NK-2 homeodomain proteins. *Proc Natl Acad Sci U S A* **97**, 9443 (Aug 15, 2000).

111. J. T. Hill, K. R. Anderson, T. L. Mastracci, K. H. Kaestner, L. Sussel, Novel computational analysis of protein binding array data identifies direct targets of Nkx2.2 in the pancreas. *BMC bioinformatics* **12**, 62 (2011).

112. P. Minoo, G. Su, H. Drum, P. Bringas, S. Kimura, Defects in tracheoesophageal and lung morphogenesis in Nkx2.1(-/-) mouse embryos. *Dev Biol* **209**, 60 (May 1, 1999).

113. B. Yuan *et al.*, Inhibition of distal lung morphogenesis in Nkx2.1(-/-) embryos. *Developmental dynamics : an official publication of the American Association of Anatomists* **217**, 180 (Feb, 2000).

114. V. Kolla *et al.*, Thyroid transcription factor in differentiating type II cells: regulation, isoforms, and target genes. *American journal of respiratory cell and molecular biology* **36**, 213 (Feb, 2007).

115. L. Pradhan *et al.*, Crystal structure of the human NKX2.5 homeodomain in complex with DNA target. *Biochemistry* **51**, 6312 (Aug 14, 2012).

116. T. J. Lints, L. M. Parsons, L. Hartley, I. Lyons, R. P. Harvey, Nkx-2.5: a novel murine homeobox gene expressed in early heart progenitor cells and their myogenic descendants. *Development* **119**, 419 (Oct, 1993).

117. I. Lyons *et al.*, Myogenic and morphogenetic defects in the heart tubes of murine embryos lacking the homeo box gene Nkx2-5. *Genes Dev* **9**, 1654 (Jul 1, 1995).

118. M. Tanaka, Z. Chen, S. Bartunkova, N. Yamasaki, S. Izumo, The cardiac homeobox gene Csx/Nkx2.5 lies genetically upstream of multiple genes essential for heart development. *Development* **126**, 1269 (Mar, 1999).

119. Y. Hiroi *et al.*, Tbx5 associates with Nkx2-5 and synergistically promotes cardiomyocyte differentiation. *Nature genetics* **28**, 276 (Jul, 2001).

120. B. G. Bruneau *et al.*, A murine model of Holt-Oram syndrome defines roles of the T-box transcription factor Tbx5 in cardiogenesis and disease. *Cell* **106**, 709 (Sep 21, 2001).

121. L. E. Briggs *et al.*, Perinatal loss of Nkx2-5 results in rapid conduction and contraction defects. *Circulation research* **103**, 580 (Sep 12, 2008).

122. M. Takeda *et al.*, Slow progressive conduction and contraction defects in loss of Nkx2-5 mice after cardiomyocyte terminal differentiation. *Lab Invest* **89**, 983 (Sep, 2009).

123. D. Durocher, F. Charron, R. Warren, R. J. Schwartz, M. Nemer, The cardiac transcription factors Nkx2-5 and GATA-4 are mutual cofactors. *EMBO J* **16**, 5687 (Sep 15, 1997).

124. A. C. Houweling, M. M. van Borren, A. F. Moorman, V. M. Christoffels, Expression and regulation of the atrial natriuretic factor encoding gene Nppa during development and disease. *Cardiovasc Res* **67**, 583 (Sep 1, 2005).

125. S. M. Reamon-Buettner, J. Borlak, NKX2-5: an update on this hypermutable homeodomain protein and its role in human congenital heart disease (CHD). *Human mutation* **31**, 1185 (Nov, 2010).

126. J. Briscoe *et al.*, Homeobox gene Nkx2.2 and specification of neuronal identity by graded Sonic hedgehog signalling. *Nature* **398**, 622 (Apr 15, 1999).

127. J. Briscoe, A. Pierani, T. M. Jessell, J. Ericson, A homeodomain protein code specifies progenitor cell identity and neuronal fate in the ventral neural tube. *Cell* **101**, 435 (May 12, 2000).

128. X. Xu *et al.*, Selective expression of Nkx-2.2 transcription factor in chicken oligodendrocyte progenitors and implications for the embryonic origin of oligodendrocytes. *Molecular and cellular neurosciences* **16**, 740 (Dec, 2000).

129. Y. Qi *et al.*, Control of oligodendrocyte differentiation by the Nkx2.2 homeodomain transcription factor. *Development* **128**, 2723 (Jul, 2001).

130. C. Soula *et al.*, Distinct sites of origin of oligodendrocytes and somatic motoneurons in the chick spinal cord: oligodendrocytes arise from Nkx2.2-expressing progenitors by a Shh-dependent mechanism. *Development* **128**, 1369 (Apr, 2001).

131. Q. Zhou, G. Choi, D. J. Anderson, The bHLH transcription factor Olig2 promotes oligodendrocyte differentiation in collaboration with Nkx2.2. *Neuron* **31**, 791 (Sep 13, 2001).

132. H. Fu *et al.*, Dual origin of spinal oligodendrocyte progenitors and evidence for the cooperative role of Olig2 and Nkx2.2 in the control of oligodendrocyte differentiation. *Development* **129**, 681 (Feb, 2002).

133. Q. Zhu *et al.*, Genetic evidence that Nkx2.2 and Pdgfra are major determinants of the timing of oligodendrocyte differentiation in the developing CNS. *Development* **141**, 548 (Feb, 2014).

134. Z. Liu *et al.*, Induction of oligodendrocyte differentiation by Olig2 and Sox10: evidence for reciprocal interactions and dosage-dependent mechanisms. *Dev Biol* **302**, 683 (Feb 15, 2007).

135. Q. Wei, W. K. Miskimins, R. Miskimins, Stage-specific expression of myelin basic protein in oligodendrocytes involves Nkx2.2-mediated repression that is relieved by the Sp1 transcription factor. *J Biol Chem* **280**, 16284 (Apr 22, 2005).

136. S. Ji, J. R. Doucette, A. J. Nazarali, Sirt2 is a novel in vivo downstream target of Nkx2.2 and enhances oligodendroglial cell differentiation. *Journal of molecular cell biology* **3**, 351 (Dec, 2011).

137. W. Li *et al.*, Sirtuin 2, a mammalian homolog of yeast silent information regulator-2 longevity regulator, is an oligodendroglial protein that decelerates cell differentiation through deacetylating alpha-tubulin. *J Neurosci* **27**, 2606 (Mar 7, 2007).

138. H. B. Werner *et al.*, Proteolipid protein is required for transport of sirtuin 2 into CNS myelin. *J Neurosci* **27**, 7717 (Jul 18, 2007).

139. N. P. Pringle, W. D. Richardson, A singularity of PDGF alpha-receptor expression in the dorsoventral axis of the neural tube may define the origin of the oligodendrocyte lineage. *Development* **117**, 525 (Feb, 1993).

140. R. D. McKinnon, S. Waldron, M. E. Kiel, PDGF alpha-receptor signal strength controls an RTK rheostat that integrates phosphoinositol 3'-kinase and phospholipase Cgamma pathways during oligodendrocyte maturation. *J Neurosci* **25**, 3499 (Apr 6, 2005).

141. J. Muhr, E. Andersson, M. Persson, T. M. Jessell, J. Ericson, Groucho-mediated transcriptional repression establishes progenitor cell pattern and neuronal fate in the ventral neural tube. *Cell* **104**, 861 (Mar 23, 2001).

142. T. Muraguchi *et al.*, NKX2.2 suppresses self-renewal of glioma-initiating cells. *Cancer Res* **71**, 1135 (Feb 1, 2010).

143. B. A. Vesely *et al.*, Four cardiac hormones eliminate 4-fold more human glioblastoma cells than the green mamba snake peptide. *Cancer Lett* **254**, 94 (Aug 28, 2007).

144. B. Hessabi, I. Schmidt, R. Walther, The homeodomain of Nkx2.2 carries two cooperatively acting nuclear localization signals. *Biochem Biophys Res Commun* **270**, 695 (Apr 21, 2000).

145. T. Sun *et al.*, Cross-repressive interaction of the Olig2 and Nkx2.2 transcription factors in developing neural tube associated with formation of a specific physical complex. *J Neurosci* **23**, 9547 (Oct 22, 2003).

146. M. Beitzinger, L. Peters, J. Y. Zhu, E. Kremmer, G. Meister, Identification of human microRNA targets from isolated argonaute protein complexes. *RNA biology* **4**, 76 (Jun, 2007).

147. J. Pfaff *et al.*, Structural features of Argonaute-GW182 protein interactions. *Proceedings of the National Academy of Sciences of the United States of America* **110**, E3770 (Oct 1, 2013).

148. C. Mayr, M. T. Hemann, D. P. Bartel, Disrupting the pairing between let-7 and Hmga2 enhances oncogenic transformation. *Science* **315**, 1576 (Mar 16, 2007).

149. L. Salmena, L. Poliseno, Y. Tay, L. Kats, P. P. Pandolfi, A ceRNA hypothesis: the Rosetta Stone of a hidden RNA language? *Cell* **146**, 353 (Aug 5, 2011).

150. L. Poliseno *et al.*, A coding-independent function of gene and pseudogene mRNAs regulates tumour biology. *Nature* **465**, 1033 (Jun 24, 2010).

151. D. Barrick, D. U. Ferreiro, E. A. Komives, Folding landscapes of ankyrin repeat proteins: experiments meet theory. *Current opinion in structural biology* **18**, 27 (Feb, 2008).

152. H. Kasahara *et al.*, Characterization of homo- and heterodimerization of cardiac Csx/Nkx2.5 homeoprotein. *J Biol Chem* **276**, 4570 (Feb 16, 2001).

153. Y. S. Lee, A. Dutta, The tumor suppressor microRNA let-7 represses the HMGA2 oncogene. *Genes & development* **21**, 1025 (May 1, 2007).

154. I. Martinez *et al.*, Human papillomavirus type 16 reduces the expression of microRNA-218 in cervical carcinoma cells. *Oncogene* **27**, 2575 (Apr 17, 2008).

155. L. Jiang *et al.*, miR-182 as a prognostic marker for glioma progression and patient survival. *The American journal of pathology* **177**, 29 (Jul, 2010).

156. L. Song *et al.*, TGF-beta induces miR-182 to sustain NF-kappaB activation in glioma subsets. *The Journal of clinical investigation* **122**, 3563 (Oct, 2012).

157. G. S. Kapoor, Y. Zhan, G. R. Johnson, D. M. O'Rourke, Distinct domains in the SHP-2 phosphatase differentially regulate epidermal growth factor receptor/NF-kappaB activation through Gab1 in glioblastoma cells. *Molecular and cellular biology* **24**, 823 (Jan, 2004).

158. X. Tan *et al.*, cAMP response element-binding protein promotes gliomagenesis by modulating the expression of oncogenic microRNA-23a. *Proc Natl Acad Sci U S A* **109**, 15805 (Sep 25, 2012).

159. P. T. Nelson *et al.*, Microarray-based, high-throughput gene expression profiling of microRNAs. *Nature methods* **1**, 155 (Nov, 2004).

160. M. Hafner *et al.*, Transcriptome-wide identification of RNA-binding protein and microRNA target sites by PAR-CLIP. *Cell* **141**, 129 (Apr 2, 2010).

161. I. Lipchina *et al.*, Genome-wide identification of microRNA targets in human ES cells reveals a role for miR-302 in modulating BMP response. *Genes & development* **25**, 2173 (Oct 15, 2011).

162. E. R. Levin, D. G. Gardner, W. K. Samson, Natriuretic peptides. *N Engl J Med* **339**, 321 (Jul 30, 1998).

163. E. DiCicco-Bloom *et al.*, Embryonic expression and multifunctional actions of the natriuretic peptides and receptors in the developing nervous system. *Dev Biol* **271**, 161 (Jul 1, 2004).

164. J. A. Waschek, Developmental actions of natriuretic peptides in the brain and skeleton. *Cell Mol Life Sci* **61**, 2332 (Sep, 2004).

165. L. H. Cao, X. L. Yang, Natriuretic peptides and their receptors in the central nervous system. *Prog Neurobiol* **84**, 234 (Mar, 2008).

166. J. Prado, M. A. Baltrons, P. Pifarre, A. Garcia, Glial cells as sources and targets of natriuretic peptides. *Neurochem Int* **57**, 367 (Nov, 2009).

167. E. R. Levin, H. J. Frank, Natriuretic peptides inhibit rat astroglial proliferation: mediation by C receptor. *The American journal of physiology* **261**, R453 (Aug, 1991).

168. W. R. Gower, B. A. Vesely, A. A. Alli, D. L. Vesely, Four peptides decrease human colon adenocarcinoma cell number and DNA synthesis via cyclic GMP. *Int J Gastrointest Cancer* **36**, 77 (2005).

169. B. A. Vesely *et al.*, Four peptide hormones' specific decrease (up to 97%) of human prostate carcinoma cells. *Eur J Clin Invest* **35**, 700 (Nov, 2005).

170. B. A. Vesely *et al.*, Five cardiac hormones decrease the number of human small-cell lung cancer cells. *Eur J Clin Invest* **35**, 388 (Jun, 2005).

171. W. P. t. Skelton, G. Pi, A. Lenz, Y. Sun, D. L. Vesely, Cardiac hormones inhibit proliferation of pancreatic cancer but not normal cells. *Eur J Clin Invest* **40**, 706 (Aug, 2010).

172. D. L. Vesely, Cardiac hormones for the treatment of cancer. *Endocrine-related cancer* **20**, R113 (Jun, 2013).

173. Y. Sun, E. J. Eichelbaum, H. Wang, D. L. Vesely, Atrial natriuretic peptide and long acting natriuretic peptide inhibit ERK 1/2 in prostate cancer cells. *Anticancer Res* **26**, 4143 (Nov-Dec, 2006).

174. Y. Sun, E. J. Eichelbaum, H. Wang, D. L. Vesely, Atrial natriuretic peptide and long acting natriuretic peptide inhibit MEK 1/2 activation in human prostate cancer cells. *Anticancer Res* **27**, 3813 (Nov-Dec, 2007).

175. Y. Sun *et al.*, Atrial natriuretic peptide and long-acting natriuretic peptide inhibit ras in human prostate cancer cells. *Anticancer Res* **29**, 1889 (Jun, 2009).

176. M. M. Sherry, A. Reeves, J. K. Wu, B. H. Cochran, STAT3 is required for proliferation and maintenance of multipotency in glioblastoma stem cells. *Stem Cells* **27**, 2383 (Oct, 2009).

177. A. Rousseau *et al.*, Expression of oligodendroglial and astrocytic lineage markers in diffuse gliomas: use of YKL-40, ApoE, ASCL1, and NKX2-2. *Journal of neuropathology and experimental neurology* **65**, 1149 (Dec, 2006).

178. R. Smith *et al.*, Expression profiling of EWS/FLI identifies NKX2.2 as a critical target gene in Ewing's sarcoma. *Cancer cell* **9**, 405 (May, 2006).
179. L. A. Owen, A. A. Kowalewski, S. L. Lessnick, EWS/FLI mediates transcriptional repression via NKX2.2 during oncogenic transformation in Ewing's sarcoma. *PloS one* **3**, e1965 (2008).
180. M. M. Winslow *et al.*, Suppression of lung adenocarcinoma progression by Nkx2-1. *Nature* **473**, 101 (May 5, 2011).
181. E. L. Snyder *et al.*, Nkx2-1 represses a latent gastric differentiation program in lung adenocarcinoma. *Molecular cell* **50**, 185 (Apr 25, 2013).
182. H. Watanabe *et al.*, Integrated cistromic and expression analysis of amplified NKX2-1 in lung adenocarcinoma identifies LMO3 as a functional transcriptional target. *Genes Dev* **27**, 197 (Jan 15, 2013).
183. T. Yamaguchi, Y. Hosono, K. Yanagisawa, T. Takahashi, NKX2-1/TTF-1: an enigmatic oncogene that functions as a double-edged sword for cancer cell survival and progression. *Cancer cell* **23**, 718 (Jun 10, 2013).
184. A. P. Patel *et al.*, Single-cell RNA-seq highlights intratumoral heterogeneity in primary glioblastoma. *Science* **344**, 1396 (Jun 20, 2014).
185. S. N. Cohen, A. C. Chang, L. Hsu, Nonchromosomal antibiotic resistance in bacteria: genetic transformation of Escherichia coli by R-factor DNA. *Proc Natl Acad Sci U S A* **69**, 2110 (Aug, 1972).
186. R. Higuchi, G. Dollinger, P. S. Walsh, R. Griffith, Simultaneous amplification and detection of specific DNA sequences. *Biotechnology (N Y)* **10**, 413 (Apr, 1992).
187. R. Higuchi, C. Fockler, G. Dollinger, R. Watson, Kinetic PCR analysis: real-time monitoring of DNA amplification reactions. *Biotechnology (N Y)* **11**, 1026 (Sep, 1993).
188. K. J. Livak, T. D. Schmittgen, Analysis of relative gene expression data using real-time quantitative PCR and the 2(-Delta Delta C(T)) Method. *Methods* **25**, 402 (Dec, 2001).
189. U. K. Laemmli, Cleavage of structural proteins during the assembly of the head of bacteriophage T4. *Nature* **227**, 680 (Aug 15, 1970).
190. J. D. Dignam, R. M. Lebovitz, R. G. Roeder, Accurate transcription initiation by RNA polymerase II in a soluble extract from isolated mammalian nuclei. *Nucleic acids research* **11**, 1475 (Mar 11, 1983).

191. M. M. Bradford, A rapid and sensitive method for the quantitation of microgram quantities of protein utilizing the principle of protein-dye binding. *Anal Biochem* **72**, 248 (May 7, 1976).

192. H. Blum, H. Beier, J. Gross, Improved silver staining of plant proteins, RNA and DNA in polyacrylamide gels. *Electrophoresis* **8**, 93 (1987).

193. TCGA, Comprehensive genomic characterization defines human glioblastoma genes and core pathways. *Nature* **455**, 1061 (Oct 23, 2008).

194. S. Madhavan *et al.*, Rembrandt: helping personalized medicine become a reality through integrative translational research. *Molecular cancer research : MCR* **7**, 157 (Feb, 2009).

Appendix

Table A.1 contains the complete list of the mass-spectrometric analysis of FH-Nkx2.2 (co-)immunoprecipitates (see paragraph 2.2.2.).

Table A.1: Complete mass-spectrometric analysis of FH-Nkx2.2 (co-)immunoprecipitates. Identified proteins are stated as indicated with molecular weight (MW), Mascot protein scores, number of peptides (#peptides), and sequence coverage (SC).

band	identified protein	MW [kDa]	scores	#peptides	SC [%]
a	Myosin-9	226.4	842.1	20	11.0
	Nuclear pore complex protein Nup205	227.8	739.0	17	8.3
	U5 small nuclear ribonucleoprotein 200 kDa helicase	244.4	396.2	10	5.2
	Dedicator of cytokinesis protein 4	225.1	259.2	6	3.8
	HEAT repeat-containing protein 1	242.2	111.0	3	1.4
	Phosphatidylinositol 4-kinase alpha	231.2	91.6	2	0.9
	DNA-dependent protein kinase catalytic subunit	468.8	83.9	3	1.0
	Ubiquitin-40S ribosomal protein S27a	18.0	65.2	2	16.0
	Nuclear mitotic apparatus protein	238.1	63.2	1	0.8
	G-protein coupled receptor 98	692.6	48.3	1	0.1
	Dedicator of cytokinesis protein 7	242.4	44.8	1	0.7
	CAD protein	242.8	42.3	1	0.4
	Plectin	531.5	40.6	1	0.1
	Sperm-specific antigen 2	138.3	38.2	1	0.8
b	Structural maintenance of chromosomes protein 1A	143.1	257.4	6	5.3
	Bifunctional glutamate/proline-tRNA ligase	170.5	233.3	6	4.6
	OTU domain-containing protein 4	123.8	178.0	5	7.3
	Dynactin subunit 1	141.6	168.0	4	3.6
	Eukaryotic translation initiation factor 3 subunit A	166.5	117.8	4	2.3
	Heat shock 70 kDa protein 1-like	70.3	95.1	2	3.9
	Myb-binding protein 1A	148.8	94.7	3	4.4
	Clathrin heavy chain 1	191.5	78.3	2	1.5
	Homeobox protein Nkx-2.2	30.1	72.1	2	6.2
	Ig alpha-1 chain C region	37.6	67.8	1	2.8

Table continued on next page

band	identified protein	MW [kDa]	scores	#peptides	SC [%]
	Integrin alpha-X	127.7	60.0	2	2.9
	Insulin receptor substrate 4	133.7	58.5	2	2.1
	Plectin	531.5	54.3	1	0.1
	Nesprin-2	795.9	53.2	1	0.1
	Ubiquitin-40S ribosomal protein S27a	18.0	47.9	1	10.3
	Tyrosine-protein phosphatase non-receptor type 1	49.9	45.6	1	1.8
	Lactadherin	43.1	45.2	1	2.3
	Midasin	632.4	44.1	1	0.2
	Sperm-specific antigen 2	138.3	43.5	1	0.8
	Nesprin-1	1010.4	43.0	1	0.1
	Copine-2	61.2	39.5	1	1.6
	Long-chain fatty acid transport protein 4	72.0	39.3	1	1.2
c	Heterogeneous nuclear ribonucleoprotein U	90.5	678.2	14	21.3
	Tyrosine-protein kinase JAK1	133.2	490.7	13	13.1
	Importin-8	119.9	451.6	8	8.6
	Matrin-3	94.6	384.5	10	15.7
	Kinesin-like protein KIF11	119.1	329.9	9	9.2
	Helicase-like transcription factor	113.9	319.6	7	8.2
	Poly [ADP-ribose] polymerase 1	113.0	319.6	8	10.4
	116 kDa U5 small nuclear ribonucleoprotein component	109.4	262.7	9	10.6
	RNA-binding protein 10	103.5	201.1	4	5.3
	Cullin-associated NEDD8-dissociated protein 1	136.3	126.9	3	2.7
	Ankyrin repeat and FYVE domain-containing protein 1	128.3	96.2	2	2.7
	Ig kappa chain V-II region Cum	12.7	93.1	1	11.3
	Importin-7	119.4	83.0	2	1.9
	Ubiquitin carboxyl-terminal hydrolase 15	112.3	81.7	2	2.1
	Importin-4	118.6	74.4	2	2.4
	Putative trypsin-6	26.5	70.1	6	4.0
	Ryanodine receptor 2	564.2	53.0	1	0.2
	Heat shock cognate 71 kDa protein	70.9	51.0	1	2.0
	Transcriptional regulator ATRX	282.4	43.3	1	0.6
	Homeobox protein Nkx-2.2	30.1	42.3	2	7.3
	Nucleolar and coiled-body phosphoprotein 1	73.6	39.5	1	2.7
d	Kinesin-like protein KIF11	119.1	981.8	24	25.1
	Heat shock protein 105 kDa	96.8	859.7	25	22.5
	Heat shock 70 kDa protein 4	94.3	760.3	16	20.0
	Sarcoplasmic/endoplasmic reticulum calcium ATPase 2	114.7	348.0	8	10.1
	Monofunctional C1-tetrahydrofolate synthase, mitochondrial	105.7	347.5	10	11.2
	Unconventional myosin-Ic	121.6	279.5	7	6.6
	Exportin-1	123.3	238.0	8	8.9
	UDP-N-acetylglucosamine--peptide N-acetylglucosaminyltransferase 110 kDa subunit	116.8	230.3	5	5.7
	Chromodomain-helicase-DNA-binding protein 1-like	100.9	227.8	7	7.7
	ER degradation-enhancing alpha-mannosidase-like 3	104.6	198.5	6	7.8

Table continued on next page

band	identified protein	MW [kDa]	scores	#peptides	SC [%]
	C-1-tetrahydrofolate synthase, cytoplasmic	101.5	182.2	4	4.8
	Exportin-2	110.3	161.0	3	2.9
	Pre-mRNA-processing factor 6	106.9	157.9	5	6.5
	Putative ribosomal RNA methyltransferase NOP2	89.2	136.7	4	6.7
	Ribosome biogenesis protein BOP1	83.6	135.9	3	3.4
	Heat shock 70 kDa protein 1A/1B	70.0	126.6	3	5.3
	Eukaryotic translation initiation factor 3 subunit B	92.4	124.6	3	3.9
	Interleukin enhancer-binding factor 3	95.3	104.3	3	4.4
	Homeobox protein Nkx-2.2	30.1	92.9	3	12.8
	Ig kappa chain V-II region Cum	12.7	88.2	1	11.3
	26S proteasome non-ATPase regulatory subunit 1	105.8	85.1	2	2.0
	Uncharacterized protein C2orf16	224.2	74.9	1	0.5
	Serum albumin	69.3	74.2	2	3.6
	Heat shock cognate 71 kDa protein	70.9	70.2	1	2.0
	General vesicular transport factor p115	107.8	70.2	1	1.9
	DNA replication licensing factor MCM6	92.8	65.1	1	1.2
	Eukaryotic translation initiation factor 3 subunit C	105.3	64.0	2	1.9
	Replication factor C subunit 1	128.2	63.3	1	1.0
	Putative trypsin-6	26.5	57.3	6	4.0
	RING finger protein 219	81.1	51.9	1	1.4
e	Importin subunit beta-1	97.1	475.9	11	11.5
	Nucleolar RNA helicase 2	87.3	434.9	12	17.2
	MMS19 nucleotide excision repair protein homolog	113.2	396.5	12	14.9
	Sodium/potassium-transporting ATPase subunit alpha-1	112.8	159.7	3	3.4
	26S proteasome non-ATPase regulatory subunit 2	100.1	138.6	3	6.1
	A-kinase anchor protein 8	76.1	110.3	1	2.9
	Transitional endoplasmic reticulum ATPase	89.3	104.9	2	3.0
	Heat shock 70 kDa protein 1-like	70.3	98.4	2	3.9
	Methionine--tRNA ligase, cytoplasmic	101.1	97.2	4	4.1
	Ig kappa chain V-II region Cum	12.7	92.1	1	11.3
	RNA-binding protein 10	103.5	75.0	2	2.5
	Serum albumin	69.3	66.1	1	2.5
	Leucine-rich repeat-containing protein 16B	150.1	58.1	1	0.7
	Homeobox protein Nkx-2.2	30.1	56.4	2	6.2
	tRNA (cytosine(34)-C(5))-methyltransferase	86.4	49.9	1	1.4
	Plectin	531.5	47.9	0	0.0
	Histone-lysine N-methyltransferase, H3 lysine-36 and H4 lysine-20 specific	296.5	47.5	1	0.4
	Dynein heavy chain domain-containing protein 1	533.3	46.3	2	0.5
	Transducin-like enhancer protein 3	83.4	42.6	2	3.4
	Protein sel-1 homolog 1	88.7	42.3	1	2.1
	STEAP family member 1B	28.8	39.7	1	2.9
	Coiled-coil domain-containing protein 62	77.7	38.5	1	0.7
f	X-ray repair cross-complementing protein 5	82.7	1495.8	40	41.9

Table continued on next page

band	identified protein	MW [kDa]	scores	#peptides	SC [%]
	DNA replication licensing factor MCM7	81.3	1295.4	27	42.7
	Mitochondrial inner membrane protein	83.6	215.3	6	9.5
	Delta-1-pyrroline-5-carboxylate synthase	87.2	206.0	6	9.8
	Ig kappa chain V-II region MIL	12.0	172.7	2	11.6
	Heat shock 70 kDa protein 1-like	70.3	97.1	2	4.5
	Serine/threonine-protein kinase RIO1	65.5	79.3	2	4.8
	Serum albumin	69.3	73.2	2	3.6
	Serotransferrin	77.0	65.3	2	7.4
	Putative trypsin-6	26.5	56.0	6	4.0
	Eukaryotic translation initiation factor 4B	69.1	43.7	1	1.5
	Filamin-B	278.0	41.8	1	1.0
	Alpha-actinin-1	103.0	41.1	0	0.0
	Uncharacterized protein C2orf16	224.2	40.3	2	0.5
	DnaJ homolog subfamily C member 10	91.0	40.0	1	1.3
	Spectrin beta chain, non-erythrocytic 1	274.4	39.2	1	0.5
	Small G protein signaling modulator 1	129.6	38.3	1	0.8
g	78 kDa glucose-regulated protein	72.3	2489.4	46	48.6
	Eukaryotic translation initiation factor 4B	69.1	651.3	12	25.2
	Heat shock cognate 71 kDa protein	70.9	650.9	10	19.7
	Heat shock 70 kDa protein 1-like	70.3	510.9	7	13.1
	Heat shock 70 kDa protein 1A/1B	70.0	507.6	10	17.8
	ATP-dependent RNA helicase DDX3X	73.2	288.3	8	13.3
	DBIRD complex subunit ZNF326	65.6	188.9	4	8.8
	Serum albumin	69.3	123.2	3	4.8
	Ubiquitin-40S ribosomal protein S27a	18.0	116.2	2	16.0
	X-ray repair cross-complementing protein 5	82.7	106.4	2	2.9
	Serotransferrin	77.0	81.4	2	6.7
	ATP-binding cassette sub-family F member 2	71.2	80.8	2	3.7
	Ig kappa chain V-II region Cum	12.7	68.2	1	11.3
	Putative trypsin-6	26.5	61.7	5	4.0
	Nesprin-1	1010.4	59.5	0	0.0
	Homeobox protein Nkx-2.2	30.1	57.6	2	8.8
	Protein arginine N-methyltransferase 5	72.6	57.0	1	1.6
	DNA replication licensing factor MCM7	81.3	56.0	2	3.8
	Plectin	531.5	53.4	1	0.3
	Melanoma-associated antigen D2	64.9	46.1	1	2.1
	Ryanodine receptor 2	564.2	42.1	2	0.7
	Synaptopodin-2	117.4	38.1	2	1.1
	Pericentrin	377.8	38.0	2	0.6
h	Heat shock 70 kDa protein 1A/1B	70.0	2695.2	71	51.5
	Heat shock cognate 71 kDa protein	70.9	2299.3	71	50.9
	Stress-70 protein, mitochondrial	73.6	1660.8	30	40.1
	X-ray repair cross-complementing protein 6	69.8	1312.0	29	39.9

Table continued on next page

band	identified protein	MW [kDa]	scores	#peptides	SC [%]
	Heat shock 70 kDa protein 1-like	70.3	1145.3	32	31.5
	Heat shock 70 kDa protein 6	71.0	1096.3	25	21.8
	Heat shock-related 70 kDa protein 2	70.0	978.9	22	18.3
	Protein arginine N-methyltransferase 5	72.6	961.7	24	34.2
	Lamin-B1	66.4	335.8	6	11.3
	78 kDa glucose-regulated protein	72.3	259.3	6	4.3
	Replication protein A 70 kDa DNA-binding subunit	68.1	225.3	4	7.1
	Calcium-binding mitochondrial carrier protein Aralar2	74.1	197.9	4	7.6
	Ig kappa chain V-II region MIL	12.0	156.3	2	11.6
	Heterogeneous nuclear ribonucleoprotein M	77.5	92.5	2	3.6
	Zinc finger protein Helios	59.5	57.8	1	1.5
	G-protein coupled receptor 98	692.6	53.1	1	0.1
	Serotransferrin OS=Homo sapiens GN=TF PE=1 SV=3	77.0	43.6	1	5.4
i	Tubulin beta chain	49.6	1245.6	27	50.0
	Heat shock cognate 71 kDa protein	70.9	1098.7	19	26.5
	Tubulin beta-4B chain	49.8	1048.9	22	43.4
	Heat shock 70 kDa protein 1A/1B	70.0	1046.6	18	30.0
	Eukaryotic initiation factor 4A-I	46.1	758.0	17	36.9
	Vimentin	53.6	652.2	14	33.7
	Eukaryotic initiation factor 4A-III	46.8	440.8	10	24.3
	Heterogeneous nuclear ribonucleoprotein F	45.6	440.2	12	23.4
	Elongation factor 1-alpha 1	50.1	307.3	6	14.5
	Nuclease-sensitive element-binding protein 1	35.9	232.1	4	22.2
	Serpin H1	46.4	207.6	3	9.1
	Elongation factor Tu, mitochondrial	49.5	194.0	3	10.0
	Eukaryotic translation initiation factor 4B	69.1	152.3	2	4.1
	Protein arginine N-methyltransferase 5	72.6	130.0	2	4.7
	Homeobox protein Nkx-2.2	30.1	118.7	3	8.8
	Tubulin alpha-1B chain	50.1	100.7	2	5.1
	Ig kappa chain V-II region Cum	12.7	89.2	1	11.3
	26S protease regulatory subunit 7	48.6	83.6	2	6.5
	Eukaryotic translation initiation factor 3 subunit E	52.2	77.7	2	4.5
	Abnormal spindle-like microcephaly-associated protein	409.5	74.4	2	0.7
	26S protease regulatory subunit 8	45.6	67.7	3	9.9
	Splicing factor 3B subunit 4	44.4	65.3	1	3.3
	Trifunctional enzyme subunit beta, mitochondrial	51.3	62.2	1	1.9
	Elongation factor 1-gamma	50.1	59.3	1	3.0
	Putative trypsin-6	26.5	57.4	6	4.0
	Plectin	531.5	56.5	0	0.0
	Alpha-enolase	47.1	55.9	2	6.7
	ATP-dependent Clp protease ATP-binding subunit clpX-like, mitochondrial	69.2	54.1	1	2.1
	Serum albumin	69.3	52.6	2	2.5
	Transmembrane channel-like protein 3	125.6	49.8	1	0.9
	Hydroxysteroid dehydrogenase-like protein 2	45.4	48.9	1	4.3

Table continued on next page

band	identified protein	MW [kDa]	scores	#peptides	SC [%]
	Titin	3813.7	48.0	1	0.0
	Cyclin-dependent kinase 3	35.0	47.8	1	2.3
	Zinc finger protein 148	88.9	43.2	1	1.1
	Heat-stable enterotoxin receptor	123.3	41.8	1	0.9
	Rab GDP dissociation inhibitor beta	50.6	40.4	1	1.8
	Utrophin	394.2	39.0	0	0.0
	Transmembrane protein 132C	121.7	38.9	1	0.8
j	Elongation factor Tu, mitochondrial	49.5	1293.7	26	54.2
	Heat shock 70 kDa protein 1A/1B	70.0	724.7	14	22.5
	Heat shock cognate 71 kDa protein	70.9	509.6	9	16.3
	Cytochrome b-c1 complex subunit 2, mitochondrial	48.4	462.7	9	25.4
	Ornithine aminotransferase, mitochondrial	48.5	257.2	7	15.7
	Tubulin beta chain	49.6	231.9	5	14.4
	Homeobox protein Nkx-2.2	30.1	215.0	7	37.0
	Heterogeneous nuclear ribonucleoprotein F	45.6	204.6	5	14.5
	Eukaryotic initiation factor 4A-I	46.1	166.5	3	10.6
	DnaJ homolog subfamily A member 1	44.8	142.0	3	9.3
	60S ribosomal protein L3	46.1	106.7	3	7.9
	Ig kappa chain V-II region Cum	12.7	106.3	1	11.3
	Serpin H1	46.4	92.7	2	5.5
	Glutaryl-CoA dehydrogenase, mitochondrial	48.1	86.0	3	8.7
	Vimentin	53.6	79.3	2	4.3
	26S proteasome non-ATPase regulatory subunit 11	47.4	76.5	2	6.2
	Serum albumin	69.3	75.3	2	3.6
	Tubulin alpha-1B chain	50.1	70.7	2	5.1
	Elongation factor 1-alpha 1	50.1	69.4	1	2.4
	Heterogeneous nuclear ribonucleoprotein D0	38.4	63.5	1	3.9
	Ribonuclease inhibitor	49.9	60.6	2	6.5
	Eukaryotic translation initiation factor 3 subunit E	52.2	58.2	2	4.5
	Eukaryotic translation initiation factor 4B	69.1	58.1	1	2.6
	Alpha-centractin	42.6	57.8	1	4.3
	G-protein coupled receptor 98	692.6	53.3	1	0.1
	Obscurin	867.9	52.8	1	0.2
	Eukaryotic initiation factor 4A-III	46.8	50.0	2	6.3
	Protein arginine N-methyltransferase 5	72.6	48.1	1	1.6
	Eukaryotic translation initiation factor 3 subunit F	37.5	47.8	1	3.4
	Cell division cycle protein 20 homolog B	57.3	44.7	1	2.3
	Calcium-binding mitochondrial carrier protein SCaMC-1	53.3	41.7	1	2.7
k	Homeobox protein Nkx-2.2	30.1	1046.9	20	66.7
	Methylosome protein 50	36.7	586.2	10	30.4
	Heat shock 70 kDa protein 1A/1B	70.0	513.2	8	16.4
	Heat shock cognate 71 kDa protein	70.9	344.8	8	16.7
	Heterogeneous nuclear ribonucleoproteins C1/C2	33.6	340.6	7	22.5

Table continued on next page

band	identified protein	MW [kDa]	scores	#peptides	SC [%]
	Replication factor C subunit 3	40.5	235.1	6	13.8
	Actin, cytoplasmic 1	41.7	209.3	4	14.7
	Elongation factor Tu, mitochondrial	49.5	153.5	3	11.3
	Probable cytosolic iron-sulfur protein assembly protein CIAO1	37.8	96.8	2	8.8
	Ig kappa chain V-II region Cum	12.7	95.2	1	11.3
	Probable rRNA-processing protein EBP2	34.8	76.6	1	3.3
	Heterogeneous nuclear ribonucleoprotein A/B	36.2	72.2	1	3.9
	Plectin	531.5	70.9	1	0.1
	Serum albumin	69.3	68.5	1	2.5
	E3 ubiquitin-protein ligase HERC2	526.9	60.2	1	0.2
	Putative trypsin-6	26.5	54.8	6	4.0
	MMS19 nucleotide excision repair protein homolog	113.2	45.3	1	1.0
	FYVE, RhoGEF and PH domain-containing protein 3	79.4	43.6	2	2.5
	Rab-interacting lysosomal protein	44.2	42.4	1	4.7
	Plexin-D1 OS=Homo sapiens GN=PLXND1 PE=1 SV=3	211.9	40.6	1	0.4
	Zinc finger protein 148	88.9	39.4	1	1.1
	DNA excision repair protein ERCC-6	168.3	39.2	1	0.9
	Probable ATP-dependent RNA helicase DDX11	108.2	38.9	2	1.4
	Monocarboxylate transporter 1	53.9	38.5	1	3.0
1	Homeobox protein Nkx-2.2	30.1	2075.1	46	66.7
	Methylosome protein 50	36.7	538.4	11	37.4
	Heat shock 70 kDa protein 1A/1B	70.0	235.4	4	8.1
	DnaJ homolog subfamily A member 3, mitochondrial	52.5	171.2	4	8.5
	40S ribosomal protein SA	32.8	146.8	3	12.9
	7-dehydrocholesterol reductase	54.5	133.7	2	5.1
	Heterogeneous nuclear ribonucleoproteins C1/C2	33.6	115.3	2	9.2
	Heat shock cognate 71 kDa protein	70.9	93.4	2	3.9
	Ig kappa chain V-II region Cum	12.7	91.5	1	11.3
	Serum albumin	69.3	87.5	2	3.6
	Protein SET	33.5	84.4	3	8.3
	TraB domain-containing protein	42.3	80.6	1	3.2
	Putative trypsin-6	26.5	70.6	7	4.0
	Activator of 90 kDa heat shock protein ATPase homolog 1	38.3	70.4	3	13.3
	Ancient ubiquitous protein 1	53.0	60.9	3	8.0
	Keratin, type I cytoskeletal 16	51.2	59.2	3	5.1
	Developmentally-regulated GTP-binding protein 1	40.5	57.7	2	7.9
	Histone H1.2	21.4	50.6	2	9.9
	MMS19 nucleotide excision repair protein homolog	113.2	50.2	1	1.0
	Plectin	531.5	48.0	1	0.1
	Ribosome biogenesis protein BRX1 homolog	41.4	47.5	1	3.1
	Monocarboxylate transporter 1	53.9	46.2	1	3.0
	Rab-interacting lysosomal protein	44.2	45.2	1	4.7
	Casein kinase II subunit alpha	45.1	43.9	1	4.6
	Zinc finger protein 148	88.9	43.7	1	1.1

Table continued on next page

band	identified protein	MW [kDa]	scores	#peptides	SC [%]
m	Homeobox protein Nkx-2.2	30.1	3899.2	84	84.2
	Glutaminyl-peptide cyclotransferase-like protein	42.9	474.1	12	23.3
	Nucleophosmin	32.6	286.8	8	18.7
	Methylosome protein 50	36.7	246.4	6	23.4
	Homeobox protein Nkx-2.3	38.4	205.2	5	6.9
	Methylosome subunit pICln	26.2	171.1	3	18.6
	Core histone macro-H2A.1	39.6	155.9	2	11.3
	Heat shock 70 kDa protein 1A/1B	70.0	147.1	3	6.7
	Protein transport protein Sec61 subunit alpha isoform 1	52.2	138.0	3	6.3
	Poly(rC)-binding protein 1	37.5	112.9	3	9.3
	Heterogeneous nuclear ribonucleoproteins A2/B1	37.4	112.8	3	13.9
	Ig kappa chain V-II region Cum	12.7	91.8	1	11.3
	Plectin	531.5	72.8	0	0.0
	Rab-interacting lysosomal protein	44.2	67.2	1	4.7
	A-kinase anchor protein 9	453.4	55.8	2	0.4
	Stomatin-like protein 2	38.5	53.8	3	9.0
	Microtubule-actin cross-linking factor 1, isoforms 1/2/3/5	837.8	46.1	1	0.1
	Caytaxin	42.1	45.7	2	2.4
	Trypsin-3	32.5	43.5	0	0.0
	DNA polymerase zeta catalytic subunit	352.6	42.0	2	0.3
	Collagen alpha-5(VI) chain	289.7	41.6	1	0.5
	Erlin-1	38.9	40.2	1	4.3
	Centrosomal protein KIAA1731	295.0	39.4	1	0.3
	Platelet glycoprotein V	60.9	39.2	1	1.4
	Coiled-coil domain-containing protein 88B	164.7	38.9	1	0.5
	Pseudopodium-enriched atypical kinase 1	193.0	38.6	1	0.9
	5' exonuclease Apollo	60.0	38.4	1	1.3
	Solute carrier family 52, riboflavin transporter, member 1	46.3	38.3	1	1.6
n	Homeobox protein Nkx-2.2	30.1	2982.4	62	70.3
	Heterogeneous nuclear ribonucleoproteins C1/C2	33.6	434.3	9	21.6
	Glutaminyl-peptide cyclotransferase-like protein	42.9	431.4	10	25.9
	Heterogeneous nuclear ribonucleoproteins A2/B1	37.4	317.9	7	19.5
	Replication factor C subunit 2	39.1	274.7	6	23.4
	Homeobox protein Nkx-2.3	38.4	195.6	4	6.0
	Ig kappa chain V-II region Cum	12.7	92.4	1	11.3
	3-hydroxyacyl-CoA dehydratase 3	43.1	91.5	2	6.9
	DnaJ homolog subfamily A member 3, mitochondrial	52.5	87.0	3	5.8
	Heat shock 70 kDa protein 1A/1B	70.0	69.6	1	2.5
	Rab-interacting lysosomal protein	44.2	67.2	0	0.0
	Nesprin-1	1010.4	63.1	2	0.3
	Heterogeneous nuclear ribonucleoprotein H3	36.9	55.7	1	3.5
	A-kinase anchor protein 9	453.4	55.6	2	0.4
	1-phosphatidylinositol 4,5-bisphosphate phosphodiesterase beta-3	138.7	51.6	1	1.2
	Golgin subfamily B member 1	375.8	50.1	1	0.2

Table continued on next page

band	identified protein	MW [kDa]	scores	#peptides	SC [%]
	Mucin-16	2353.1	50.1	1	0.0
	Unconventional myosin-IXb	243.2	45.9	1	0.5
	Poly(rC)-binding protein 1	37.5	45.8	1	3.1
	DDB1- and CUL4-associated factor 7	38.9	45.2	1	4.4
	G-protein coupled receptor 98	692.6	44.8	1	0.1
	Spectrin alpha chain, erythrocytic 1	279.8	44.7	0	0.0
	Heat shock cognate 71 kDa protein	70.9	43.9	1	2.6
	Platelet glycoprotein V	60.9	43.1	1.4	3.92
	Putative uncharacterized protein C8orf73	77.1	41.6	1.1	16.13

Danksagung

Zu allererst danke ich natürlich Prof. Gunter Meister für die Möglichkeit, dass ich meine Doktorarbeit in deiner Arbeitsgruppe durchführen konnte! Vielen Dank Gunter für die Betreuung dieser Arbeit, die hilfreichen Anregungen und Diskussionen sowie das mich gesetzte Vertrauen dieses Thema bearbeiten zu können.

Bei Herrn Prof. Christoph Klein bedanke ich mich für die Bereitschaft, das Zweitgutachten für diese Arbeit anzufertigen.

Allen Mitgliedern des Lehrstuhls Biochemie I gilt mein Dank für die Unterstützung, die mir während meiner Zeit zu Teil wurde. Für die gute und freundliche Arbeits-atmosphäre danke ich insbesondere folgenden aktiven und ehemaligen Mitgliedern des Lehrstuhls: Sigrun Ammon, Corinna Friedrich, Eduard Hochmuth, Norbert Eichner, Gerhard Lehmann, Johannes Danner, Nicholas Strieder, Simone Harlander sowie Marie-Theresa Wickert.

Vier Personen aus meiner Zeit am Lehrstuhl, die weit mehr als "nur" werte Kollegen sind, verdienen noch einen ganz besonderen Dank:

Liebe Judith, dir danke ich für die gute Zeit, die zahlreichen Meetings, bei denen nicht nur fachliches besprochen wurde und den nicht-weggefrorenen Spaß. Vielen herzlichen Dank auch für das Gegenlesen dieser Arbeit!

Lieber Leo, auch dir danke ich sehr für die Unterstützung während meiner Arbeit, insbesondere für die Zeit, die du für mich an der Äkta geopfert hast. Vor allem auch Danke für all den Spaß und Freude im Labor und darüber hinaus. Ich werde unsere kleinen "Streitigkeiten" vermissen.

Lieber Philipp, lieber Daniele: Euch beiden gebührt ein sehr großes Danke! Ohne euch wäre ich wahrscheinlich nicht soweit gekommen.
Philipp, ich bin sehr froh, dass es dich damals zu uns an den Lehrstuhl verschlagen hat und dass sich durch deine Zeit bei uns eine tiefe Freundschaft entwickeln konnte. Diese Zeit wird von meiner Doktorarbeit immer in allerbester Erinnerung bleiben! Danke für deine Tipps zu jeder Lebenslage und dein stets offenes Ohr.
Daniele, von ganzem Herzen Danke für die vielen Ratschläge, den wunderbar witzigen Schmarrn, den wir zusammen gemacht haben, und vor allem für deine Freundschaft, die mittlerweile schon lange besteht und hoffentlich noch viel länger bestehen wird!

Zum Schluss danke ich ausdrücklich meiner Familie, auf deren Unterstützung ich immer zählen kann. Vielen Dank hierfür!